A unified developmental model of maps, complex cells and surround modulation in the primary visual cortex

Jan Antolik

Doctor of Philosophy

Institute for Adaptive and Neural Computation
School of Informatics
University of Edinburgh

2010

Abstract

For human and animal vision, the perception of local visual features can depend on the spatial arrangement of the surrounding visual stimuli. In the earliest stages of visual processing this phenomenon is called surround modulation, where the response of visually selective neurons is influenced by the response of neighboring neurons. Surround modulation has been implicated in numerous important perceptual phenomena, such as contour integration and figure-ground segregation. In cats, one of the major potential neural substrates for surround modulation are lateral connections between cortical neurons in layer 2/3, which typically contains ”complex” cells that appear to combine responses from ”simple” cells in layer 4C. Interestingly, these lateral connections have also been implicated in the development of functional maps in primary visual cortex, such as smooth, well-organized maps for the preference of oriented lines.

Together, this evidence suggests a common underlying substrate the lateral interactions in layer 2/3—as the driving force behind development of orientation maps for both simple and complex cells, and at the same time expression of surround modulation in adult animals. However, previously these phenomena have been studied largely in isolation, and we are not aware of a computational model that can account for all of them simultaneously and show how they are related. In this thesis we resolve this problem by building a single, unified computational model that can explain the development of orientation maps, the development of simple and complex cells, and surround modulation.

First we build a simple, single-layer model of orientation map development based on ALISSOM, which has more realistic single cell properties (such as contrast gain control and contrast invariant orientation tuning) than its predecessor. Then we extend this model by adding layer 2/3, and show how the model can explain development of orientation maps of both simple and complex cells. As the last step towards a developmental model of surround modulation, we replace Mexican-hat-like lateral connectivity in layer 2/3 of the model with a more realistic configuration based on long-range excitation and short-range inhibitory cells, extending a simpler model by Judith Law.

The resulting unified model of V1 explains how orientation maps of simple and complex cells can develop, while individual neurons in the developed model express realistic orientation tuning and various surround modulation properties. In doing so, we not only offer a consistent explanation behind all these phenomena, but also create a very rich model of V1 in which the interactions between various V1 properties can be studied. The model allows us to formulate several novel predictions that relate the

variation of single cell properties to their location in the orientation preference maps in V1, and we show how these predictions can be tested experimentally. Overall, this model represents a synthesis of a wide body of experimental evidence, forming a compact hypothesis for much of the development and behavior of neurons in the visual cortex.

Acknowledgements

First of all, I would like to thank my supervisor Jim Bednar whose guidance and encouragement from the initial to the final level enabled me to progress in my research and to develop an understanding of the subject. I am indebted to members of Institute of Adaptive and Neural Computation for support and help. Especially big thanks to Judith Law, Chris Ball and Nicolas Heess for all the advice and helpful discussions, and to Adrianna Teriakidis and Cian O'Donnell for making sure that the final text is readable. Great thank you also to Pat Ferguson for all the care and Mark Van Rossum, David Willshaw and Peggy Seriès for all the helpful input I received throughout the years. Further thanks goes to Yishai Elyada without whom this thesis would never met the deadline.

I would like to thank my friends in and outside of academia, Atila, Adrianna, Chris, Graeme, Gurprit, Mike, Michael, Tim and Tom; that made the last 4 years in Edinburgh so much fun and gave me the energy to finish this endeavor.

I am very grateful to my family. They always understood how much it means to me to continue with further education and were always supporting my decision.

Finally, a special thanks to Tanja for making my PhD-study time even nicer and memorable. It was fun to be on the PhD journey together and reaching the goal at the same time.

Declaration

I declare that this thesis was composed by myself, that the work contained herein is my own except where explicitly stated otherwise in the text, and that this work has not been submitted for any other degree or professional qualification except as specified.

(*Jan Antolik*)

Table of Contents

Chapter 1

Introduction

The brain is the information processing centre of all higher organisms. Undoubtedly the most notable property of this organ is its immense adaptability to external stimuli. This is manifested not only during adulthood as the ability to acquire new memories and skills, but also, already during its pre and post-natal development, when the brain forms its basic adult functions in tandem with input coming from the environment. Remarkably this is true even at the earliest stages of the brain's information processing pipeline, such as early visual, auditory and somatosensory cortical areas. It is one of the underlying assumptions of this thesis that both these types of adaptability — during development and during adulthood — have largely overlapping underlying mechanisms, particularly some form of activity-based synaptic plasticity.

Neuroscience has produced an immense amount of data on both the function and anatomy of the brain. However, our transformation of all this knowledge into a general coherent understanding of how the brain works have so far been very limited. This is probably best manifested by the first cortical visual processing area. V1 amounts to only a fraction of cerebral cortex, but — thanks to the last 50 years of intense research — is the most studied part of the brain. Despite this, our understanding of what this small part of cortex does is probably best represented by the title of a recent review on V1: 'What is the other 85% of V1 doing?' [148].

One of the main reasons behind our poor understanding of the brain, other than that it is an immensely complicated dynamical system, is the fact that the experimental evidence is very fragmented. A natural remedy to this situation is to complement the experimental studies with computational and modeling approaches, in order to create links between the fragments of understanding. This way we can uncover the general underlying principles, and not less importantly also guide the future experimental

studies towards experiments that shed the most light on the outstanding problems. It is my belief that so far even computational neuroscience has unfortunately been primarily following the fragmented pattern of knowledge coming from experimental studies, focusing on producing small isolated models of only a few target properties.

In this thesis we follow a modeling approach that is more systematic and incremental, and that we believe is more likely to lead to integration of the present knowledge into more general understanding of the brain and of the cortex in particular. We base our models on a well-established model architecture (LISSOM [132]), particularly on its latest variant ALISSOM [119], which already reproduces many previous experimental findings. We extend this model significantly to both more accurately represent the anatomical and functional properties of adult brain, and at the same time explain how these properties can develop from initially random or isotropic connectivity. In this way, we achieve a model that explains phenomena at several temporal scales (both long-term development and short-term adult properties) and at several spatial scales (population properties, such as maps, and single-cell properties, such as receptive fields and surround modulation of individual neurons). We further propose extensions to the model that can start to explain interaction between multiple cortical areas.

In this thesis we will focus on the study of the early visual system, particular the primary visual sensory cortical area, V1. In our models we will investigate both the adult function and the development of this area. As stated above, the main advantage of focusing on this particular area is the large number of experimental studies that have explored it, and the wide range of experimental techniques that have been applied to its exploration. These techniques have created knowledge at both short and long term temporal scales (e.g. electrophysiology and chronic optical imaging, respectively), and at both small and large spatial scales (e.g. two-photon imaging and optical imaging, respectively). This wealth and range of data is particularly important for our modeling approach, which reproduces V1 properties at various temporal and spatial scales, and thus requires all this information to be properly constrained.

One of the cerebral cortex's most notable large-scale properties, which clearly undergoes development both pre- and post-natally [54], are the various topographic maps. These are known to be present throughout cortex, and are implicated in a number of functional properties of V1 (such as surround modulation [107]), and of cortex in general. This makes topographical organization a particularly important feature of cortex, and thus a very desirable target for study. A number of previous modeling studies have investigated the possible mechanisms behind map development [154, 81, 132],

and there have also been a few that have focused on the role of maps in adult cortex [177, 204]. However, a model showing both how these maps can develop and how and why the developed structures lead to the adult functional properties of V1 is so far missing. By studying in a single model both the possible mechanisms of the development of these maps, and also the role of the developed maps in adult cortical function, we fill this missing gap in our understanding of the development and adult function of V1. This nicely demonstrates the advantage of our more inclusive approach, which allows us to incorporate a large number of properties into a single model, and subsequently explore the interactions between them. Even though many functional maps have been so far identified in V1, e.g. orientation preference, position preference, ocular dominance, direction preference, color preference, spatial frequency preference, and temporal frequency preference, in this thesis we will focus only on the first two, which, together with ocular dominance, have so far been the most studied. All of these techniques and approaches can be extended to these other dimensions in future work, using techniques already demonstrated in previous work using closely related models.

A particular focus of this work is to help understand the phenomenon of surround modulation (SM). The response of neurons in primary visual cortex is not only influenced by the stimuli confined to their classical receptive field, but also by the spatial context within which the visual stimuli are embedded [120]. Neurons in V1 receive inputs from three main sources: afferent input from lateral geniculate nucleus (LGN), input from other V1 neurons in the map via lateral connections, and input from extra-striate areas via feedback connections. Various studies have indicated participation of all of these sources in the phenomenon of contextual modulation (CM) [60, 179, 14, 49, 204] . In this thesis, we will focus on the second source of SM, believed to be the main: the lateral connections in V1. Interestingly, lateral connections have been previously implicated also in the formation of functional maps in V1, being the source of Mexican-hat lateral interactions [200]. This highlights the need to study the phenomenon of SM in the context of V1 map formation. The main goal of this thesis, therefore, is to create a model which shows how orientation (and position) preference maps, and connection patterns within them, can develop, and at the same time show that these neurons' connection patterns in the developed model explain the SM properties of adult V1 known from experimental studies.

Furthermore, an interesting consequence of the integrative modeling approach adopted in this thesis is that we were able to show that two V1 phenomena previously explained by advanced plasticity rules, can in the models proposed here be implemented

with simpler plasticity mechanisms, as will be discussed in chapter 5. This is due to the fact, that some of the computational power of the advanced plasticity rules can be offloaded onto the dynamics of the networks. This demonstrated the importance in considering realistic, highly heterogeneous network architectures — such as those proposed in this thesis — as they enable rich and specific network dynamics, that can be in turn harnessed for various computational roles. We believe that the highly specific wiring of cortex is a good evidence that such phenomena are likely to occur in animal brain.

1.1 Summary of aims

An important feature of SM is that its properties are strongly dependent on the contrast of the stimulus. In order to study SM, it is critical that a model have realistic behavior with respect to contrast. Previous models of development have been highly unrealistic in this sense. In chapter 3 we show how adding retinal or LGN gain control mechanisms to the ALISSOM model can give realistic contrast-invariant tuning and patterns of response with respect to contrast that match experimental results. The most important novel feature of the ALISSOM model is the use of homeostatic plasticity to show how orientation maps in V1 develop in a stable way. Previous models have been unable to explain how development could be stable, despite the ongoing changes in cortical circuity and the afferent input during development (e.g. pre-natal activity such as retinal waves and post-natal natural visual input). In the rest of chapter 3 we show that by introducing the above changes to the ALISSOM model, we can simplify the homeostatic rule, while still maintaining stable orientation map development. Furthermore we show that our modifications allow us to eliminate the last free parameter that was required in the ALISSOM model to ensure stable map development for wide range of input statistics. The resulting modified ALISSOM model is then used as the base for the rest of the models introduced in this thesis.

In chapter 4 we focus on making the functional and anatomical properties of our model more realistic. As stated above, the main source of contextual modulation in V1 that this thesis focuses on are the lateral connections. Although the lateral connectivity is present throughout all cortical layers, it is particularly strong [27, 28] and spatially extended [173, 157, 28] in layer 2/3. Also, unlike in cortical layer 4C, the lateral connectivity in layer 2/3 is not isotropic, but forms a so called ‘daisy’ pattern correlated with the orientation preference maps with respect to the orientation preference of the

source neurons[173, 157] . The above, together with the fact that SM is known to have orientation-specific effects, strongly suggests that the lateral connectivity in layer 2/3 should be considered as the primary substrate underlying SM.

A related issue is that previous experimental studies have shown a relationship between cortical depth and the presence of simple and complex cell classes [155, 92]. Simple cells are V1 neurons that respond to a drifting sinusoidal grating only when it is precisely aligned with the on and off subregions of cell's receptive field (RF). On the other hand, the response of complex cells is largely phase invariant i.e. the cell will respond to all phases of a sine grating. A recent study by Martinez et al. [92] argued that in cat, neurons with simple receptive fields are exclusively present in upper layer 6 and layer 4. Data in macaque monkey are not as clear, but researchers have also reported a trend from simple cells dominating in layer 4 to complex cells dominating in layer 2/3 [155]. Together with the fact that layer 4C is the primary target of the thalamic axons, above evidence suggests, that a model exploring SM in the context of lateral connectivity should model layer 2/3 as being populated primarily with complex cells. There has so far been only a single model explicitly modeling lateral connectivity and showing how maps of complex cells can develop [149]. However, this model has several disadvantages, the main one being that it places the strong long-range lateral connections between neurons receiving direct thalamic input and having simple-cell-like properties — i.e. a homologue of layer 4C. Furthermore, this model also requires a very specific pattern of connectivity to be established before development, for which there is no experimental evidence. Therefore, in chapter 4 we present a new model of the development of simple cells in layer 4C and complex cells in layer 2/3 that rectifies the above problems. In this way, we not only pave the way towards our final goal, but also present a significantly more realistic model of complex-cell map development.

In chapter 5 we focus on a direct contradiction between previous models of development and experimental evidence about the pattern of long-range connections. Previous models of map development relying on lateral connectivity as the underlying substrate for self-organisation have been using Mexican-hat shaped lateral connectivity, with short-range lateral excitation and long-range lateral inhibition [144, 132]. This is, however, in direct contradiction to experimental evidence showing that the source of long-range lateral connectivity is excitatory pyramidal neurons, and that these primarily target other excitatory neurons [83, 114, 126]. Recently, my colleague Judith Law has solved this problem by constructing a model that uses realistic lateral connectivity, i.e. short-range inhibitory and long-range excitatory, and is able to develop

orientation preference maps [119]. As we have discussed above, the lateral connectivity in layer 2/3 of V1 is believed to be the main substrate behind SM, and therefore it is imperative that a model studying SM uses a realistic configuration. So, as the last step towards a developmental model of surround modulation, in chapter 5 we incorporate this new, more realistic configuration of lateral connections into the model presented in chapter 4, and show that this altered architecture can still account for all the desirable properties of the original model, that we have discussed.

Using this more realistic model, we perform a wide range of surround modulation analysis on populations of model neurons, focusing on two particular features: size tuning curves and orientation contrast responses. We show that neurons in our model exhibit a wide range of surround modulation properties consistent with experimental evidence. The model explains how the patterns of activity arise from the connectivity and how the connectivity arises from development. Having a model with realistic functional topographical properties and that also exhibits SM puts us in a unique position to link these two V1 phenomena. We offer a number of predictions on how the various parameters of the surround modulation properties of neurons in our model correlate with their position in the map or their orientation selectivity. This again illustrates the advantage of constructing more complex models incorporating a large number of properties, and would not be possible with simple approaches.

Finally, in the last chapter we discuss a number of possible extensions of our model that can further improve the understanding of contextual modulation and other phenomena in the early visual system. As we mentioned at the beginning of this chapter, lateral connections are only one of three major sources that can potentially participate in the contextual modulation properties of V1 neurons. The first of the remaining sources is the feed-forward projection from LGN. It turns out that our implementation of gain control is in fact tightly related to a possible mechanism of surround modulation already at the level of LGN or retina [159], which can be investiaged further in detail. The other source of SM is the feedback connectivity from higher-level cortical areas. Our model of map development, unlike most of its predecessors, already contains the equivalent of layer 2/3 with complex cells — the primary source of output from V1 to extra-striate areas. This means that extension of our model to include extra-striate areas should now be straightforward. Together this positions our model as the ideal test bed for future investigation of the interplay between these three sources of SM, and V1 in general, helping us to understand what computations are performed in V1 and how its circuitry arises through development.

Chapter 2

Background

2.1 The early visual system

In this thesis we build a model of the early visual system, focusing primarily on information processing in the primary visual cortex. One of the main goals is to bring together in a single model as many of the known properties of primary visual cortex as possible. Due to this and the limited number of experimental studies exploring these properties in various animal species, when designing and evaluating our models, we will rely on the data from the following four species: macaque monkey, cat, ferret and tree shrew. Although it is fair to say that the early visual system among these species is similar, there are number of known differences. Therefore, to achieve maximal consistency, we will primarily focus our models to replicate data from cat, and resort to the other species only if appropriate data is not available. We will begin this chapter with a brief description of the early visual system, followed by a more detailed discussion of aspects of primary visual cortex particularly relevant to this thesis. A more thorough review of the early visual system can be found for example in [21].

The early visual system pathway is depicted in detail in figure 2.1. The light sensitive sensors of the visual system are the photoreceptors located in the retina. From these the information is passed to retinal ganglion cells (RGCs). In the center of the visual field, RGCs make one-to-one projections to the lateral geniculate nucleus (LGN), which is typically considered to be a relay station passing the information to the primary visual cortical area, also known as 'striate' cortex or area V1. The connections from the two eyes to the LGN cross in the optic chiasm, such that the information from the left side of the retina in both eyes is channelled into the part of V1 situated in the left hemisphere, and vice versa. An important property of this retino-geniculate

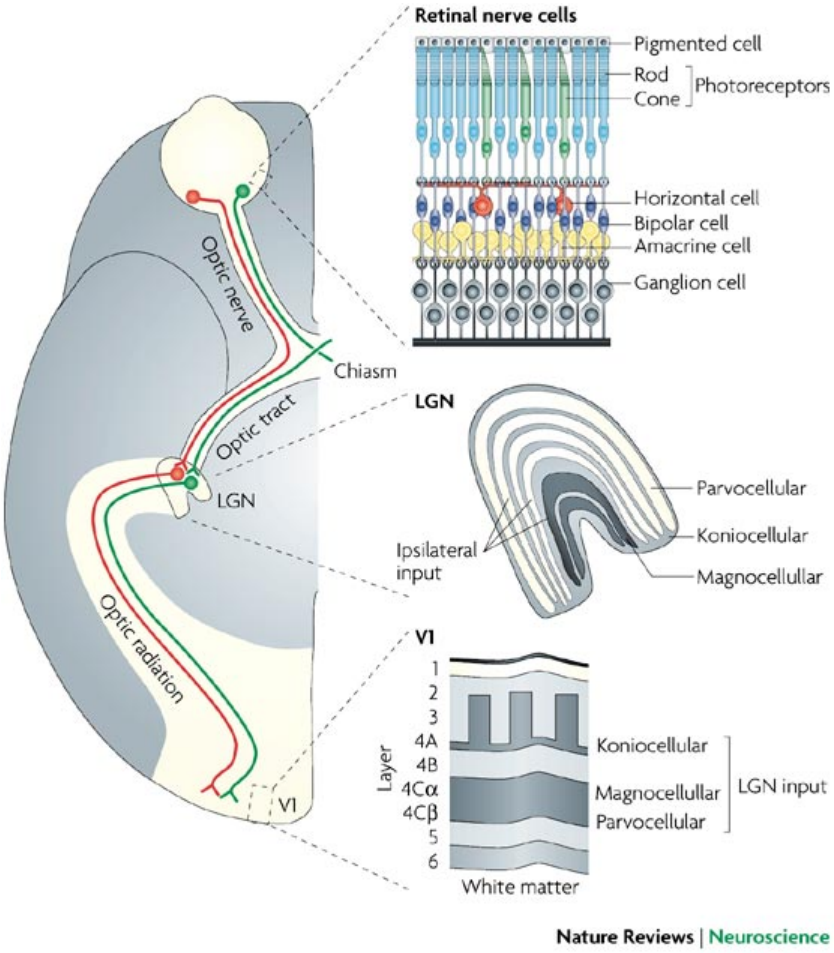

Figure 2.1: Anatomy of the visual pathway from the retina through the lateral geniculate nucleus to the primary visual cortex (V1) in the macaque monkey. The first processing step of the visual pathway is the retina, where light entering the eye activates the photoreceptors. Signals from photoreceptors are then passed through bipolar cells onto ganglion cells, whose axons form the optic nerve that passes the signals to LGN. Ganglion cells from the temporal retina (away from the nose) project to the ipsilateral LGN (red lines) and those from the nasal retina (towards the nose) project to the contralateral LGN (green lines). The projections from retina form a smooth mapping in LGN, such that nearby locations in the retina are connected to nearby locations in the LGN. This way the same retinotopical mapping is formed in each of the LGN layers. The main target of the axons of LGN neurons is V1, where they terminate primarily in layer 4C. Depending on the layer where the LGN neurons originate they innervate different V1 layers: parvocellular cells project mainly to layer 4Cβ, magnocelular to layer 4Cα, and koniocellular cells to layer 4A and lower layer 3. Reprinted from [175].

pathway is that it forms a smooth mapping from the retinotopic space onto the LGN space, meaning that nearby locations in visual space are connected to nearby locations in LGN. This retinotopical organization is maintained throughout most of the visual cortex.

The LGN is a layered structure, where cells in different layers exhibit different properties. For example, in the macaque monkey, magnocellular (M) cells (which have large receptive fields), parvocellular (P) cells (which have smaller receptive fields), and koniocellular (K) cells are separated into different, eye-specific layers (figure 2.1). In this thesis we will focus on the parvocellular pathway, as it is believed to be primarily involved in the shape recognition.

Figure 2.2: Schematic depictions of receptive field types in the retina, LGN and V1. Regions of the receptive fields where bright spots of light excite the neuron are plotted white (On subregions), regions where dark spots of light excite it are plotted black (Off subregions) and regions where contrast has no direct effect are plotted in medium gray. (a,b) RFs in retina and LGN have typical center-surround arrangement where the maximal response is elicited if the center of the RF is stimulated with a light patch surrounded by dark surround (On cells) or vice-vers (Off cells). Unlike the isotropic RFs in LGN and retina, which are not selective to orientation, most V1 neurons have orientation-selective RFs that can be well represented by Gabor functions. These typically consist of two or three elongated subregions as shown above: (c) A two-lobe arrangement, here favoring a 45° edge, and (d) a three-lobe pattern, favoring a 135° white line against a dark background. Reprinted with permission from [132].

The most common method to characterize the functional properties of neurons in early visual system is to identify their classical receptive field (CRF), which is defined as the area of visual space that neuron responds to by emitting action potentials (spikes). The On-centre and Off-centre receptive fields of RGC and LGN cells (figure 2.2 a,b) perform a basic type of contrast detection. The RGCs can be considered to do a convolution of the visual input with a difference-of-gaussians kernel, effectively

performing edge-detection or edge enhancement [158].

2.1.1 Anatomy of the primary visual cortex

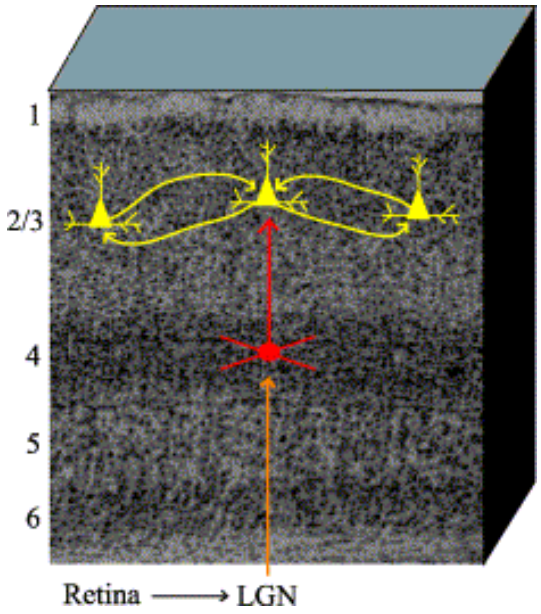

Figure 2.3: Elements of the cortical circuit in cat primary visual cortex. A Nissl-stained histological section through primary visual cortex shows the cortical laminae. The schematic overlay depicts the flow of visual information through primary feed-forward and recurrent pathways to a layer 2/3 neuron (central, yellow cell). The feed-forward pathway travels from the retina, to the lateral geniculate nucleus in the thalamus (LGN), to cortical layer 4 (red cell), and on to layer 2/3. Recurrent, or horizontal, connections between layer 2/3 neurons (flanking yellow cells) are one source for the modulatory effects of the receptive field surround. Reprinted from [55].

The cortex is a large, folded, layered sheet of neurons and connections covering most of the visible surface of the brain. By convention, the cortical sheet is divided into 6 main layers, which are sometimes further grouped or subdivided. The layers are distinguished by the distribution of the different types of cortical neurons that occupy them and also by the major axonal projections that either arrive or originate there. An example of the laminar structure of the primary visual cortex in cat can be seen in figure 2.3.

The cortex is composed of a variety of cells, the two main categories being excitatory and inhibitory cells. There are two main types of excitatory cells; pyramidal neurons and spiny stellate cells. A large number of different types of cortical inhibitory

neurons (more than 40) have been identified [124]. Both excitatory and inhibitory cells vary widely in both physiological and morphological properties.

A specific pattern of both incoming and outgoing connectivity and connectivity between cortical layers has been identified for cat primary visual cortex (see figure 2.4). The main feed-forward input to V1 comes from the (LGN), which transmits input from the retina and sends axonal projections that target mainly layer 4. Layer 4 is subdivided into 4 sublayers: 4A,4B and 4Cα,4Cβ. Parvocellular cells project mainly to layer 4Cβ, magnocellular to layer 4Cα, and koniocellular cells to layer 4A. Layer 4B receives connections primarily from layer 4Cβ but also from layer 4Cα, and sends projections to the middle temporal (MT) visual area and to V2. Layer 4C contains both spiny stellate and pyramidal neurons, whereas the remaining cortical layers are dominated by pyramidal neurons [180]. It is the spiny stellate cells that receive the bulk of the thalamic projections [27]. Spiny stellate cells confine their axons to layer 4C and connect to other spiny stellate cells and pyramidal neurons. Interestingly, despite the huge number of synaptic bouttons formed on single layer 4C spiny stellate cells (tens of thousands) the number of LGN cells converging to single spiny stellate cells in layer 4C is low (30 cells in cat [8]), with the most recent unpublished evidence (Kevan Martin, 2009, personal communication) suggesting that as few as 5 synaptic boutons per stellate cell originate from the thalamus.

The main target of layer 4C pyramidal neurons is the supra-granular layer 2/3, which thus appears to be the second major processing stage of the visual signal in V1. A major anatomical characteristic of layer 2/3 is the existence of strong long-range lateral connectivity, originating in the excitatory pyramidal neurons. These connections can span 6-8 millimeters and are restricted within layer 2/3 [13]. Furthermore, this lateral connectivity becomes patchy at longer distances, and it has been shown that this patchiness coincides with functional properties of the layer 2/3 neurons such as orientation preference [36, 173]. Furthermore, as Buzás et al. [42] show, even though long-range connections of local populations of neurons are clearly biased towards similar orientations, there is a great variability between the individual neurons within the local population. However, due to the local network effects in the local populations of neurons it is reasonable to still expect strong orientation biases on single cell level. Although it turns out that the long range lateral connections in layer 2/3 target mostly excitatory pyramidal neurons (80%) as opposed to inhibitory inter-neurons (20%) [83, 114, 126], studies undertaken with high-contrast stimuli showed that the overall effect seems to be inhibitory [80]. Layer 2/3 is also the major source of output

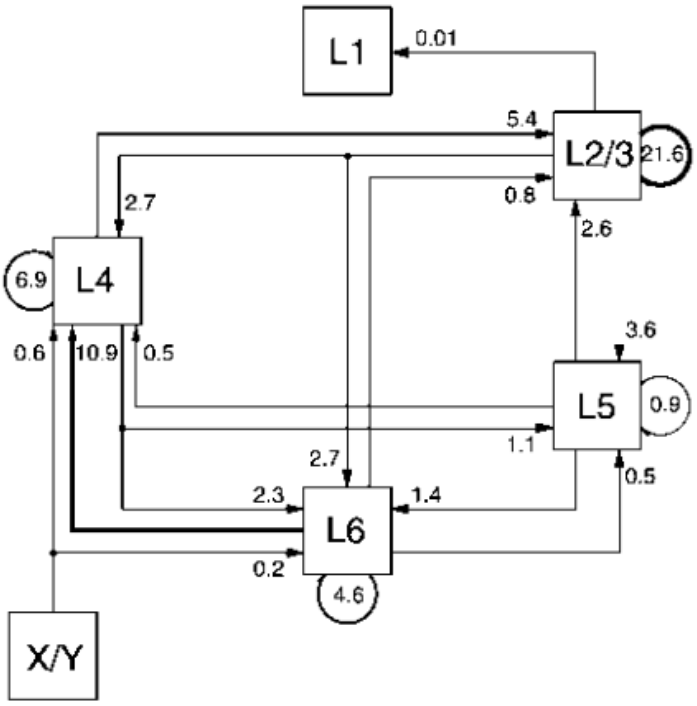

Figure 2.4: Number of synapses involved in the projections between excitatory and excitatory neurons between cortical layers in cat, including the X-type and Y-type afferents from the dorsal LGN. Each arrow is labeled with a number indicating the proportion of all the synapses in V1 that are formed between excitatory neurons in the examined volume of cortex (this means that the depicted projections will not add up to 1.0 as synapses formed by axons incoming from different cortical areas or other brain structures are not accounted for). Reprinted from [27].

into other cortical areas.

The exact role of layer 5 in cortical visual processing is not known yet, but the prevailing hypothesis is that it has a modulatory effect on superficial cortical layers (ie. layers 1-3) [44]. The main input to layer 5 comes from layer 2/3 [39] and thus it can be considered as the third processing step of the visual input from thalamus. Most layer 5 pyramidal neurons preferentially target layers 2–4B where they form non-specific axonal arborizations [45]. Another important anatomical feature of layer 5 is that it sends numerous feedback projections back into LGNd, thus providing feedback to this relay area.

Similarly to layer 5, the role of layer 6 in processing of visual information is not clear. It receives input from both layer 2/3 and 5 and sends strong projections back to layer 4. It is the strongest anatomical input (in terms of number of synapses) to layer 4. Similarly to layer 5, layer 6 sends a feedback projection back to the thalamus.

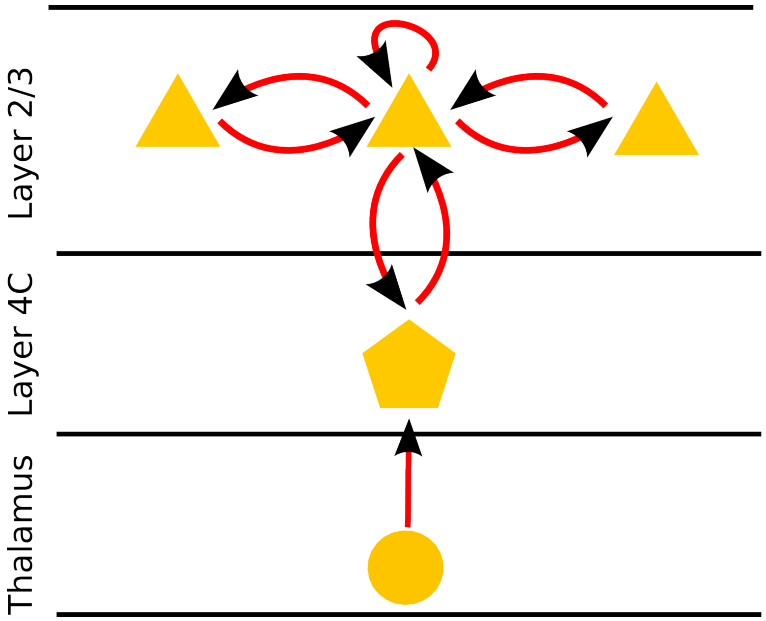

Figure 2.5: This figure shows the simplification of the excitatory cortical connectivity that we will use in this study. The input from thalamus arrives to cortical layer 4C, and is passed onto layer 2/3 neurons. The major long range lateral interactions occur in layer 2/3. Layer 4C additionally receives strong direct local feedback from layer 2/3, which in real cortex corresponds to the pathway reaching to layer 4C from layer 2/3 via layers 5 and 6. We also simulate local inhibitory interneurons in layer 2/3 (not shown).

We consider the known anatomical features to be a very important constraint for modeling. However, due to the limitations of our current knowledge on cortical anatomy,

and due to the natural need to make simplifications while formulating computational models, in this study we consider the following simplified view of V1 anatomy, summarized in figure 2.5:

1. **Layer 4C** - As stated above, in this thesis we focus on modeling the parvocellular pathway. Consequently in our models we will model only layer 4C*beta* - the primary recipient of parvocellular input. We consider only one cell type in layer 4C, effectively combining effects of the excitatory stellate and pyramidal cells. We assume that the lateral connectivity in this model is shorter and several times weaker than the one in layer 2/3. This layer is dominated by simple cells, and the orientation preference of these neurons is due to the specific set of thalamic axons synapsing on them, whose source neurons have preferences arranged along an axis in visual space (see section 2.1.2).

2. **Layer 2/3** - this layer receives a feed-forward input from layer 4C via narrow excitatory intra-columnar projections. This layer is the major provider of the lateral interactions in V1 due to its very strong lateral connectivity. Crucially, the long range connection should be excitatory, synapsing at both excitatory and inhibitory neurons, and inhibitory neurons should have comparatively shorter axonal arborization. This layer is dominated by complex cells. They inherit their orientation selectivity from the layer 4C neurons they receive input from, and achieve phase invariance by pooling inputs from simple cells with different phase preference.

3. **Layer 5 and 6** - in this study we do not consider the feedback pathway from V1 to LGN, nor from extrastriate cortex to V1. Because it is currently not clear what the roles of layer 5 and 6 in visual processing are, other than providing feedback from layer 2/3 into layer 4, we do not explicitly model these two layers. For simplicity and in order to save computational resources we instead consider a direct pathway from layer 2/3 to layer 4C.

2.1.2 Functional properties of primary visual cortex

The visual cortex is organised in a columnar fashion. Neurons within a single vertical column (perpendicular to the cortical surface) respond to similar visual stimuli. Neurons in V1 typically respond best to high-contrast lines, bars, or gratings of a certain orientation [94].

The early studies of Hubel & Wiesel [94] identified two functionally different classes of cells in primary visual cortex. The first class — simple cells — respond to a drifting sinusoidal grating only when it is precisely aligned with the ON and OFF subregions of the cell's receptive field (RF). On the other hand, the response of cells in the second class — the complex cells — is largely phase invariant, i.e., the cell will respond to many or all phases of a sine grating (see figure 2.6). Studies have shown a relationship between cortical depth and cell class [155, 92]. A recent study by Martinez et al. [92] argued that in cat, neurons with simple receptive fields are exclusively present in layer 4 and upper layer 6, the layers that receive the majority of thalamic input. Data in macaque monkey are not as clear, but evidence suggests a trend from simple cells dominating in layer 4 to complex cells dominating in layer 2/3 [155].

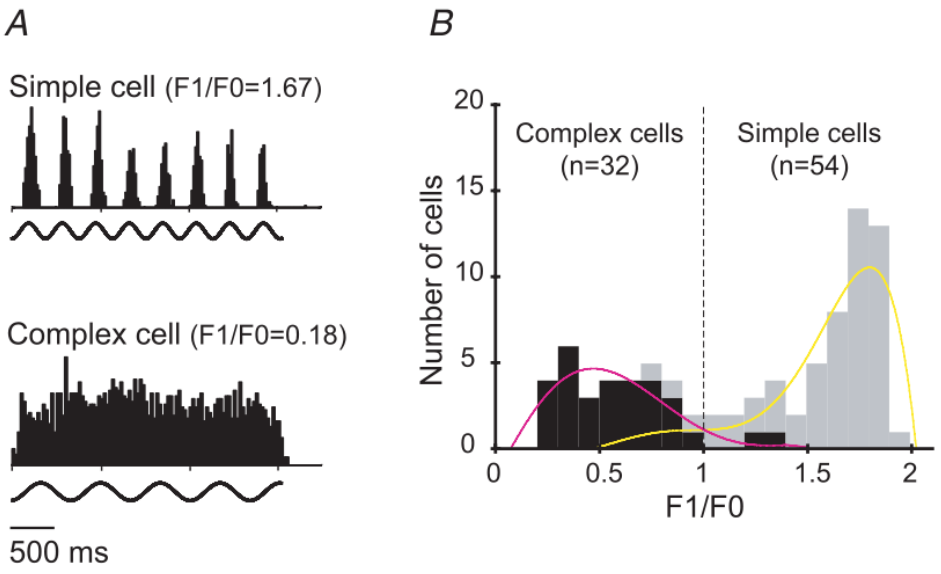

Figure 2.6: A, Peristimulus time histogram (PSTH) of responses of a typical simple (upper PSTH) and a complex cell (lower PSTH) in area V1. The action potentials of the cells were generated in response to the presentation of optimised drifting sine gratings covering their CRFs. The sinusoidal lines below each PSTH represent the temporal frequency modulation of the visual stimulus energy. The PSTH of the simple cell (F1/F0 = 1.65) and that of the complex cell (F1/F0 = 0.18) are based on the accumulation of 8 trials. B, frequency histogram of F1/F0 ratios for the sample of V1 neurones. The cells were qualitatively identified as simple (shaded columns) or complex (filled columns) on the basis of the presence or absence, respectively, of spatially separated light on and light off discharge subregions in their CRFs. Reprinted from [19].

In line with these laminar differences in the functional properties of neurons in V1, Hubel and Wiesel suggested that V1 RFs can be constructed by a simple hierarchical architecture, where simple cells in layer 4C receive inputs from a small number of cells in LGN, whose RFs are specifically aligned, forming the orientation selectivity of the layer 4C neuron's RF. Similarly, neurons in layer 2/3 can pool responses from cells in layer 4C of the same orientation preference, but different phase preference, thus forming the phase invariant RFs of complex cells (see figure 2.7). It is possible to extend this hierarchical idea of RF construction further and hypothesise neurons that response to complex shapes, such as the neurons found in higher level areas, by pooling responses from specific combinations of lower level neurons.

This hierarchical description of early visual system has dominated literature since the early studies of Hubel and Wiesel. However, as discussed above, V1 is dominated by lateral connections, suggesting that V1 is highly recurrent dynamical system and thus the simple hierarchical model is not capturing important aspects of V1. Numerous experimental studies examined the role of recurrent connectivity in several functional V1 properties, including orientation tuning [172] and simple/complex cell type division [171], and corresponding models were formulated explaining these V1 properties via recurrent network dynamics rather than the simple feed-forward model proposed by Hubel and Wiesel [29, 172, 51, 130, 203]. For example Sillito [171] found that blocking inhibition in simple cells in cat V1 lead to loss of the subdivision of their receptive fields into antagonistic ON and OFF regions, a characteristic of complex cells. A follow up study by Sillito et al. [172] found that blocking inhibition in previously sharply-tuned simple cells renders them unselective to orientation. These findings indicate that the activity surrounding neurons (particularly inhibitory in this case) is essential for the expression of orientation tuning and simple/complex properties, and underlies the limitations of the simple hierarchical view of early visual cortex.

Above description of V1 functional properties was mainly based on the spiking (i.e. supra-threshold) properties of V1 neurons. However, several previous studies have shown that examining the sub-threshold neural behavior via intracellular recordings reveals important principles underlying the supra-threshold behavior. A study of Monier et al. [136] have shown a great diversity of tuning of excitatory and inhibitory currents impinging on neurons in V1, that are not always tuned to the preferred orientation of the spiking response, indicating that the orientation tuning of a V1 cells arise as a complex interplay between inhibition and excitation, which differ from cell to cell.

They hypothesized that the observed diversity is consequence of the varying inhomogeneities in functional intracortical connectivity. In a similar manner recent study by Liu et al. [93], have examined the ON and OFF subfield of the inhibitory and excitatory synaptic inputs in mouse V1 neurons. They found that in both cells whose spiking ON and OFF subfields overlapped (putatively complex cells) and in which they were segregated (putatively simple cells) all four synaptic subfields had substantial overlap. Overall these studies show that the excitatory and inhibitory inputs of V1 neurons are spatially much broader and variable, and the very specific tuning properties of V1 neuron arise due to the potentially small relative differences between these broad synaptic currents.

An important feature of the primary visual cortex is its functional topological organisation. If one traverses V1 in the horizontal direction along the surface, one will see that various RF properties of the cells change smoothly. Thus, if one measures the RF properties of neurons in an area of cortex and plots them, a map-like structure appears. The best known and most studied examples of such maps are retinotopic, ocular dominance, and orientation preference maps (see figure 2.8). As follows from the vertical homogeneity of cortical columns, an orientation preference map is present throughout all cortical layers and is aligned — meaning that when one traverses cortex vertically (perpendicular to the surface) one will find neurons with similar position and orientation preference [95]. Furthermore there is a relationship between the functional topological maps and connectivity in V1: if one overlays the pattern of lateral connections formed in layer 2/3 over the orientation map, one finds that the long range lateral connections preferentially connect neurons of similar orientations (see figure 2.8).

The organization of absolute phase preference — eg. the phase of the sine-grating with respect to visual field which elicits highest response from the neuron — is much less clear. Study in cat [122] have found that nearby neurons tend to have opposite phase preferences, whereas study in macaque by [16] found that nearby neurons tend to have correlated phase preference. Furthermore, the relative phase which describes the alignment of the ON and OFF RF subfields with respect to the center of RF, was found not to cluster in cat V1 [61]. It is important to note that findings about relative phase do not transfer to absolute phase, as it is possible that two neurons with opposite relative phase can still have highly overlapping ON and OFF RF subregions due to the local scatter of receptive fields centers. This fact has not been fully appreciated by several experimental and modeling studies which further added to confusion.

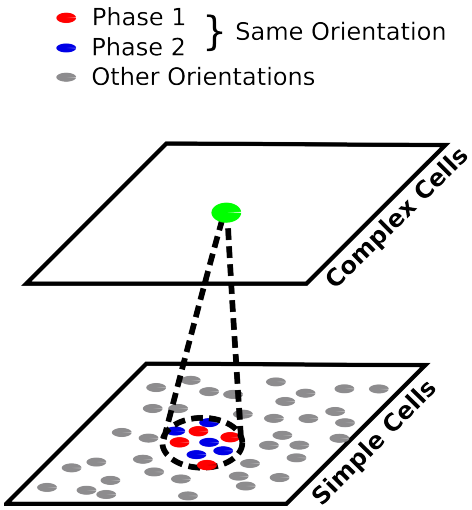

Figure 2.7: Model of complex cells that achieves phase invariance by indiscriminately pooling activities from a narrow region of simple cells of similar orientations but scattered phase.

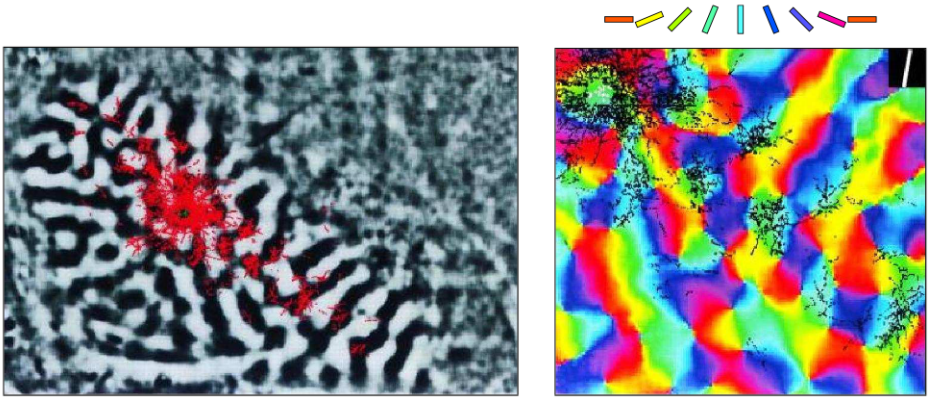

(*a*) Vertical and horizontal orientations (*b*) All orientations

Figure 2.8: Lateral connections in the tree shrew layer 2/3 orientation map. (a) The vertical and horizontal orientation preferences in a 8mm $\times$ 5mm section of V1 in the adult tree shrew, measured using optical imaging. The areas responding to vertical stimuli are plotted in black, and those responding to horizontal stimuli in white. The green dot indicates the dye injection location, and red color indicates locations where the dye have propagated. Short-range lateral connections target all orientations equally, but long-range connections go to neurons that have similar orientation preferences and are extended along the orientation preference of the source neurons. (b) The same information plotted on a 2.5mm $\times$ 2mm section of the full orientation map to the right and below the injection site. Reprinted from [36].

2.1.3 Development of visual cortex

In the previous section we described how the functional properties of adult V1 neurons can arise from the complex and specific connectivity that is present in the developed cortex. How can such specific connectivity develop? It is widely agreed that the RF properties of individual neurons cannot be directly encoded in the genetic code on a connection by connection basis, but rather some more subtle process must happen during development that leads to the specific wiring of adult neurons. There are two main candidate substrates for this development process: a molecularly mediated developmental process, and activity-mediated synaptic remodeling.

One of the central hypotheses behind the models presented in this thesis is that a specific interplay between these two mechanisms is involved: First, molecular development determines the high level anatomical structure of the cortex, such as the layered organisation, the type of neurons with their basic morphological parameters such as the extents of their dendritic and axonal arbours and their gross patterns of connectivity between visual areas [167, 125]. Second, this developmental process is then followed by activity based adaptation that further refines the isotropic or locally random connectivity laid out by molecular development, based on either internally generated or externally induced patterns of activity, leading to specific neuron-to-neuron connectivity that can explain properties such as orientation selectivity, ocular dominance and surround modulation of individual neurons.

Thus, both molecular and activity-based development have an important role. The molecular developmental process sets the basic architecture and dynamics of the system. When this system is set up, it is further refined based on its dynamics and the adaptation mechanisms operating at the synaptic level. In this thesis we focus on explaining the adaptation stage of the development. Thus in our models we assume that the general architecture set up by the molecular developmental mechanisms is present at the beginning of our simulations, and we proceed to simulate the effects of the synaptic adaptation (which in our models is governed by a simple Hebbian learning rule) when the cortex is stimulated with external or internally generated patterns of incoming neural activity.

The most compelling evidence showing that external activity is an important factor in the development of V1 comes from a number of studies that have altered visual input during development in various ways. They showed that such procedures impair various functional properties of V1 [94, 30, 102] (see figure 2.10 for illustration). For

example, if an animal is reared in darkness during its early development, its V1 neurons do not achieve orientation selectivity and consequently orientation maps do not develop [202]. On the other hand, the same studies indicate that the natural visual input cannot be the only factor behind maturation of RF in V1, as V1 neurons of dark reared animals still express many functional properties (e.g., ocular dominance and orientation selectivity), albeit impaired. Under an assumption of activity-driven development of these properties, the above experiments indicate that some other source of internally generated input (as opposed to natural visual stimulation) has to be involved. Although the specific sources of this input are not known, the most common theory is that early development is driven by genetically determined internal activity patterns, such as the coordinated spontaneous activity that occurs in the developing retina [208]. A number of experimental studies have supported this theory by showing that disrupting retinal waves during development leads to abnormal development of the visual system [82, 178, 53].

The process of early development of V1 discussed above is gradual. This has been most directly demonstrated in chronic optical imaging studies performed in ferrets [52, 54, 78] that show that functional properties of V1 develop slowly to become more adult-like at a large scale. Figure 2.9 shows orientation map of a young ferret at several time points during development. The maps are initially faint and become more prominent and refined as time progresses, reflecting the maturation of RF and thus increasing orientation selectivity of individual neurons in cortex. An interesting feature revealed by these studies is the remarkable stability of the map development. When one examines orientation preference at any given point in the map, one should see that from the time point where a given site becomes orientation selective it maintains approximately the same orientation preference during the remaining development. This level of stability is especially striking given the ongoing maturation and refinement of the local cortical circuitry during this period.

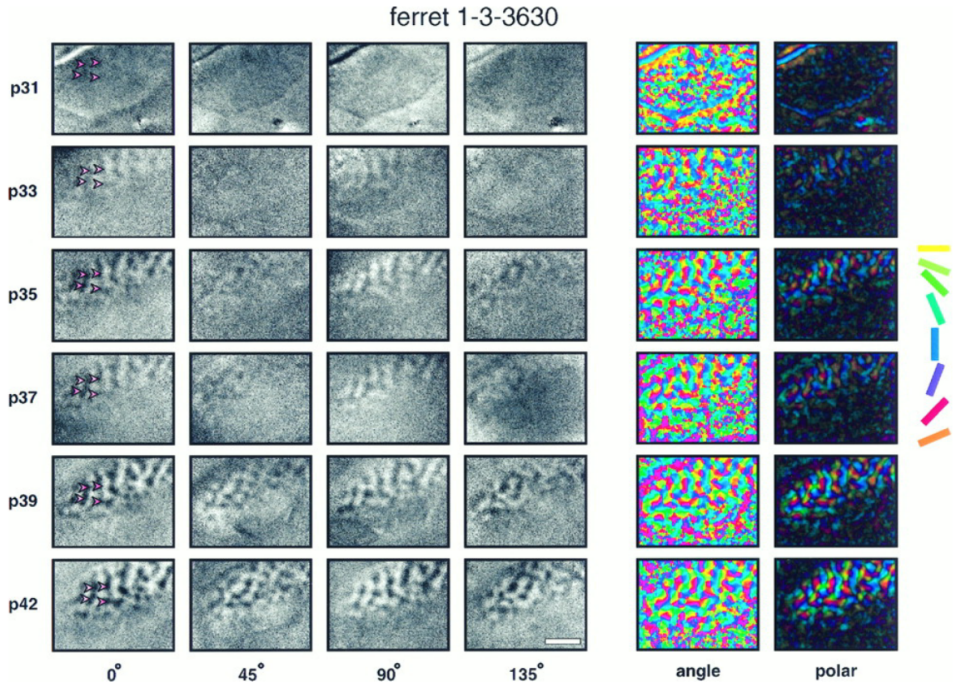

Figure 2.9: Stability of orientation map development measured by optical imaging. All maps were obtained from single ferret at six different postnatal ages. Each row shows maps recorded in the primary visual cortex at the post-natal age (in days) indicated at the left of the row. First four columns show single-condition maps recorded in response to a particular orientation of a moving square-wave grating. Individual iso-orientation domains remain stable over time and do not change their position, shape, or size. Last two columns show the combined angle maps, the color of each pixel indicates the preferred orientation of cells at that location in cortex (see color key on the right). In polar maps, the color indicates the preferred orientation, whereas the strength of orientation tuning is coded as the brightness of the pixel. At early ages, the polar maps are almost completely dark, indicating that there were no regions of the cortex that showed strong orientation-selective responses. With increasing age iso-orientation domains become more pronounced. These domains become more strongly responsive over time, and more domains appear as the maps mature, without changing the overall map pattern. Scale bar, 2mm. Reprinted from [54].

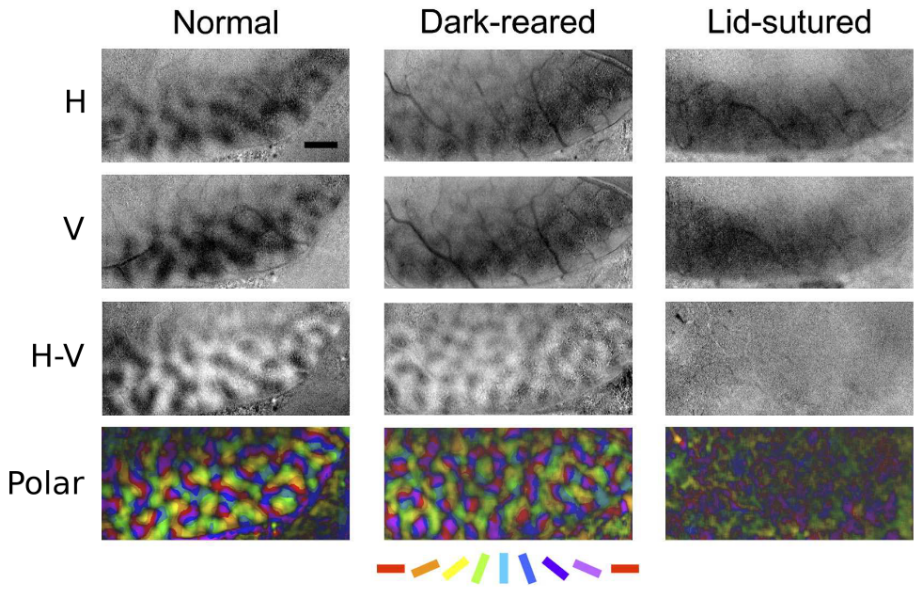

Figure 2.10: The effect of dark rearing and lid suture on orientation map development in ferrets. The top two rows show single-condition maps recorded in response to horizontal (H) and vertical (V) grating stimuli. The third row shows difference images generated by subtracting horizontal and vertical single-condition maps (scale bar = 1mm). The bottom row shows the combined polar-magnitude maps. The color of each pixel indicates the preferred orientation of cells at that location in cortex (see color key on the bottom), whereas the brightness represents the magnitude of selectivity. The orientation maps appear well formed but weaker in dark-reared ferrets. In contrast, orientation maps in lid-sututred ferrets are nearly undetectable. This indicates that the impact of abnormal visual experience is much more destructive for the developmental of the orientation preference maps than absence of visual inputs. Reprinted from [201].

2.1.4 Surround Modulation

In the previous sections we have described V1 mostly in terms of a simple feed-forward hierarchical system. This can capture a number of V1 neurons' properties, particularly in anesthetized animals. However, it is clear that the architecture and processing of V1 is more complex. Surround modulation is probably the best known and well studied functional property of V1 neurons that is inconsistent with a purely feed-forward architecture.

As briefly discussed in the introductory chapter, by definition, a visual stimulus presented outside of the CRF cannot, on its own, elicit a response from a neuron. However, experimental studies have shown that if one presents a stimulus to the RF of neuron in V1 which elicits a certain firing rate, the firing rate can be enhanced or suppressed by presenting a second stimulus in the RF surround [32, 60, 195, 106]. This means that visual stimuli outside of a neuron's RF can modulate its firing rate. This phenomenon is referred in the literature as contextual modulation or surround modulation (SM). In the past, such contextual effects have been mainly associated with primary visual cortex and higher cortical areas, but there is new substantial evidence that these mechanisms operate already at the level of LGN [35] or retina [174]. This means that surround-modulation effects can be passed on to V1 neurons via feed-forward connections, and that some surround-modulation properties measured in V1 are a reflection of processes in the retina or LGN. There is, however, evidence that the surround effects in LGN are spatially less extended [105, 159]. Furthermore, some surround modulation effects are orientation dependent, which appears to rule out an explanation in terms of LGN or retina processing, which is not selective for orientation [107]. Therefore, additional mechanisms present in V1 or higher cortical areas are required to explain the full range of surround-modulation effects observed in V1.

The most commonly implicated substrate responsible for surround modulation in V1 are the excitatory long-range lateral connections between pyramidal neurons in layer 2/3. They extend sufficiently far (8mm) [76] to account for most of the spatial extent of SM effects, and at the same time exhibit the orientation bias required to explain orientation-specific surround modulation. On the other hand, several experimental studies provided evidence showing that long-range lateral connection in V1 cannot be the sole source of surround modulation. For example, several studies have shown contextual effects from beyond the reach of V1 lateral connections, and others suggest that these connections might be too slow to account for the fast onset of sur-

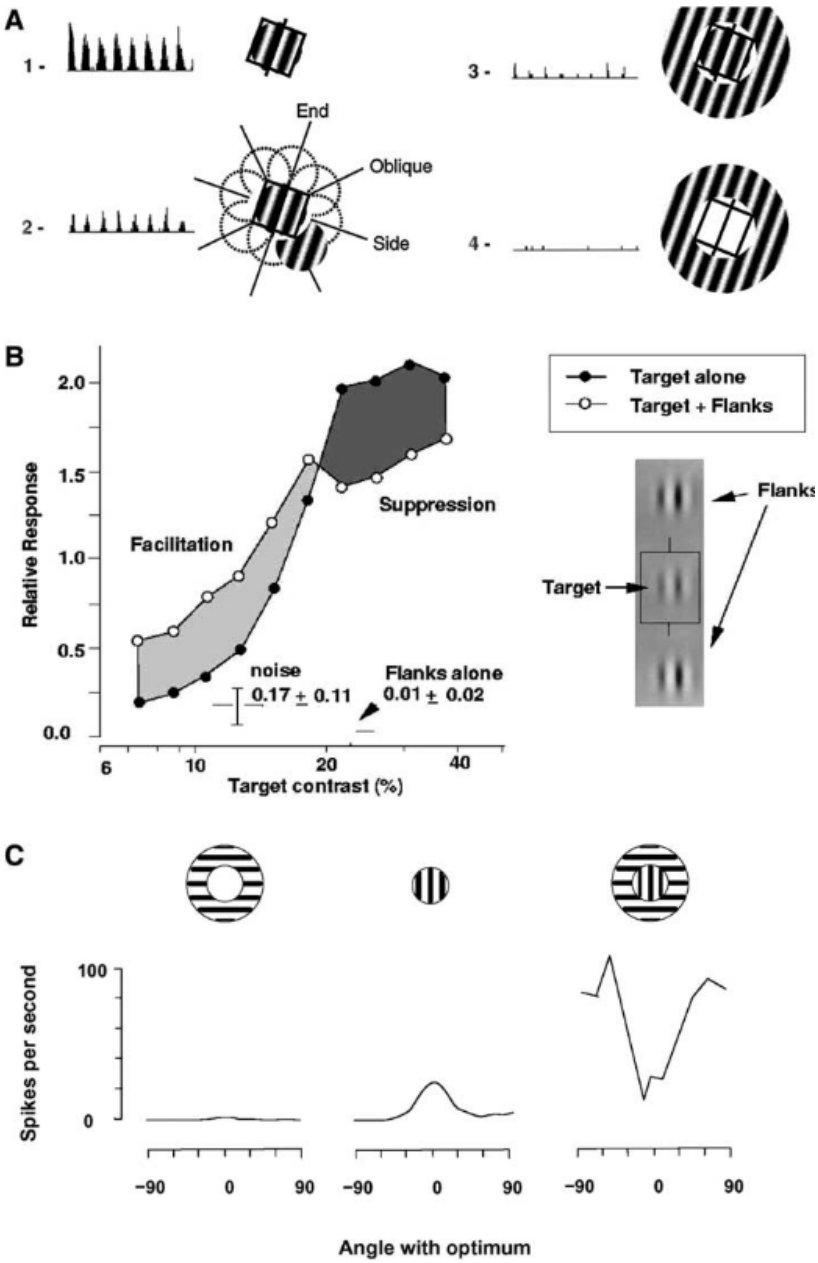

Figure 2.11: (A) Example of surround suppression in a single neuron in cat V1. 1. Response to an optimal drifting grating placed in CRF. 2. Placing second stimulus outside of the neuron's CRF suppresses the response of the cell. 3. Influence of an annular surround. 4. Response to the surround stimulus alone does not evoke response. Reproduced from Walker et al. [195]. (B) Contrast-response functions of a single cell in cat area 17 when only a target is shown (filled circle) and when it is flanked by two other collinear Gabor elements (open circles). The cell response is facilitated at low contrast and suppressed at high contrasts. Reproduced from Polat et al. [160]. (C) Facilitation for cross-oriented configurations (orientation contrast selectivity). Orientation tuning of one simple cell in macaque V1 in response to a central drifting grating alone and surround grating alone, and influence of the surround orientation when the central grating is is shown at the cell's preferred orientation. Reproduced from Jones and Sillito [107].

round modulation [14]. These findings lead to hypothesis that the fast conducting, and spatially extended feedback connections from higher-level visual areas play some role in surround modulation.

The most commonly studied contextual effect in V1 is called "size tuning" (see figure 2.11A). When one presents a V1 neuron with a sinusoidal patch of optimal parameters (orientation,phase and spatial frequency) centred in the neuron's RF, the response of the neuron will increase as the size of the sinusoidal patch increases. However, at some point, as the grating reaches beyond the CRF and starts to activate the neuron's RF surround, the activity of the neuron starts to decrease. These findings have led to the general belief that the surround effects are largely suppressive. However, more recently it has been shown that if a neuron is stimulated with low-contrast stimuli, surround stimuli can also be facilitatory [100]. Another example of contrast-dependence of size tuning is the shift of the summation peak towards larger diameters at low contrasts (see figure 2.11B).

Another property of surround modulation that is receiving increasing attention is its dependence on orientation. A number of studies have shown that if one varies the orientation of the flanking grating with respect to a centre grating of optimal parameters, one observes the strongest suppression when the centre and surround are colinear, and less suppression or even facilitation in the orthogonal configuration (see figure 2.11C).

Furthermore a study by Bardy et al. [19] have shown the interdependence between surround modulation and expression of simple/complex cell types. Authors have shown that complex cells increase their F1/F0 ratios when also the area outside of their CRF is stimulated compared to stimulation of the center only. In this way the stimulation of the surround converted 50% of complex cells in their sample to simple cells. This mechanism supports the idea that the expression of simple and complex subtypes is not hard-wired but is rather dependent on the interactions of the inhibition and excitation impinging on the cells and can be dynamically changed. This idea is further supported by recent experiments by Crowder et al. [59] who have shown that many cells that have been identified to be complex when measured at 100% contrast become simple if measured at low contrast, which presumably reduces the amount of excitation arriving to the cells.

Surround modulation has been implicated in a number of important perceptual phenomena, such as contour integration [71, 89, 7], figure-ground segregation [117, 213], and attention [156]. For example, in psychophysical experiments where subjects judge the contrast of a central grating, they perceive the contrast of the central grating to be

higher if it is presented alone, than if it is surrounded by another iso-oriented grating [46]. This is in line with the response magnitude of neurons in V1 when presented with analogous stimuli as can be judged from their size tuning properties discussed above. Similarly, by performing contour integration experiments in humans, Field et al. [71] identified set of rules, consistent with an idea of "association field" that integrates information across neighboring filters tuned to similar orientions. These findings are in agreement with the orientation specific contextual interactions found in V1 neurons [107]. This evidence suggests that surround modulation might, therefore, represent an important link between early- and high-level vision, which highlights the importance of a detailed understanding of its function and the neural substrate and mechanisms underlying it.

2.2 Map development models

Computational models of map development offer a mechanistic explanation for how the functional structures reviewed in section 2.1 arise. The most convenient way to categories existing models of orientation map development in V1 is based on the substrate they assume as the source of initial orientation maps. Ringach [154] suggests that the initial orientation maps in cortex are induced by *retinal mosaics*. Retinal ganglion cells (RGCs) are arranged on a nearly hexagonal grid or mosaic and the ON and OFF RGCs are offset from each other. Sampling from such systematically arranged cells can convey some initial orientation selectivity to V1. Although this model produces smooth orientation maps with some of the features found in animal maps, the model orientation maps do not, for example, exhibit the regular periodicity characterized by the ring-like 2D Fourier transform — i.e. the power is not evenly distributed across all orientations in a narrow band of frequencies.

Because the final maps exhibit this property [69] and because the map shape does not appear to change significantly over development, it seems unlikely that the final map structure is significantly affected by this bias. The most serious criticism of this model is that it is not clear how maps of orientation preference that are similar regardless of the eye to which the stimuli are presented (as found by Godecke and Bonhoeffer [77]) could be formed using this model, given that the retinal mosaic will differ in the two eyes.

Unlike the Ringach model, most models of V1 orientation map development assume some form of self-organization, induced by synaptic remodeling at the cortical

level, as the process responsible for the map development (reviewed in [183]). Generally these models are based on the principle of competition and cooperation. Typically, models assume that neurons 'cooperate' over short distances and 'compete' over longer distances, using a Mexican-hat profile of lateral interactions. Based on unsupervised learning rules, nearby neurons develop selectivity for similar patterns, whereas the competitive component ensures that a wide range of patterns is represented across the whole network. Overall, such processes will lead to some form of smooth topographical mapping, similar to those measured in adult cortex. Models typically cite the long-range lateral connections in V1 as a candidate substrate for the lateral interactions driving the development. Some models assume the self-organization process is driven by spontaneous activity patterns in V1 changing the strength of these lateral connections, while others consider changes in the afferent connections from the LGN, driven either by spontaneous retinal or LGN activity, or by visual stimulation.

The most recent model based on spontaneous cortical activity from Barwinska and von der Malsburg [79], shows that ring-shaped cortical waves along with synaptic adaptability of long-range lateral connections can induce patchy lateral connectivity elongated in one direction. Furthermore, this pattern of connectivity will change smoothly along the cortical surface, such that long-range lateral connections of nearby neurons innervate similar cortical patches and are elongated in similar direction. As previous models have shown, such a systematic pattern of lateral connectivity can then induce initial orientation maps [168, 68]. Although it is known that the above connectivity pattern of lateral connections is present in adult animals [36] (figure 2.8), the afferent connections from LGN arrive to cortex already before the lateral connections start to form the patchy pattern [201]. Furthermore, when one takes into consideration the cortical magnification factor and the fact that the orientation preference bias stems from the elongated pattern of long-range lateral connections, it follows that the neurons should initially be selective to only very large elongated stimuli, a hypothesis for which there is as yet no support.

Most models instead focus on the thalamocortical connectivity, starting with the earliest model of V1 development by von der Malsburg [194] in 1973. This model assumed a small two-dimensional grid of V1 units, each representing a single cortical column. Each unit has fixed excitatory lateral connections to neighbouring units and fixed inhibitory lateral connections to units farther away, together implementing Mexican-hat lateral interactions. The afferent weights of each unit were modified according to a Hebbian learning rule with divisive normalization, while being trained

with oriented bars. This led to units developing orientation preference, forming a large-scale orientation maps before such a map has been experimentally measured. A large number of models based on similar principles followed the study by von der Marlsburg, explaining other aspects of orientation map development and other topologically organised cortical features [81, 25, 41, 69, 134, 182, 185]. Comprehensive reviews of the numerous models can be found in [69, 132, 183].

Nearly all models including plastic afferent connections assume fixed and isotropic lateral interactions. However it is known that lateral connections in V1 undergo development, and become progressively highly structured. Furthermore, these specific patterns of lateral connectivity are implicated in a number of phenomena in adult cortex. Therefore an important advancement was the introduction of models that explicitly model lateral connections and their adaptation during development [131, 4, 20, 38, 108, 198]. The most fully developed of these is the LISSOM (Laterally Interconnected Synergetically Self-Organizing Map) model [132], which reproduces many previous experimental findings, including feature maps for orientation, spatial frequency, disparity, ocular dominance, color, and motion direction, known visual after-effects, and both pre- and post-natal development.

In this thesis we will extend the LISSOM model to account for three important phenomena that have not yet had a satisfying computational explanation. First, current variants of LISSOM and other developmental models do not exhibit realistic properties with respect to contrast of the visual stimulus, which limits the range of phenomena that can be investigated. Therefore in chapter 4, we extend the LISSOM with a gain control mechanism that addresses some of these issues. LISSOM and most other models so far account for only one of the two main functional types of V1 neurons — simple cells — whereas the complex cells are missing. In chapter 4 we introduce a model based on LISSOM that shows how orientation maps of both simple and complex cells can develop, driven by pre-natal intrinsically generated inputs and subsequent normal visual inputs. Finally, in the last result chapter we conclude our work by introducing more realistic lateral connectivity into this model, and subsequently show that the resulting model, whilst preserving all the desired properties of the above models, exhibits realistic surround modulation properties present in adult V1 cortex, providing a comprehensive explanation of how specific structures arising during development lead to the complex variety of phenomena observed in adult V1. In the following two section we will discuss previous models related to complex-cell map development and surround modulation.

2.2.1 Complex cell development models

One of the first studies to demonstrate how complex-cell–like properties can emerge by stimulus-driven self-organization was the work of Földiák [73], which introduced a local learning rule (trace rule) that was able to develop complex cell RFs when trained with a temporal sequence of smoothly translating bars. Another study, by Einhäuser et al. [67], has recently shown that a two-layer network using a competitive Hebbian learning rule can develop the properties of complex cells when fed with natural images. One of the most recent models of complex cell development is by Karklin et. al. [109], who have shown that a model that learns the statistical distributions that characterize local image regions, when trained on natural images, will also develop units with complex cell like characteristics.

The above studies explain the development of RFs of individual complex cells in isolation. Therefore they cannot explain an important aspect of V1 development — the development of the functional topographic maps in V1. Sullivan et al. [181] addressed this problem, by combining Földiák's trace rule with a self-organising map algorithm. This model assumes orientation preference in simple cells to be fixed prior to development, and thus explains only how maps can develop in complex cells, but not in simple cells, and does not show how neurons can become selective for orientation in the first place.

The two studies that came closest to explaining how maps of complex cells develop are the models by Hyvärinen et al.[99] and by Olson et al. [149]. The first study is an example of a normative model formulated at the level of Bayesian probabilistic theory. The main limitation of this model is that it thus cannot explain how the process it describes is implemented in the neural substrate and indeed it relies on biologically implausible mechanisms (as detailed in chapter 4). It also does not separate evolutionary and developmental processes. The Olson et al. model consists of two layers, the first containing ensembles of simple cells organised in a two dimensional lattice. Within these ensembles, the authors assume that at the beginning of development there exists very specific connectivity. This assumption, however, is not currently supported by experimental evidence. In this work we will present a new model of V1 developmental which will rectify all these problems and limitations and thus provide the most consistent biologically plausible explanation of complex cell map development so far.

2.2.2 Surround modulation models

Numerous computational models explaining various aspects of surround modulation at various levels of detail have been proposed in the past. One convenient way to broadly catogorize them is by their scope into those that approach the problem from single neuron perspective, and those that focus on explanations involving populations of neurons.

An example of first category are models by Sceniak et al. [160, 159] that model the interactions between the CRF and surround as difference-of-Gaussians where the first gaussian corresponds to the excitatory drive from the CRF and the second Gaussian corresponds to the suppressive surround. Sceniak et al. showed that this type of model provides good fits to the size tuning curves in both LGN [160] and V1 [159]. Furthermore, Bonin et al. [35] have later showed that a similar model, where the surround acts divisively, can explain both gain control and size tuning in LGN neurons.

This phenomenological approach has been taken one step further in models that explicitly model V1 connectivity [121, 177, 192] and thus improve the grounding of the surround modulation models with respect to V1 anatomy. For example Li have proposed a computational model relying on local lateral connections in V1, which explains the perceptual pop-out of boundries in visual stimuli. This due to the difference in contextual influences near and far away from boundries which make neurons near boundries more activated. In this way the model explains how texture or region segmentation can be implemented within V1 circuitry without the need of higher-level visual ares.

The first large scale model showing how surround modulation can arise from the lateral connectivity in V1 was by Somers et al. [177]. This model works with a two dimensional grids of excitatory and inhibitory neurons, interconnected via short-range and long-range lateral connectivity. The afferent receptive fields of individual neurons, and the strength of the long-range lateral connections are determined by their position in an overlaid experimentally measured orientation map. The main contribution of this study is that it shows how the lateral connectivity in V1 can lead to size tuning, i.e. a maximum response to one specific pattern size. It correctly predicts the expansion of the summation at low contrast, and it also replicates the dependence of the magnitude of the surround suppression on the orientation of the surround.

A similar study by Wielaard et al. [204] shows a model of similar architecture — a two dimensional grid of neurons initialised with an orientation map. The most

important architectural difference of this model from the Somers et al. study is that it explicitly assumes only local lateral connectivity. The advantage of this study is that the individual neurons in the model exhibit a number of basic functional properties such as orientation preference and a realistic distribution of modulation ratios, thus embedding the surround modulation into more realistic context. With this architecture, Wielaard et al. were able to show basic size tuning properties including the expansion of summation at low contrast. However, due to a lack of orientation-specific long-range lateral connectivity, this study lacks explanation for the orientation-specific surround modulation properties of V1 neurons.

The most recent theoretical advancement of our understanding of surround modulation comes from the study by Schwabe et al. [161]. Unlike the previous two studies, their model is only one-dimensional, representing orientation columns along a hypothetical line laid along the V1 surface. It simulates a single sheet of excitatory and single sheet of inhibitory neurons, laterally interconnected via both short and long range lateral connectivity. As for the Somers et al. model, their model neurons lack realistic functional properties such as orientation tuning or phase invariance. The main novel feature of this study is the addition of extra-striate feedback connections to the model. This study demonstrate the basic size tuning properties of V1 neurons, but again due to the lack of orientation specificity in the model, orientation contrast is not replicated. Unlike both previous studies, this model predicts the counter suppression phenomenon [100]. The main contribution of this study is the demonstration of how surround modulation effects that are known to be still present at very large distances, beyond the monosynaptic reach of long range lateral connections, can be explained by inclusion of the extra-striate feedback into the model.

The main substrate responsible for the surround modulation in all these models (together with feedback from higher level areas in case of the model by Schwabe et al.) are the lateral connections. As has been discuss in detail in this chapter, these have been also linked to the development of orientation maps, a cortical feature already assumed in two of the above models. In this work we will present a developmental model of V1, that can explain how orientation maps develop, while individual model neurons after development express realistic surround modulation properties. This way we provide a consistent explanation of all these phenomena in a single model.

Chapter 3

A simpler, more robust, and more realistic model of visual development

The starting point for this thesis is the Adaptive LISSOM (ALISSOM) model presented in the 2009 PhD thesis by Judith Law [119]. The main improvement of the ALISSOM model over the basic LISSOM model [132] are the static extents of the long-range lateral connections, as opposed to the more complicated and less plausible shrinking configuration used in LISSOM, and the homeostatic regulation of excitability governed by the Triesch rule [188]. These changes mean that ALISSOM has many fewer free parameters compared to LISSOM, and as shown in [119], unlike LISSOM, it can show how stable maps can develop in V1. Overall this makes ALISSOM the most advanced variation of the LISSOM architecture, and therefore we will consider this model as the starting point for our model development.

Despite all the above features, ALISSOM still lacks several V1 properties that are necessary for achieving the goals that we have outlined in chapter 1:

1. **Gain control** - as shown in number of studies, surround modulation effects are highly dependent on contrast of the stimulus [160, 100, 196]. It is also known that the response to different contrasts of visual stimuli of neurons in RGC, LGN and V1 are not linear [174, 35, 152], unlike in ALISSOM model. Therefore we extend the ALISSOM model with a simple gain-control mechanism that ensures these experimental constraints are met.

2. **Contrast invariant orientation tuning width** - one well established functional characteristic of most V1 neurons is the fact that if one measures the orientation tuning curve of a given V1 neuron, and the width of the tuning curve at half

of the maximum peak, this width will be identical regardless of the contrast at which the orientation tuning curve was measured. This is an important property, because it ensures that the selectivity of a neuron for orientation is independent of contrast. Consequently if any property of V1 depends on the contrast (such as surround modulation) it is likely to be affected by the contrast invariance of orientation tuning width. Because ALISSOM does not exhibit this property, we will modify the model to account for it.

3. **Robustness of self-organization** - orientation preference maps develop in V1 of animals under a wide range of different conditions of visual stimulation during development. This indicates that the self-organizing process of map development is very robust to differences in the statistical properties of visual stimulation. Despite the progress ALISSOM model has shown in achieving such robustness of development, it still had one free parameter that had to be tuned to ensure stable self-organization for a given training input set. Beside the existence of such a free parameter being biologically unrealistic, achieving self-organization properties robust to the statistical properties of training stimuli in a model has practical benefits. It turns out that by addition of the above two properties into the ALISSOM model, we can achieve robust self-organization even with a much simpler homeostatic rule than the one used in the ALISSOM model and eliminate the last parameter that had to be adjusted depending on the input set to achieve stable development of maps.

In this chapter we introduce a new model referred to as GCA-LISSOM, which is derived from the ALISSOM model by implementing the above modifications. The GCA-LISSOM model maintains all main novel properties of ALISSOM, including non-shrinking extents of lateral connectivity and stable map development. At the same time, we add new properties: realistic contrast response and orientation tuning properties of neurons after development, and enhanced robustness to statistics of visual stimuli during development. In this way we achieve a model with all properties required for the next step towards the goals outlined in chapter 1.

In order to demonstrate the individual contributions of the discussed modifications to the ALISSOM model, we will proceed to present 4 intermediate models in this chapter, gradually incorporating the new elements. First in section 3.2 we will present a new model of LGN/RGC expressing realistic gain control. Next, in section 3.3, we will first show that exchanging the sigmoid transfer function for a linear threshold and

adding the new model of the LGN into a instance of fully developed ALISSOM improves the orientation tuning properties of model neurons. We will then proceed to show that these modifications are compatible with development by running simulations in which the two modifications are present from the start of development, but the homeostatic mechanisms present in ALISSOM, which are incompatible with the new linear threshold function, are switched off. Finally, in section 3.4 we will introduce a new homeostatic mechanism into the modified ALISSOM model, thus completing the new GCA-ALISSOM model, and show that this model maintains all the main novel properties of the original ALISSOM model, while improving its gain control and orientation tuning properties, yet reducing the number of free parameters.

3.1 ALISSOM

Before we proceed to introduce our modifications let us describe the model we have chosen as the starting point of our study. The ALISSOM model introduced in the 2009 PhD thesis by Judith Law [119], is based on the LISSOM model architecture, described in detail in [132]. Following the LISSOM architecture, the ALISSOM model consists of four 2D sheets of firing-rate single-compartment neural units, representing retina, LGN (On and Off) and V1 (see figure 3.1). A sheet corresponds to a rectangular portion of a continuous two-dimensional plane and contains a two-dimensional array of firing-rate single-compartment neural units. Dimensions are therefore defined in sheet coordinates rather than numbers of units so that parameter values are independent of the number of units [23].

The number of units simulated in each sheet is determined by setting the density of units per unit length in both sheet dimensions. The size of V1 (1.0×1.0) the RGC/LGN (2.6×2.6) and retina (3.2×3.2) sheets are chosen to ensure that each unit in the receiving sheet has a complete set of connections, thus minimizing edge effects. The density of units per 1.0×1.0 area is 48×48 for the Retina (photoreceptors) and RGC/LGN sheets, and 96×96 for the V1 sheet.

The activation level for a unit at position j in an RGC/LGN sheet at time t is defined as:

$$\eta_j(t) = f(\sum_{i\in F_j} \Psi_i(t)\omega_{ij}) \tag{3.1}$$

The activation function f is a half-wave rectifying function that ensures positive activation values, Ψ_i is the activation of unit i taken from the set of photoreceptors from

which RGC/LGN unit j receives input (its connection field F_j), ω_{ij} is the connection weight from unit i in the retina to unit j in the RGC/LGN. Photoreceptors to RGC/LGN weights in the ON and OFF channels are set to fixed strengths with a difference-of-Gaussians kernel ($\sigma_{center} = 0.073$, $\sigma_{surround} = 0.29$, in sheet dimensions), with ON connection fields having a positive center and a negative surround and vice versa for OFF.

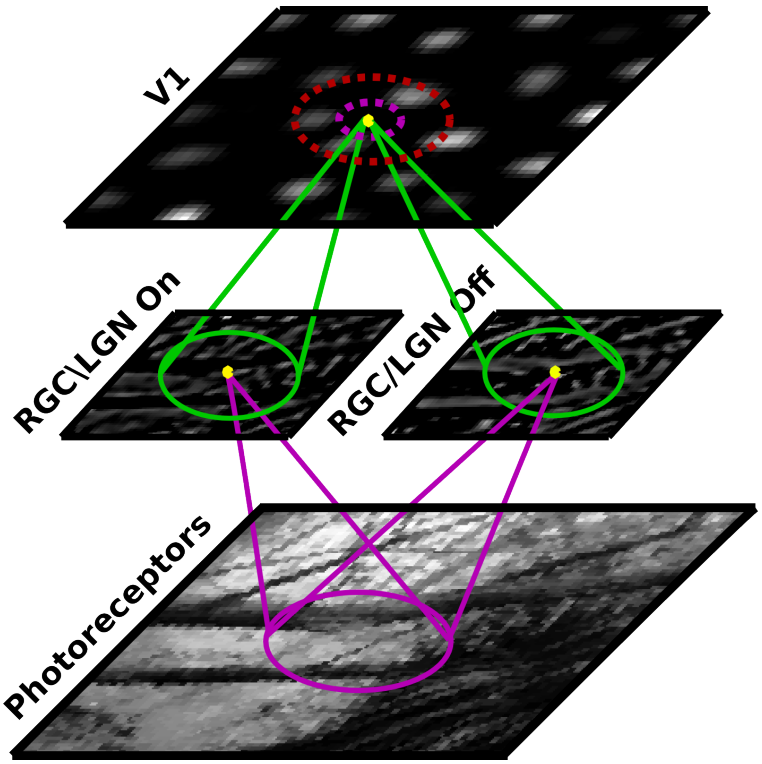

Figure 3.1: Architecture of the ALISSOM model. The model consists of four 2D sheets of firing-rate single-compartment neural units, representing retina, LGN and V1. The projections from Retina to LGN have difference-of-Gaussian shaped connection fields. The output of the LGN units is the dot product of the retinal input with their projections that is passed via a piece-wise linear transfer function. The information from LGN to V1 is passed via excitatory connection fields which are adapted during the development by Hebbian learning. The V1 units use a sigmoid transfer function. The information within V1 travels laterally via short range excitatory and longer range inhibitory connections. During development the excitatory lateral connections are fixed while the inhibitory are adapted via Hebbian learning. A typical profile of activity to a natural image in an early stage of development is also depicted. One can see the typical 'blobby' profile of activity in V1, that reflects the tendency of the lateral connections to force locally correlated activity upon the V1 neurons.

Units in the cortical sheets each receive two types of projections represented as matrices of weights: afferent (one from LGN ON and on from LGN OFF sheet) and lateral (one corresponding to short-range excitatory and one to long-range inhibitory lateral connections) (figure 3.1). Similarly to previous LISSOM models, the ALISSOM model operates in settling phases—for each input, the network runs for 10 update steps, during which the activity in the cortical sheets settles. At the beginning of each settling phase the activity in the cortical sheet is reset to 0. Formally, the contribution X_{jp} to the activation of unit j in the V1 sheet from each projection p at settling step t is given by:

$$X_{jp}(t) = \sum_{i \in F_{jp}} \Psi_i(t-1)\omega_{ij} \tag{3.2}$$

where $\Psi_i(t)$ is the activation of unit i taken from the set of neurons in the input sheet of projection p from which unit j receives input (its connection field F_{jp}), and ω_{ij} is the connection weight from unit i in the input sheet of projection p to unit j. All connection field weights are initialized with 2D Gaussian profiles multiplied with uniform random noise, and cut off at specified distance (0.271 for the two afferent projections, 0.02 for the short range excitatory and 0.229 for the lateral inhibitory projection). Contributions from each projection are weighted and summed to form the overall input of unit i:

$$Y_i(t) = \sum_p \gamma_p X_{ip}(t) \tag{3.3}$$

where γ_p is a constant determining the sign and strength of projection p. Finally, the output of unit i is computed by passing this quantity via a sigmoid transfer function f:

$$\Psi_i(t) = f(Y_i(t)) \tag{3.4}$$

where

$$f(x) = \frac{1}{1+e^{\alpha x - \beta}} \tag{3.5}$$

Crucially, the ALISSOM model uses a homeostatic rule introduced by Triesch [188] to govern the slope and threshold of the transfer function (parameters α and β), independently for each neuron. Such changes in intrinsic excitability has been demonstrated in neurons by several studies [62, 211], indicating that changes in threshold and slope of transfer function are plausible way to model this type of homeostasis. Specifically, the Triesch rule was derived such that it drives the neuron to have an exponential distribution of firing rates with a fixed pre-specified mean, and the resulting update rules are dependent only on the overall input and output of the cell. however

the specific biophysical mechanisms that could potentially underly it are currently now known.

At the end of each settling phase, the weights in the afferent projections from LGN ON and LGN OFF sheets to the V1 sheet, and weights in the long-range inhibitory projection are adjusted with a unsupervised Hebbian learning with divisive normalization based on the activations of the units at the end of the settling phase. A more detailed description of the learning mechanism and of the input patterns is given in section 4.2.

3.1.1 Network dynamics

The defining feature of the LISSOM architecture, present also in ALISSOM, is the pattern of short range excitatory and long-range inhibitory connections surrounding each neuron in the cortical sheet. A sigmoid non-linearity is used as the transfer function for the cortical units. Due to the recurrent nature of the ALISSOM model, for each input presentation, the activity is transmitted between and within the model sheets via the described projections for several steps. Because the lateral excitatory and inhibitory connections are balanced, for each input presentation, the cortical activity gradually settles. In general, the areas which are more activated relatively to their surrounding area via the feed-forward connections will gradually become more active, while the surrounding areas of neurons will become more and more inhibited, resulting in the typical 'blobby' activity pattern (see figure 3.1). At the end of each settling phase the weights of the plastic projections are updated according to a Hebbian learning rule (based on the activity at the end of settling). To prevent runaway increase of weights, the connection field of each neuron is normalized after each Hebbian update.

The main role of the lateral connections in the LISSOM architecture is the facilitation of development of smooth topographic functional maps. The Mexican-hat-like profile of the lateral connections ensures that regardless of the input stimuli, the activity in the V1 model sheet settles into a pattern where nearby neurons will have highly correlated activity—i.e., the characteristic pattern of 'blobby' activity evolves as shown in figure 3.1. Such locally correlated pattern of activity combined with the Hebbian adaptation of the afferent weights in turn ensures that nearby neurons will tend to develop similar receptive fields. This property of the developed model then gives rise to the various functional maps that have been demonstrated in the LISSOM model. Similar principles of functional map development based on Mexican-hat–like lateral interactions have been demonstrated in numerous other models, though typically without the

modifiable lateral connections crucial for this thesis.

The size and shape of the individual activity blobs evolving in the model in response to the retinal input will be related both to the shape of the Mexican-hat like lateral connections (for example broader local excitatory connections will tend to produce broader blobs of activity) and to the shape of the transfer function of individual neurons (for example more rapidly rising transfer functions will tend to produce 'sharper' blobs). In general, various structural parameters of the model inevitably influence the patterns of activity that evolve in the model in response to retinal input. Importantly, stereotypical patterns of activity in the model during development will in turn influence the final patterns of functional maps in the developed model. Therefore analyzing the stereotypical patterns of activity (e.g. blobs) evolving in the model can help us to not only understand the immediate response properties of neurons in the model, but also the nature of the functional maps that eventually develop. We will use this reasoning in section 3.3 to understand some of the limitations of the ALISSOM model.

3.2 Gain control

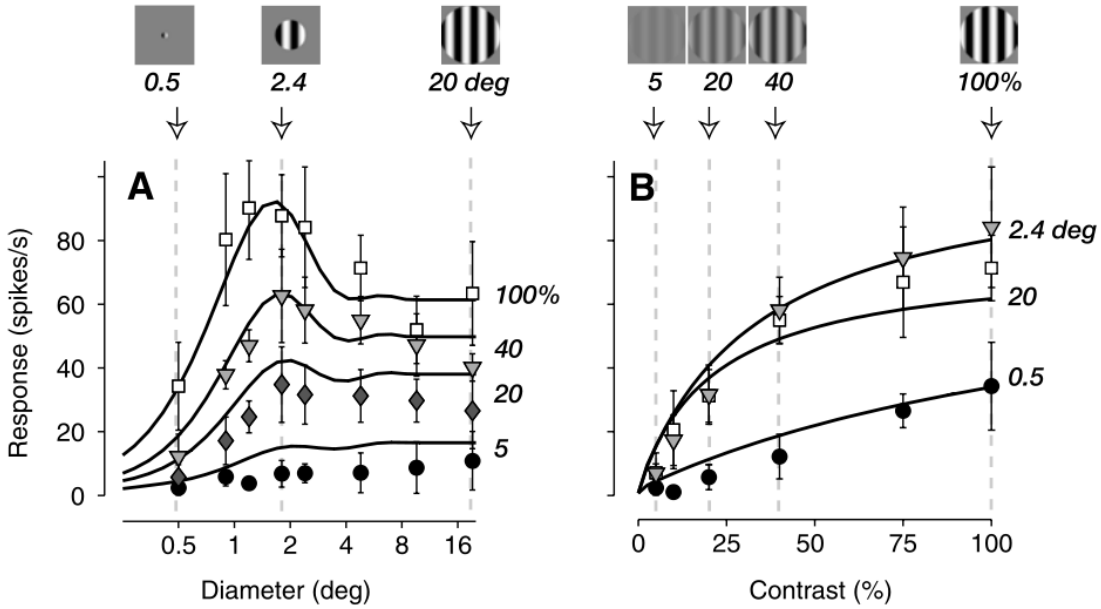

Figure 3.2: Size tuning and contrast saturation in cat LGN. Stimuli are gratings varying in diameter and contrast. A, Responses as a function of diameter, for selected contrasts. B, Same data, plotted as a function of contrast, for selected diameters. Reprinted from [35].

The response of neurons in the visual system does not increase linearly with increasing contrast, but instead gradually saturates (see figure 3.2B). Such non-linearity is observed already in retinal ganglion cells [174] and can be measured in the subsequent stages of visual processing in LGN [35], V1 [152] and other higher visual areas (figure 3.2B). The benefit of such gradual saturation of neural response to increasing contrast is usually explained as improvement of the dynamic range of neuron. This is because neurons have limited maximal firing rate and can thus represent only a limited range of inputs within their dynamic range. The gain control thus increases the range of inputs that are mapped onto output firing rates that are not saturated. Another phenomenon that cannot be explained solely by the classical center-surround receptive field is that responses of neurons are suppressed if a second stimulus is presented outside of the CRF (see figure 3.2A).

In V1 and higher level visual areas, besides the above instantaneous adaption to contrast, one can also observe another much slower type of adaptation: the contrast response functions shift primarily to the right with increasing mean contrast at 40s timescales [146]. This shift of contrast response functions is accompanied by the change of their slope, indicating a divisive effect [74]. Furthermore the changes in gain are not necessarily externally driven, as it has been shown that attention seems to act through a gain control mechanism as well in areas V4 and MT [129, 187]. This diverse set of gain control phenomena has been accompanied by a numerous hypothesis as to what are the underlying mechanisms responsible for them. For example rectifying mechanism [84], network interactions [193], shunting inhibition [47], synaptic depression [1] and shunting inhibition combined with synaptic noise [50] have been proposed as the possible candidates. However, the true biological substrate of gain control is still unknown.

In this thesis we are not interested in advancing our knowledge of gain control mechanisms in visual cortex. Rather we recognize the important role of contrast in surround modulation and for this reason we want to ensure that our model V1 neurons have realistic contrast response. An elegant solution explaining both contrast gain control and size tuning in LGN (that is thus passed to V1 neurons) with a single mechanism, that we will adopt here, has been proposed recently by Bonin et al. [35]. Their model involves a linear and a nonlinear pathway (see figure 3.3). The linear pathway consists of the standard difference-of-Gaussians RGC/LGN receptive field L, whereas the non-linear pathway computes a measure of local contrast c_{local} and acts as a suppressive field. The measure of local contrast then acts divisively on the CRF, thus

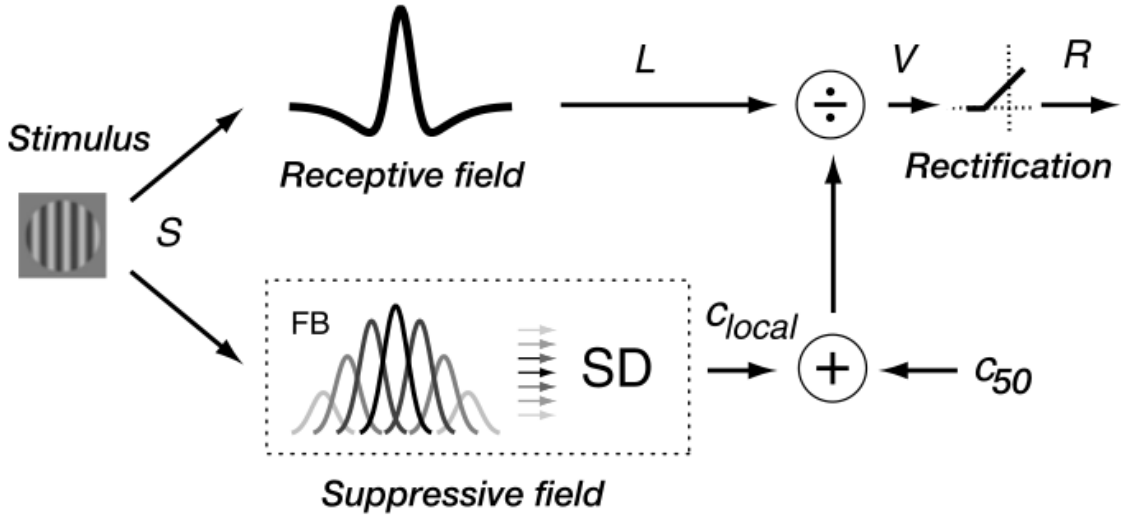

Figure 3.3: Bonin et al. model of LGN responses. The model includes a receptive field and a suppressive field. The receptive field has the classical centersurround organization (difference of Gaussians). The suppressive field computes the SD of the outputs of a Gaussian-weighted bank of difference of Gaussians filters (FB) and sums the result to a constant, c50. The difference of Gaussians filters are depicted as Gaussians in the figure. The signals from receptive field and suppressive field meet at a divisive stage. The output of the division is then rectified to yield positive firing rates. Reprinted from [35].

achieving the contrast response saturation:

$$V = V_{max} \frac{L}{c_{50} + c_{local}}$$

where V is the response of the neuron, V_{max} captures the overall responsiveness of the neuron and c_{50} determines the strength of the suppressive fields. The local contrast is computed by first passing the stimulus through a bank of difference-of-Gaussian filters. The response of the filters is then squared and weighted by a Gaussian envelope, thus achieving the locality property. The authors fitted the free parameters of this model to data from cat LGN, and showed that the model provides good fits to LGN responses for a variety of stimuli.

The suppressive field in the Bonin et al. model estimates the local contrast by calculating the standard deviation of a bank of difference-of-Gaussian contrast detectors weighted by a Gaussian envelope. Note that RGC (or LGN neurons) are themselves contrast detectors, with a difference-of-Gaussian kernel. Therefore, a natural way to simplify this model and implement it within our modeling paradigm based on two-

dimensional lattices of neurons, is to introduce lateral connections with Gaussian profile into our model of RGC/LGN neurons, acting divisively on the target neuron (see figure 3.4). Such mechanism is further supported by existence of such lateral connections both in retina [128] and LGN [34].

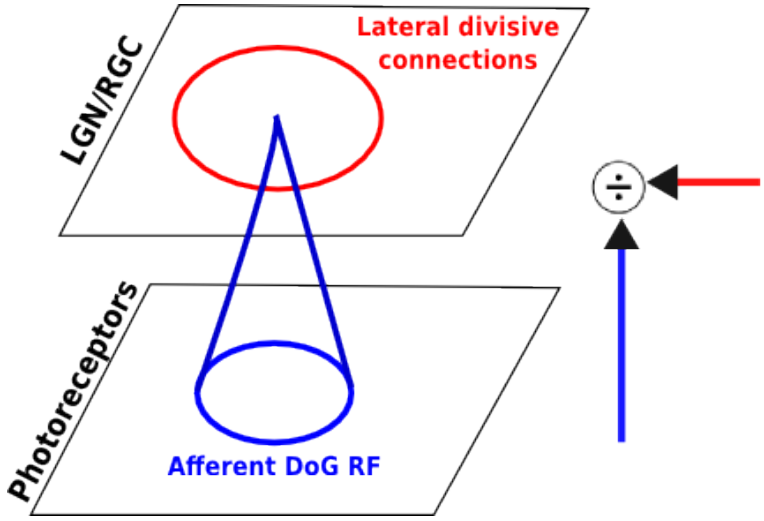

Figure 3.4: Architecture of the new LGN model. Each LGN neuron has the standard feed-forward difference-of-Gaussians RF. Each neuron also receives lateral connections with a Gaussian profile. The activation from the afferent connections is combined divisively with the lateral contributions to achieve contrast response saturation.

Let us now formalize the newly proposed LGN model. The model corresponds to the ALISSOM LGN model described in section 3.1, with added divisive lateral connectivity. The activation level for a unit at position j in an RGC/LGN sheet at time t is defined as:

$$\eta_j(t) = f\left(\frac{A_j(t)}{c+\gamma_L \sum_{k\in\Phi} A_k(t) l_{kj}}\right) \tag{3.6}$$

where

$$A_j(t) = \gamma_F \sum_{i\in F_j} \Psi_i(t)\omega_{ij} \tag{3.7}$$

The activation function f is a half-wave rectifying function that ensures positive activation values, constant γ_F defines the overall strength of the afferent connections from retina, constant γ_L defines the strength of the lateral connections in RGC/LGN, c is a constant that defines the slope of the gain, Ψ_i is the activation of unit i taken from the set of photoreceptors from which RGC/LGN unit j receives input (its connection field F_j), ω_{ij} is the connection weight from unit i in the retina to unit j in the RGC/LGN, l_{kj}

is the lateral connection weight between RGC/LGN neuron k and j and Φ is the set of neurons in RGC/LGN. Photoreceptors to RGC/LGN weights in the ON and OFF channels are set to fixed strengths with a difference-of-Gaussians kernel ($\sigma_{center} = 0.07$, $\sigma_{surround} = 0.2$, in sheet dimensions), with ON connection fields having a positive center and a negative surround and vice versa for OFF. The lateral RGC/LGN weights are Gaussian with kernel size $\sigma_{center} = 0.5$.

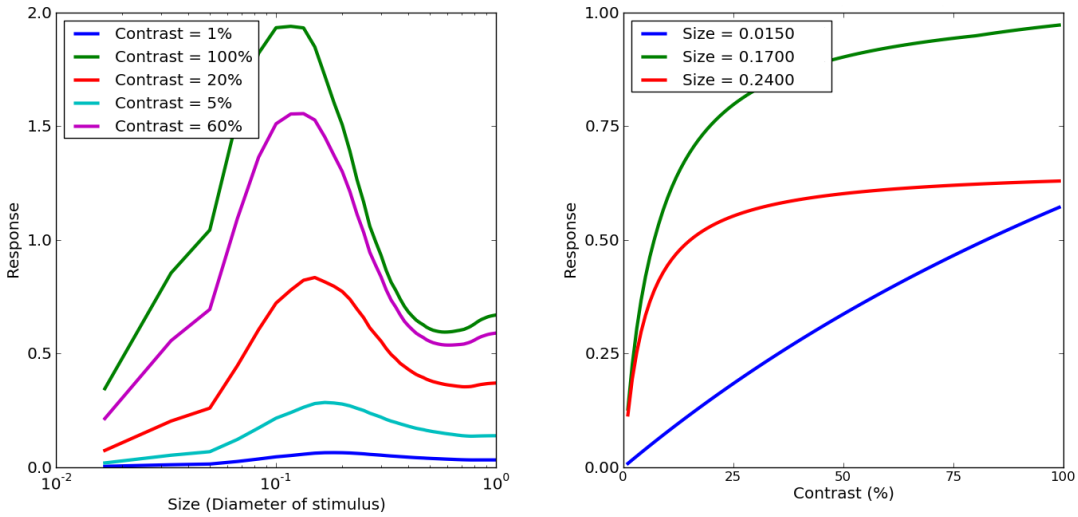

Figure 3.5: Contrast and size tuning curve of the LGN model. A, The response of model LGN neurons to increasing size (in retinotopic coordinates) of sinusoidal grating patch at different contrasts. B, The contrast response of model LGN neurons. These figures show the qualitative match of our model with the Bonin et al. data (see figure 3.2).

Figure 3.5 shows the response for different contrasts and sizes of a sine-grating patch. When compared to the data from cat (figure 3.2), we can see a good qualitative match of our LGN model with the experimental results. Our model represents a concrete and simple 2D implementation of the Bonin et al. model, and links the abstract mechanism of local contrast measurement to a specific neuronal substrate—lateral connections—while showing a good qualitative match of the response with the experimental results.

3.3 Contrast invariant orientation tuning width

3.3.1 The effects of sigmoid non-linearity in ALISSOM model

As discussed in section 3.1, ALISSOM model uses a sigmoid function in place of the transfer function for cortical neurons. The saturation of the sigmoid function causes several undesired effects in the model. First, because sigmoid saturates at high contrast, the blobs of the activity formed due to the Mexican-hat like interactions in the cortical sheet will saturate in the center if the feed-forward input to the model is strong enough. Consequently, increasing the strength of the feed-forward inputs to the model even further, will lead to the increase of the size of saturated regions, instead of multiplicative scaling of the activity blobs that would ensure the same shape of the blobs apart from the scaling. This causes several undesired effects on the development of the model. Firstly, the size of the blobs is tightly related to the size of the orientation domains that develop in the model. This means that if, for example, the strength of the input significantly changes during the development (such as during the transition from the pre- to post-natal phase), the spatial frequency (in cortical space) of the map structure could change, which is in contradiction with the stable development of orientation maps shown experimentally [54].

Secondly, the sigmoid function has a detrimental effect on the shape of orientation tuning curves of individual neurons (see figure 3.6). This can again be linked to the saturation of the sigmoid function. Even at non-preferred orientations, the excitation due to the overlap of the input stimulus with the feed-forward connection field of a neuron will be non-zero, and will increase with contrast, such that with enough contrast any neuron will respond, regardless of preferred orientation. In models with lateral inhibitory connectivity such as ALISSOM, under the right conditions, lateral interactions can ensure that the response of neurons to non-preferred orientation is suppressed to zero. This is because while neurons not selective to the orientation presented in their RF will still receive some afferent excitation, they will be at the same time inhibited by neurons preferring the orientation of the presented stimulus. These neurons will, by definition, be relatively more excited by the afferent pathway at the onset of the stimulus, and the winner take all influence of Mexican-hat-like lateral connection will further increase the relative difference of activations between these two groups of neurons over the course of settling. Also note, that the existence of orientation maps guarantees that for each group of neurons preferring certain orientation, there exists a group of neurons preferring other orientations close by.

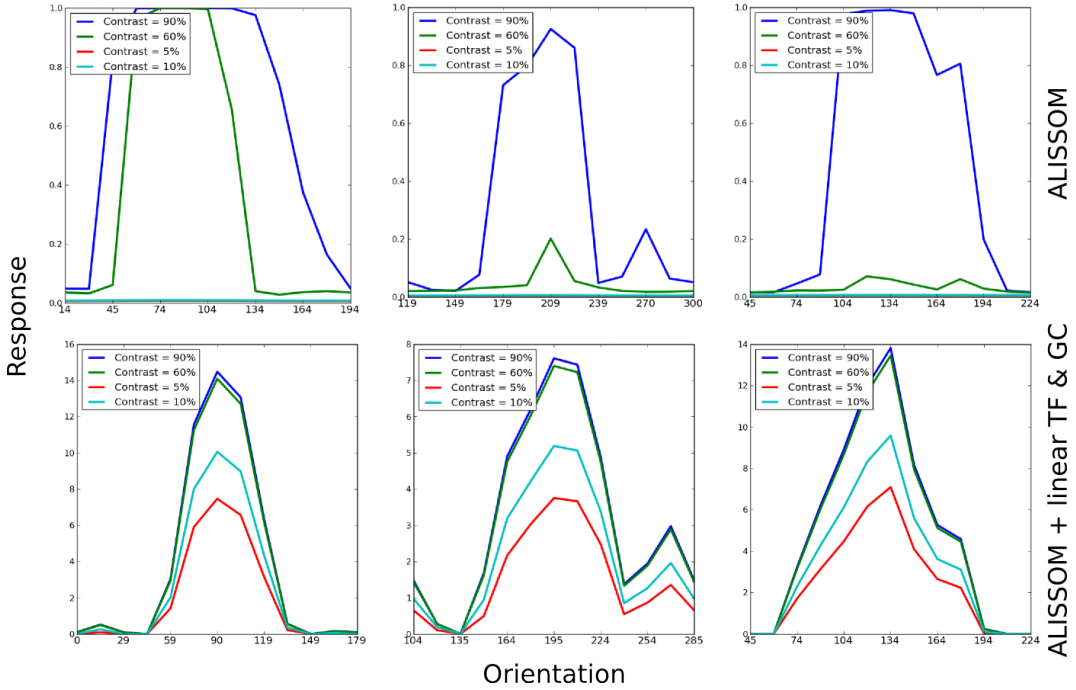

Figure 3.6: Ilustration of the beneficial effect of gain control mechanism and linear transfer function on the orientation tuning curves. Top row shows an example of orientation tuning curves of three ALISSOM neurons at positions (0.0,0.0), (0.0,0.1), (0.1,0.0) in the cortical sheet. The bottom row shows orientation tuning curves of the same neurons in the same instance of the ALISSOM model, but after the gain control mechanism in the LGN/RGC sheet and linear transfer function instead of sigmoid was added to the model instance. As illustrated in these 3 example neurons, many neurons in the ALISSOM model lose orientation selectivity with increasing contrast, and the majority of neurons do not have contrast invariant width of their tuning curve. After the modifying the ALISSOM model, neurons exhibit more realistic orientation tuning curves.

However, with a saturating transfer function, the relative difference between the response for preferred and non-preferred orientation decreases with increasing contrast. This effect can be so strong that the lateral connections are not capable of compensating for it, and thus the orientation tuning curves will broaden with increasing contrast, as happens in previous LISSOM models (see figure 3.6).

3.3.2 Sigmoid transfer function vs. linear transfer function

One possible solution to the above problems is to prevent the activities in the cortical sheet from reaching levels that will be in the saturating region of the f-I curve. Note that this would not mean that the activity of a neuron would never saturate under physiological conditions, only that this saturation would be due to the saturation of the input to the neuron rather than directly due to the saturation of its f-I curve. At the same time, if the mechanisms preventing the neuron reaching the saturating region of its f-I curve are bypassed, for example by directly injecting current into the neuron, saturation of the response due to its f-I curve can still be observed.

Preventing the activity of neurons to reach the saturating regions of the f-I curve in the ALISSOM model, however, turns out to be very difficult, especially due to the changes to lateral connectivity and strength of the visual input during development. For example the ALISSOM model employs the Triesch [188] rule to govern the threshold and slope of the sigmoid transfer function of individual neurons in order to achieve a stable level of activity in cortical sheet regardless of the input strength. This homeostatic rule was derived such that, for a given neuron, it attempts to achieve exponential distribution of activities with a specified fixed mean [188]. As shown in figure 3.7 the distribution of activities in ALISSOM model after development does approximate an exponential distribution for low activity values. However, one can see an increasing diversion from the exponential distribution with increasing activity level, and a cluster of activities around value 1.0. This cluster of activities close to 1.0 indicates that even under the Triesch rule the system often reaches saturation and that that the Triesch rule is not fully achieving the desired exponential activity distribution.

Note that despite that Triesch rule does not guarantee the exponential firing rate distribution, it does ensure the prespecified mean firing rate of neurons and thus any homeostatic mechanism relying only on the correct mean firing rate will be unaffected. This explains why the ALISSOM model with Triesch rule still achieves stable map development.

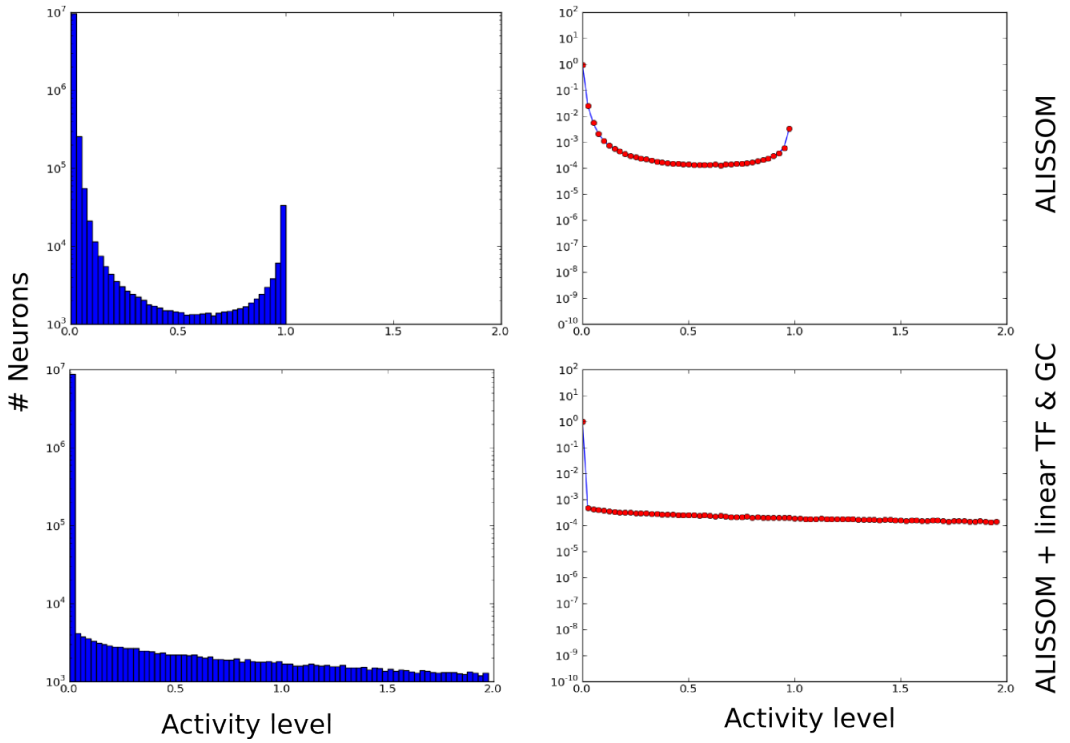

Figure 3.7: Distribution of activity levels of neurons after development in the ALISSOM model (top row) and the ALISSOM model with added gain control mechanism and linear threshold transfer function (bottom row). Both models ran for 10000 iterations, by which time they have developed stable RFs and orientation maps. At this point the simulations were run for another 1000 steps during which activity of all neurons was recorded and pooled together. Left: Raw histogram of activity levels of all neurons. Right: To allow for easier visualization of the exponential distribution the histograms are on the right shown as line graphs. Due to the logarithmic y axis exponential distributions appear as straight lines. Recorded activities in the ALISSOM model initially follow exponential distribution, but diverge increasingly with increasing activity level. Eventually there is an increase in frequency of high activity values—an indication of saturation. In contrast, the distribution of activities in the modified ALISSOM model closely follows an exponential distribution apart from increased occurrence of 0 activities.

We have attempted to avoid the saturation both by changing various free parameters of the model and by using different homeostatic rules, however we were not successful at reliably preventing a sigmoid activation function from often reaching saturation. We believe this tendency is due to the Mexican–hat like lateral interactions in the network that drive the system into a stable state which has the form of highly activated blobs of neurons, surrounded by low activity areas. This, coupled with the sigmoid nonlinearity which has approximately exponential shape in the interval between minus infinity and half maximal response, means that within the blobs of even moderately activated neurons there is high tendency of the system to run away into the maximum of 1.0 defined by the sigmoid function. The only obvious way to prevent this is to make sure the system is permanently operating in the 'shallow' parts of the sigmoid tuning curve ie., keeping activity levels very low.

Two straightforward ways to do this are either to increase the ratio between the strength of inhibitory and excitatory lateral connections, or to let a homeostatic rule (such as the Triesch rule) maintain the average activity of neurons at very low values. However, our empirical attempts to implement either of these solutions show that decreasing the activity in the network to the levels that prevent saturation also puts the network in the mode where activity does not become 'blobby' or only very weakly 'blobby', which in turn prevents orientation maps from developing. In short, we hypothesize that there is no overlap between the parametrization of the model in which it operates at low, non-saturating activities, and the parametrization in which the model is driven into the 'blobby' activity profiles.

It is an interesting scientific question, whether one can achieve a map development in a network of laterally connected neurons with Mexican-hat-like interactions and sigmoid transfer functions, while avoiding saturation during the development. However, the relative complexity of the ALISSOM model makes it unsuitable for answering this question. A possible future work could address this question by turning to a highly simplified version of the LISSOM model and either perform a systematic parameter search or attempt to solve this problem analytically.

Instead, the practical solution to our problem comes from confronting the sigmoid transfer function with experimental evidence. Even though, in more abstract firing-rate based models such as ours, this function is often assumed to be a good approximation of the 'f-I' curve describing the relationship between the input current and firing rate, a number of studies suggest that in many neurons a more accurate abstraction is a linear transfer function with threshold [17, 2, 170, 56]:

$$f(x) = \begin{cases} \alpha x & \text{if x} > \theta \\ 0 & \text{if x} <= \theta \end{cases} \tag{3.8}$$

where α is the gain and θ the threshold. One might argue that this function is not realistic, because neurons naturally cannot increase their firing rates indefinitely and firing must saturate eventually. However, this is true only providing that the input to the neurons under natural conditions actually reaches a level that would lead to saturation. There are number of mechanisms, such as the gain control discussed in previous section or sufficiently strong local inhibition, that can prevent such a situation. In vivo, V1 neurons do not reach firing rates that would be in the saturating regions of their f-I curves, as suggested by their peak firing rates when stimulated with natural movies [210] or the low firing rates at which their contrast response curves saturate [164]. Note, that if however these mechanisms are bypassed, for example by directly injecting current into the neuron in a patching experiment, the saturating region of the f-I curve can still be revealed [162].

In light of this evidence we decided to exchange the sigmoid transfer function in our model with a linear threshold. As illustrated in figure 3.6, if we exchange the sigmoid transfer function with linear-threshold one in the same instance of the ALISSOM model as presented in figure 3.6, add a gain control mechanism in the RGC/LGN such as described in the previous section, and adjust the strength of lateral connections to compensate for these changes, we significantly improve the orientation tuning curves, both in terms of selectivity and contrast invariance. This shows that applying the above changes in a fully developed model instance achieves our goals.

Could these changes, however, interfere with the development of the model? In order to answer this question, we ran another simulation with all these changes present already at the beginning of the development. Because we have exchanged the sigmoid transfer function with linear threshold one, we cannot use the Triesch rule as the homeostatic mechanism in this new model. For this simulation we keep the threshold of the linear transfer function fixed and thus the responsiveness of the neurons in this simulation is not governed by any homeostatic mechanisms. We will address this issue in the next section.

As illustrated in figure 3.8, the modified ALISSOM model with added gain control mechanism and linear transfer functions develops realistic RFs and orientation maps, while still showing improved orientation tuning properties after development. Furthermore, if we plot the histogram of activity levels of neurons after development, we can see that we are now avoiding the clustering of firing rates at any particular higher value,

an improvement over the ALISSOM model (see figure 3.7). Furthermore, as indicated by the straight line of the histogram of activities in the logarithmic plot, the distribution of activities in the new model well approximates an exponential distribution.

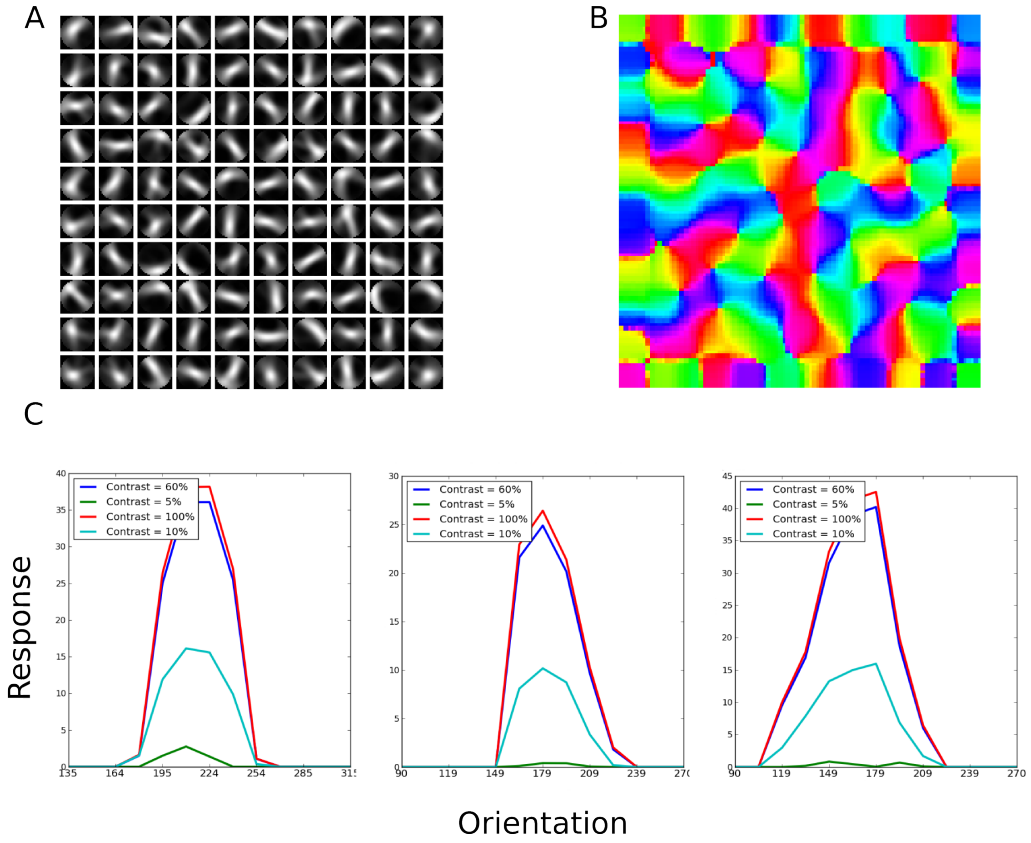

Figure 3.8: Results from the modified ALISSOM model with added gain control mechanism, linear-threshold transfer function, adjusted parameters during all of development, and no homeostatic mechanism trained on Gaussian patches for 10000 iterations. Connection field of the neurons after development (A). Orientation map (B). Examples of orientation tuning curves, at arbitrary positions (0.0,0.0),(0.0,0.1),(0.1,0.0) in the cortical sheet (C). This figure shows that the proposed changes to the ALISSOM model are consistent with development of orientation selective neurons and orientation maps, while ensuring both the selectivity and the contrast invariance of neurons in the network.

In conclusion, while simplifying the model of V1 neurons by exchanging sigmoid transfer function with linear one, and introducing gain control mechanism, we have improved the orientation tuning properties of our model. All other important properties of ALISSOM, such as non-shrinking lateral connections and robust development of orientation maps, are preserved, except for the homeostatic mechanism and the stable development that it allows. We will address this last issue in the following section.

3.4 Robustness of self-organization

Experimental evidence from ferrets [52, 54] and cats [57, 78] indicates that orientation preference maps in V1 develop in a stable way. That is, once neurons became orientation selective in a particular point in the map, their orientation preference remains largely unchanged for the rest of the development. This stability is remarkable given the massive circuit reorganization and changes in V1 inputs occurring at this time. One of the main novel properties of the ALISSOM model introduced by Judith Law in her recent PhD thesis [119], was that it showed how such stability can be achieved in a computational model of map development. As mentioned earlier, the main mechanism responsible for this property was the Triesch homeostatic rule [188] governing the slope and threshold of the sigmoid transfer function of each neuron. This homeostatic mechanism had a key role in the stability of map development, as it ensured that the activity of individual neurons had similar statistical properties for wide range of different input stimuli sets. One remaining limitation of this model was that it still required a single free parameter to be adjusted with respect to the training inputs to ensure stable development.

In the previous section we modified the ALISSOM model by replacing the sigmoid transfer function with a linear threshold transfer function, in order to achieve more realistic tuning properties of individual neurons. Because the Triesch rule has been derived only for sigmoid transfer function we can not use it directly in our new model. It may be possible to re-derive the Triesch rule for linear-threshold transfer function, but we decided to first examine the possibility of using a simplified homeostatic rule that only maintains the average activity of a neuron at a desired level by adjusting the threshold of the linear-threshold transfer function.

As presented in the rest of this chapter, it turns out that this simplified homeostatic rule, in combination with the changes discussed in previous sections, ensures stable development of maps. This means that even with the simplified homeostatic rule we maintain all key properties of the ALISSOM model in the model, called GCA-LISSOM.

The Triesch homeostatic learning rule adjusts the slope and threshold of the transfer function of a given neuron such that distribution of its firing rates follows an exponential distribution of pre-specified mean. Since the activity distribution in ALISSOM was not approaching an exponential distribution even with this constraint, we will drop the requirement that neuron's firing rates have to follow an exponential distribution, and

only require neurons to have a fixed mean rate of firing. In such a case, one can specify a very simple, purely reactive homeostatic rule, where each neuron computes its recent activity mean and shifts the threshold in the direction specified by the difference between its recent mean activity and the desired mean. Assuming that activity of neuron n at time t $\Psi_n(t)$ is computed by passing its overall synaptic input $x(t)$ at time t through a linear threshold transfer function f with threshold $\theta_n(t)$:

$$\Psi_n(t) = f_n(x(t)) = \begin{cases} \alpha x(t) & \text{if x} > \theta_n(t) \\ 0 & \text{if x} \leq \theta_n(t) \end{cases} \tag{3.9}$$

we define the homeostatic rule as:

$$\theta_n(t+1) = \theta_n(t) + \xi(\varphi_n(t) - \mu) \tag{3.10}$$

where μ is the desired target average activity, ξ is a time constant regulating the speed of adaptation and $\varphi_n(t)$ is the recent average activity of neuron n at time t, computed as follows:

$$\varphi_n(t) = \zeta\varphi_n(t-1) + (1-\zeta)\Psi_n(t) \tag{3.11}$$

where ζ is the time constant controlling the exponential decay rate of averaging. This mechanism represents a simple form of a PID controller—a feedback control loop mechanism that has been extensively studied in control theory [26].

In order to assess the stability of a map development, we compute an 'orientation similarity index' periodically during the development, as in reference [54]. The similarity of two maps is calculated by averaging the differences of preferred orientations across all corresponding pairs of pixels in the two maps, and subtracting the resulting number from 1.0. This yields values of 1.0 for identical maps and approximately 0.5 for maps that are uncorrelated. To assess the stability of the map development, we calculate the similarity of the orientation maps over the course of development to the final orientation map. If one plots these similarity values as a function of simulation time, fast monotonically rising curves indicate stable development.

In figure 3.9 we present the final orientation maps, afferent connection fields and example orientation tuning curves, along with the the evolution of selectivity and orientation similarity indexes for six simulation runs of the GCA-LISSOM model, each lasting 20000 iterations. Each row in figure 3.9 shows a simulation run using different training inputs, either Gaussian blobs of different peak amplitudes (0.5,1.0,2.0) or of different frequency of occurrence per iteration (1 or 4), or a natural image dataset.

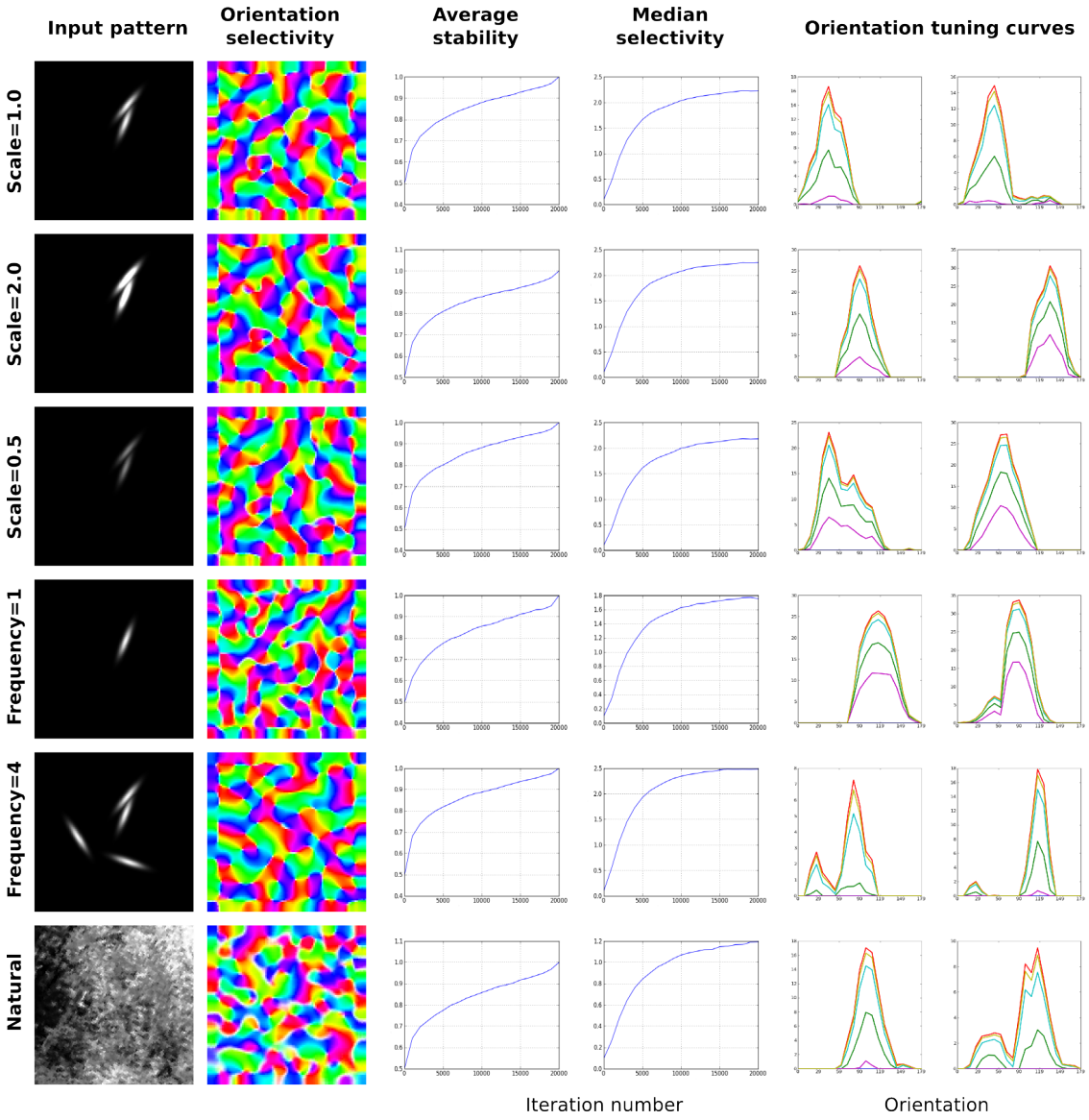

Figure 3.9: Stable development under different input statistics conditions. Each column corresponds to one instance of our GCA-LISSOM model, run with identical parameters for 20000 iterations, and trained on 6 different input statistics (from top to bottom): Pair of Gaussians with scale 1.0, 2.0 and 0.5, one Gaussian per iteration (frequency 1), 4 Gaussians per iteration (frequency 4) ot a set of natural images. The first column shows an example stimulus from that training set. The second column shows final orientation preference and selectivity map. The third column shows the evolution of the average stability over the course of development. The fourth column shows the evolution of the median of the selectivity over the course of development. The last three columns show three example orientation tuning curves, measured at 4 different contrasts at the end of development.

Figure 3.9 demonstrates that the GCA-LISSOM model can develop smooth, stable orientation maps for a wide range of input statistics, without the need to change any of its parameters, while achieving realistic orientation tuning properties for individual neurons.

3.5 Discussion

The goal of the work presented in this chapter was to build a robust, practical model of the self-organization and function of V1, starting from the existing ALISSOM model. This step was an essential prerequisite being able to address the main aims of this thesis.

First, to account for the known dependencies of surround modulation effects on the contrast of the stimulus and given the unrealistic contrast saturation in the previous versions of the LISSOM family of models, we introduced a form of gain control. We did this by assuming divisive lateral connections in the model LGN/RGC. As demonstrated in figure 3.9, this simple mechanism can account for both the typical saturating contrast response curve and for the contrast-dependent size-tuning effects found in the LGN. The divisive lateral connections can be considered as a neural implementation of the previous more abstract model by Bonin et al., which was shown to produce good quantitative fits to cat LGN data [35]. Such mechanism is supported by existence of lateral connections both in retina [128] and LGN [34]. An additional possible mechanism contributing to the gain control in LGN, not accounted for in this study, could also be the strong cortical feedback from V1 to LGN, which has been found by several previous studies [139, 10]. However, given that the gain control is already present at the level of retina which does not receive feedback from V1 (or LGN) indicates that the cortical feedback could not be the only mechanism responsible for gain control in LGN. The introduction of the gain control mechanism will in future allow us to investigate the interaction between the surround modulation effects present already in LGN and those observed in V1.

The second property examined in this chapter is the contrast-invariant width of the orientation tuning curve. This property of V1 neurons represents a tight interplay between the contrast response of V1 neurons and their orientation tuning. Because both contrast response and orientation tuning are known to interact with surround modulation, it is necessary for our model to account for not only both of them separately but also for their interactions. As discussed above, we identified the saturation of the

transfer function curve (when modeled as a sigmoid), the equivalent of an f-I curve for our model neurons, as the main cause of the poor orientation tuning properties of the ALISSOM V1 neurons. Consequently, we replaced the sigmoid transfer function with a linear threshold function. As shown in figure 3.9, together with the gain control mechanism introduced in the previous step, this change ensures a realistic orientation tuning responses of individual neurons in the network.

Even though it is known that the f-I curve of neurons saturates, the assumption of the linear threshold function is realistic given the low peak firing rates V1 neurons reach in vivo [210, 163], suggesting that neurons might operate only in the linear regime of their f-I curves and that the saturation of firing rates with increasing contrast is instead due to other mechanisms (such as the saturation of the feed-forward inputs from the LGN and the lateral interactions).

Numerous previous models of contrast-invariant orientation tuning have been proposed in the literature, including models based on 'push-pull' mechanisms [66], feed-forward excitation from LGN in combination with the effects of intrinsic noise on the firing threshold [72] and lateral interactions [176, 84]. Recently, a first study has shown how development of orientation maps can be combined with 'push-pull' effects to achieve contrast invariant orientation tuning within single model [212]. It remains to be seen which of these mechanisms, or their combination will be confirmed experimentally. Our main contribution towards this topic is to show in a single model that one of these mechanisms—the lateral interactions—is compatible with both development of orientation maps (and other V1 properties as shown in chapters 4 and 5) and with a contrast-invariant orientation tuning width. This shows, that theoretically, assuming the gain control mechanisms in RGC/LGN and Mexican hat like interactions in V1 are realistic, 'push-pull' organization is not necessary prerequisite for contrast invariant orientation tuning width. However, our work does not eliminate the possibility that some of the other mechanisms suggested in the literature might also be active at the same time.

One of the main novel properties of ALISSOM is that it develops orientation maps in a stable manner, as found in animals. The principal mechanism responsible for this stability is the homeostatic Triesch rule in ALISSOM that governs the threshold and slope of the sigmoid transfer function of individual neurons. GCA-LISSOM cannot rely on the Triesch rule, which was derived for sigmoid transfer function, as we have exchanged the sigmoid transfer function for linear threshold. In order to maintain the stable and robust development in GCA-LISSOM, we had to either to derive Triesch

rule for linear threshold transfer function or look for an alternative mechanism. Interestingly, we found out that a simpler homeostatic rule that only ensures that a neuron will maintain a fixed average firing rate (by adjusting the intrinsic excitability of the neuron via changes to the threshold of the transfer function) is an adequate alternative.

There are two most common ways homeostasis is believed to operate in neurons — homeostasis of synaptic strength and homeostasis of intrinsic excitability. Mathematically, these two mechanism are interchangeable, and currently there is experimental evidence supporting both types [147, 191]. The hebbian learning rule used by the proposed model applies divisive normalization, which implicitly represents a form synaptic homeostasis. Therefore to keep the two types of homeostasis conceptually different in the model we have decided to model the homeostatic mechanism proposed here as intrinsic excitability, similarly to Triesch rule used in the ALISSOM model. However, should further evidence in future show that this type of homeostasis corresponds to synaptic adaptation it should be trivial to modify the model to account for this.

As demonstrated in figure 3.9, the proposed simple homeostatic rule and the new gain control mechanism ensure stable map development for a wide range of input statistics. Moreover, thanks to the gain control, the robustness of the GCA-LISSOM model is no longer dependent on any parameter for the modeller to set for an input dataset— a clear improvement over ALISSOM. The fact that a simpler homeostatic rule can lead to stable map development and at the same time improve the robustness of the model is not entirely surprising, if we consider the two other modifications that we have introduced. The gain control increases the range of input statistics that generate similar values in LGN neurons, consequently ensuring that only extremely low input strength will significantly change the amount of input reaching V1. On the other hand, removal of the saturating transfer function ensures that the shape of the activity blobs will be maintained across a wider range of input statistics (as discussed in section 3.3), which should also make it easier for the model to maintain stable map development. Overall, we have presented a model that develops stable orientation maps for wide range of input statistics, without the need to adjust any of its parameters. It is still likely that more extreme changes in input statistics than those explored in this chapter are going to prevent the model to develop orientation maps in a stable manner, or prevent it to develop maps at all. However it is currently not known whether such extreme changes of input statistics still lead to stable orientation map development in animals, and it seems unlikely at present that we would need to account for such situations as well.

Another interesting question related to input statistics is their influence on the structure of the map (such as the frequency of the map, or the position and frequency of map discontinuities). Number of studies have formed hypothesis on why the specific structure of orientation maps in higher mammals emerges during development, including minimization of wiring costs [116], relationship to input statistics [96] and the architecture of retina [154] As can be observed in figure 3.9, the map structure in our model seems to be somewhat dependent on the statistics of the input. Note that even though development of our model is robust to input statistics in the sense that it reliably develop realistic orientation maps when trained with wide range of input statistics, it does not mean that the final map structure is always identical. Because the proposed model meets important developmental constraints ignored in other models of orientation map development (a stable map development which is robust to input statistics), it would be interesting to investigate in future which statistical properties of the inputs have what effects on the final structure of the maps in the model. Such analysis could either be done analytically, which is unlikely due to the complexity of the proposed model, or via systematic parameter search of appropriately parametrized input space. Unfortunately, the latter option is currently technically difficult, given the amount of computational resources the current model requires. However, future advances in simulation software or model simplification or improvement in hardware could make such analysis possible.

As explained above, the goal of this chapter was to build a model exhibiting functional properties that are necessary for the main goals of this thesis. However, each of the discussed modifications is related to an interesting scientific topic that could be pursued in greater detail. For example, the size tuning effects in LGN have been measured in great detail in cat [159], and one could try to achieve quantitative rather than qualitative (as in this thesis) fits to this data. Another set of issues that warrant further investigation in the context of a developmental model are the interactions between contrast invariant tuning, saturation of f-I curves, and the exponential distribution of firing rates. Finally, further analysis involving systematic parameter search is required to fully establish the region of input statistics in which our model develops stable, smooth, and selective orientation maps. However, none of these issues address the principal goals of this thesis, and therefore we leave them open for future work.

Chapter 4

Complex Cell Map Development

4.1 Introduction

The early studies of Hubel & Wiesel [94] identified two functionally different classes of cells in primary visual cortex. The first class — simple cells — respond to a drifting sinusoidal grating only when it is precisely aligned with the on and off subregions of a cell's receptive field (RF). On the other hand, the response of cells in the second class — the complex cells — is largely phase invariant, so the cell will respond to most or all phases of a sine grating. Previous studies have shown a relationship between cortical depth and the prevalence of the two cell classes [155, 92]. A recent study by Martinez et al. [92] argued that in cat, neurons with simple receptive fields are only found in layer 4 and upper layer 6, the layers that primarily receive thalamic input. Data from macaque monkey are not as clear, but show a similar trend with predominantly simple cells in layer 4 to complex cells dominating in layer 2/3 [155].

Over the years, three main types of model circuits leading to phase invariance have been proposed: hierarchical, parallel, and recurrent [127]. As Alonso et al. [127] pointed out, these three classes of models are becoming remarkably similar to each other as additional connectivity is being added to account for new physiological constraints. Regardless of which of the three classes of models is closest to reality, a fundamental question still remains largely unanswered: How does the specific and precise circuitry (assumed by each of these theories) develop? One possible explanation is that initial homogeneous cortical connectivity can be modified by activity dependent-mechanisms in such a way that, over time, adult connectivity patterns emerge [194, 206, 141]. This self-organization can be driven by intrinsic spontaneous neural activity, external visual stimuli or both.

Another feature of the primary visual cortex — whose development is often explained by self-organization — is its functional topological organization. The best known examples of topologically organized functional features are retinotopy, ocular dominance and orientation preference. In this work we will focus on the latter. Orientation preference maps are present throughout all cortical layers and are aligned — meaning that when one traverses the visual cortex vertically one will find neurons with a similar position and orientation preference [95]. Numerous models have been proposed to account for the development of orientation maps in the primary visual cortex [154, 168, 79, 133, 132].

The spatial organization of absolute phase preference is much less clear. For a fixed eye position and display screen, the absolute phase preference of a neuron is the phase of the sine-grating that elicits the highest response from the neuron. A study in cat [122] found that nearby neurons tend to have opposite phase preferences, whereas a study in macaque [16] found that nearby neurons tend to have correlated phase preference. Furthermore, relative phase, which describes the alignment of the ON and OFF RF subfields with respect to the center of RF, was found not to cluster in cat V1 [61]. It is important to note that findings about relative phase do not transfer to absolute phase, as it is possible that two neurons with opposite relative phase can still have highly overlapping ON and OFF RF subregions due to local scatter of receptive field centers. The distinction between absolute and relative phase preference has not been fully appreciated by several experimental and modeling studies, which has further added to confusion. Despite this ongoing controversy about the organization of phase in visual cortex, we believe that above studies clearly show that the representation of phase in V1 is significantly more disordered than that of orientation, (which has been shown to be smooth on single cell resolution by the recent two-photon imaging studies in cat [150]) and consequently one can expect a variety of phases being represented in a local region of cortex. As we are primarily interested in absolute phase in this work, for the sake of brevity, we will refer to the absolute phase as phase in reminder of the chapter.

The main goal of this study is to reconcile the development of orientation maps with the development of complex cells in V1. This is an important and non-trivial problem for the following reason: a natural way to construct complex cells is to let them group responses from simple cells with the same orientation preference, but with different phase preferences. Because, as discussed above, proximate simple cells are selective to variety of phases, such grouping can easily be achieved in the visual cortex by simply pooling responses from nearby simple cells indiscriminately (see figure 4.1).

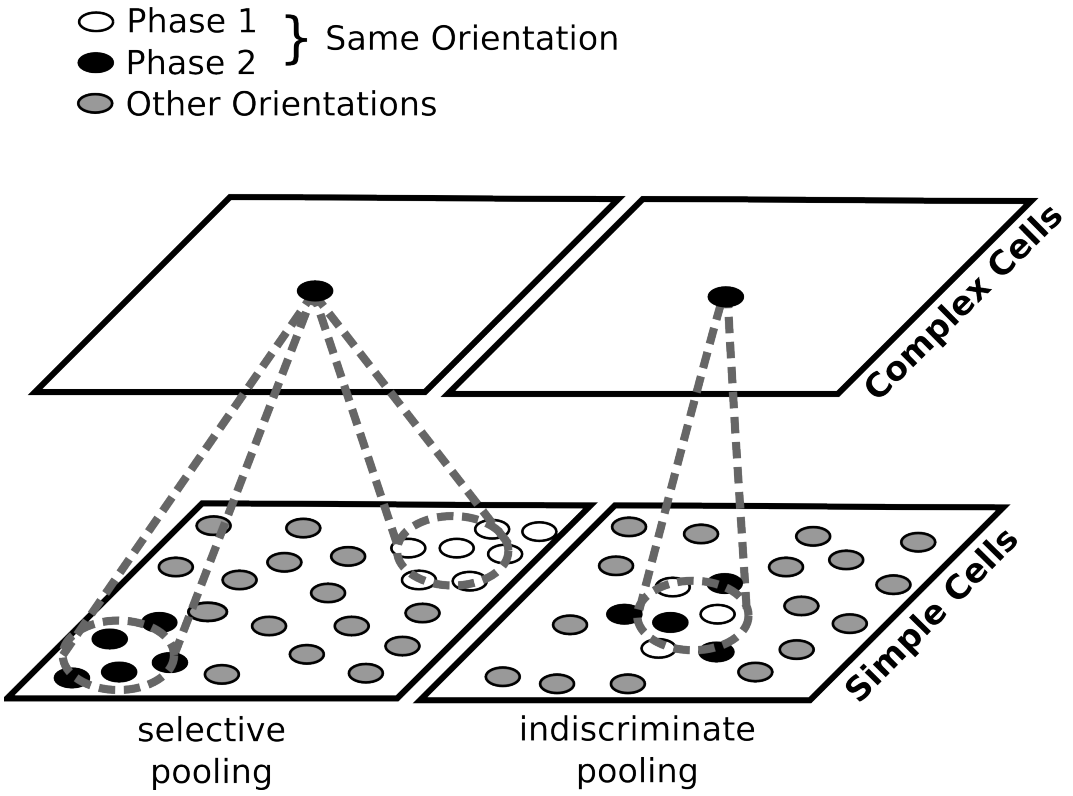

Figure 4.1: Two possible ways to construct complex cells. Left, with phase preferences clustered, a complex cell of a given orientation preference will have to pool responses of simple cells of corresponding orientation preference located at several different positions in the map in order to achieve a sufficiently phase-invariant response, while avoiding other orientations. Right, if phase is locally variable, complex cells can simply indiscriminately pool from a narrow region of the map. Variable phase ensures that it will receive inputs from simple cells selective to range of phases, while the smoothness of the orientation map will ensure that those simple cells have similar orientations. For the sake of clarity, in this figure, we approximate the continuous range of possible phases with just two.

However, most current models of map development are driven by various analogues of Hebbian learning and Mexican-hat–like lateral interactions, which ensure that nearby neurons develop highly correlated receptive fields. At the same time, phase generally represents the strongest correlation in the input, from which we can conclude that such models will tend to group similar phases together, which makes it very hard for these models to explain the formation of complex cells.

Furthermore, in this study we address an additional discrepancy between previous developmental models of map formation and known cortical anatomy. In models that are based on lateral interactions as the driving force for map development [149, 99, 168, 132], the extent and relative strengths of the lateral and afferent interactions are very important parameters. There is, however, substantial evidence suggesting the largest source of lateral interactions is the lateral connections originating from pyramidal neurons in layer 2/3 [27, 92, 55, 28]. Despite these experimental results, all previous models for orientation preference map development that we are aware of that depend on the plasticity of V1 afferent connections from LGN place the long-range lateral connectivity in an analogue of layer 4C. I.e., the layers with long-range connections in these models receive direct input from the LGN, and they develop simple cells. Thus, previous models are in conflict with the available experimental evidence.

Here we introduce a model of simple and complex cell development that results in matching orientation maps in both simple and complex cell layers, disorder in the spatial arrangement of simple cells with similar phase preferences, and realistic orientation and phase tuning curves for both simple and complex cells. At the same time, the model follows the established anatomical constraints of the connectivity in cortical layer 4C and 2/3, and does not assume any specific neuron-to-neuron connectivity at the beginning of development, an improvement over the previous models of complex cell map development.

The model contains two topographically ordered sheets of V1 cells, one representing cortical layer 4Cβ and one representing layer 2/3 with only layer 4Cβ receiving direct thalamic input. The self-organization of maps is achieved by short-range excitatory and long-range inhibitory connections in both sheets, modeling the net inhibitory interactions for high contrast stimuli at large distances [131, 132, 119]. The most important novel feature of the model is that the lateral connections in the sheet corresponding to layer 4Cβ are several times weaker than those in layer 2/3, making the layer 2/3 lateral interactions the major driving force of map development. Importantly, there is a strong anatomical evidence that this is the configuration in macaque V1

[27, 92, 55, 28]. We are not aware of any previous model of orientation map development that follows this constraint. At the same time, this arrangement is one of the key features of the model, because making the lateral connectivity weaker in the sheet representing layer 4Cβ takes away the direct self-organization pressure from layer 4Cβ. This combined with two realistic sources of variability we introduce into the model (initial local retinotopical scatter and intrinsic activity noise) allows disordered phase preference to develop in the 4Cβ sheet. The resulting development of disordered phase preference can then be harnessed by the units in layer 2/3, which pool the responses of simple cells in layer 4Cβ via narrow afferent connectivity to produce complex-cell–like RFs. In order to ensure development of RFs in layer 4Cβ and development of matching maps in both layer 4Cβ and 2/3, the model also contains feedback connectivity from layer 2/3 to layer 4Cβ, which corresponds to the known strong inter-laminar pathway starting in layer 2/3 and reaching back to layer 4 via layer 5 and 6 [27, 92].

This model demonstrates that it is possible to develop a map of complex cells using only known mechanisms and anatomical features of primate V1, unlike previous models. Furthermore the model produces realistic single cell properties, such as realistically shaped orientation tuning curves for both simple and complex neurons, and realistic contrast responses. The specific connectivity that develops in the model also allows us to formulate specific predictions: First, we predict clustering of the (albeit weak) phase preference of complex cells in layer 2/3, and second we predict a relationship between modulation ratios and the position of cells in the orientation maps.

Finally, in the proposed model we simulate both prenatal and postnatal developmental phases, driven by retinal waves before eye opening and then by natural images. The simple and repetitive patterns of retinal waves help to establish initial smooth orientation maps, reducing the dependence on the less predictable patterns of natural image stimulation. Simulating them also helps the model account for findings that orientation maps are present even at eye opening [54, 57]. However, the retinal waves do not play a critical role in this model, and just like with previous models in the LISSOM family, it should also be possible to adjust the model such that it can show development of maps driven purely by natural stimuli. In any case, the retinal waves as implemented here represent an advance over previous models of prenatal development. Many of those models have assumed anti-correlated activities between ON and OFF LGN channels, as is true in normal vision. However, retinal waves activate both ON and OFF retinal ganglion cells nearly simultaneously [113], implying that the activation patterns between ON and OFF LGN cells with the same retinotopic preference

will be highly correlated during prenatal development. In the proposed model we simulate retinal waves that activate both ON and OFF channels at the same time. As will be discussed in further detail in section 4.2.1, by randomizing the relative strength of connections from ON and OFF LGN sheets to individual layer 4C model neurons—as recently found for the macaque [209]—we show that initial orientation map development can be driven by this more realistic simulation of retinal waves. The model thus represents a novel and more realistic simulation of how retinal waves or other spontaneous activity could drive initial development of orientation maps.

4.1.1 Related Models

One of the first studies to demonstrate how complex-cell–like properties can emerge from stimulus-driven self-organization was the work of Földiák [73], which introduced a local learning rule (trace rule) that developed complex-cell RFs when trained with a temporal sequence of smoothly translating bars. Einhäuser et al. [67] has recently shown that a two-layer network using a competitive Hebbian learning rule can develop the properties of complex cells, when trained on natural images. A very recent model by Karklin et. al. [109] develops complex cells by learning the statistical distributions that characterize local natural image regions. None of these models, however, can explain the emergence of functional topological organization, such as orientation maps, which is important because of the striking difference between the observed organizations for phase and for orientation.

Sullivan et al. [181] address the problem of complex cell map development by combining Földiák's trace rule with a self-organizing map algorithm. Their model consists of two layers of neurons. The first layer is a fixed sheet containing hard-wired simple cells with various orientation and position preferences. The cells in the second layer are fully connected to the cells in the first layer and adapt their afferent connections based on a combination of Hebbian, winner takes all and trace rules. When stimulated with oriented moving stimuli, this model develops receptive fields that are invariant to position but selective to orientation, and also ensures that nearby neurons have similar orientation preferences. The main drawback of this model is that it still does not explain how orientation maps and disordered phase representation can develop in the layer containing simple cells; it assumes that these have already developed.

So far, there have been three models showing how maps of simple cells with disordered phase preference and correspondingly organized maps of complex cells can

develop. In order to understand the contributions of these models it is helpful to emphasize the main underlying problem, which is how to reconcile the development of disordered phase preference with the Mexican-hat–like lateral interactions driving nearby cells to develop correlated RFs. Because simple cells are strongly phase selective, two simple cells preferring the same orientation but opposite phases will respond in an anti-correlated manner when presented with a range of sinusoidal gratings of the same orientation but varying phases. This means that any self-organizing rule forcing nearby neurons to develop correlated RFs will not allow cells selective to opposite phase to develop next to each other, in contradiction with the observed disordered phase preference (figure 4.2 left).

One way to overcome this problem, allowing neurons selective to opposite phases to develop nearby, is to map the responses of phase opposite cells to the same values, and then apply the lateral interactions (or mechanisms analogous to them) over this transformed representation. A simple and elegant, albeit not biologically plausible, way to achieve this is to allow neurons to have signed responses rather than only positive "firing rates'. That is, the response of an idealized neuron preferring phase a, to a sinusoidal stimulus of phase $a+\pi$, will be -1. One can then pass activities of such neurons through a squaring function that ensure that the response of each neuron to its preferred phase and anti-phase are equal (figure 4.2 right). However, this approach is arguably just a trick, as it is hard to link the negative activities and the squaring operation to any known neural mechanisms.

There have been two studies that have used this trick to achieve development of disordered phase preference, complex cells and topographic maps. First, Hyvärinen et al. [99] employed a hierarchical two-layer model where signed units with simple-cell–like RFs emerge in the first layer. The second layer contains units that locally pool squared activations of units in the first layer. A topographic extension of the independent component analysis (ICA) learning rule is used to self-organize the model, and leads to the development of orientation maps. Due to the signed responses of simple cells and the squaring of their output, this learning rule also ensures disordered phase preference representation across the simple cells, which in turn ensures that units in the second layer, which simply pool local activities from the first layer, become complex cells.

Similarly, Weber [198] uses a two layer model, with the first layer containing 'feature cells' with bottom up and top down weights. During training, these cells are allowed to have negative responses which are then squared. The second layer con-

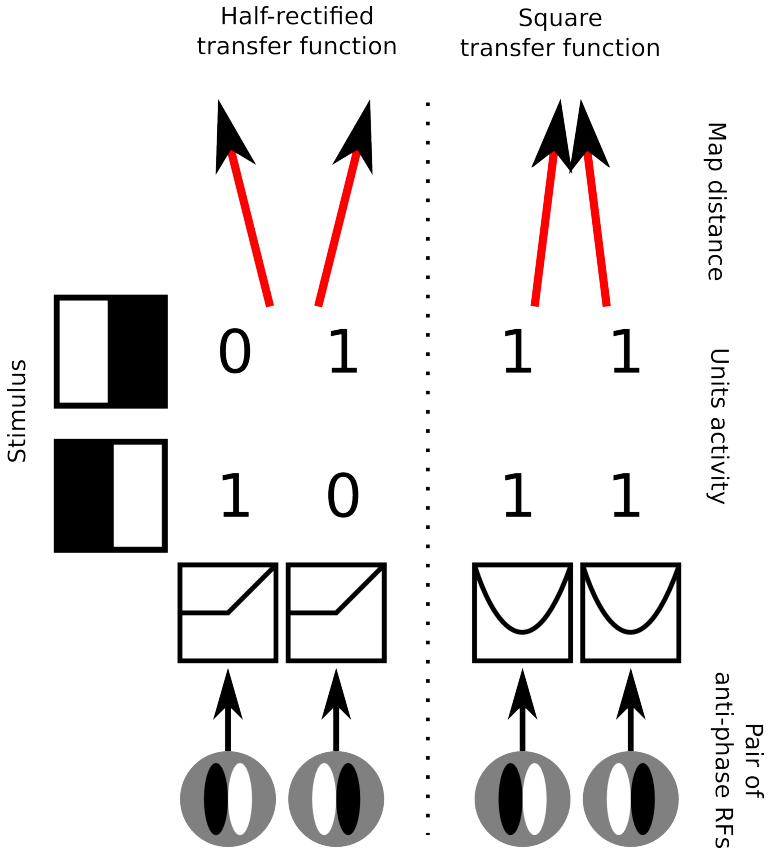

Figure 4.2: Demonstration of the underlying conflict between disordered phase preference, development of simple cells, and mexican-hat–like lateral interactions. Left, an example of a pair of simple cells with half-rectified transfer functions that are selective to the same orientation but opposite phase. When such cells are presented with stimuli of preferred orientation, they will have mutually anti-correlated activities. Mexican-hat–like lateral interactions constrain nearby neurons to have highly correlated activities, causing neurons selective for the same orientation but opposite phase to develop in different map locations. Right, an example configuration that resolves this conflict by applying a squaring transfer function to the response of the simple cells. This ensures that the activity of neurons will become correlated and thus allows them to occupy nearby locations in the map, but renders their output non-simple-cell–like.

tains 'attractor cells', with lateral weights, which become complex cells. The feature cells in this model are trained with a sparse coding paradigm and develop orientation preference, orientation maps and disordered phase preference.

Neither Weber nor Hyvärinen et al. propose a biological circuit that could implement their algorithms. Overall, this lack of grounding in cortical anatomy is the main limitation of the Hyvärinen and Weber probabilistic models. As Hyvärinen et al. mention these models represent the combined effect of evolution, prenatal, and postnatal development. Therefore it is not possible to say which properties of the model correspond to putatively hardwired architecture of cortical connections, and which to activity-based adaptive mechanisms. Furthermore, the simulations in both studies were performed with small sheets of neurons because of the very high computational requirements of the models, which prevents assessment of the smoothness and regularity of the developed orientation maps in comparison with experimental maps.

As we have noted above, the idea of negative activations of neurons together with their squaring is not biologically plausible. Olson et al. [149] address this problem by assuming instead specifically hard-wired ensembles of neurons, that they call dipoles, each with only positive activations. Each such dipole consists of two pairs of neurons that strongly inhibit each other, and thus will have anti-correlated activities during development. The BCM learning rule used in this study will ensure that in each dipole the two pairs of neurons will develop receptive fields selective to opposite phases. In this way, a dipole has a role analogous to that of the signed units with squaring in the previous two studies. Similarly to the above studies, the model of Olson et al. consists of two layers, the first containing the ensembles of simple cells (dipoles). The dipoles are laterally connected via short-range excitatory and long range inhibitory connections that drive map formation in the first layer. This in turn allows modeling of complex cells in the second layer as units that simply pool the activations from simple cells via Gaussian afferent connections. The main limitation of this model is that it requires arbitrary specific wiring between pairs of simple cells at the beginning of the simulation. However, currently there is no evidence for such specific connectivity in undeveloped primary visual cortex. Furthermore, the model does not show how strong orientation-selective responses for complex cells can develop, because the model's complex cells have elevated responses to all orientations. Also, the authors do not present orientation maps in the complex layer, preventing comparison with animal maps and with their simple cell layer maps. Experimental evidence suggests simple and complex cells within a column should exhibit similar orientation preferences [31].

In this study we present a model of complex cell map development that does not rely on negative activations or arbitrary pre-specified connectivity. Instead, the key idea is to weaken the lateral interactions in the layer that is — after development — predominantly occupied by simple cells moving them to the layer that is occupied by complex cells, in line with experimental evidence. This means that nearby neurons are not forced to develop correlated phase response, as complex cells are not selective to phase and the activity of simple cells is not directly shaped by the strong lateral interactions. The second essential ingredient of the model is the feedback connectivity from layer 2/3 to layer 4C, which ensures that a matching map can develop in layer 4Cβ even without the presence of strong lateral interactions. Finally, we introduce two realistic sources of variability — initial local scatter of centers of the afferent projection from LGN to layer 4Cβ and weak intrinsic noise of neural activity — which ensure that the initial responses of neurons are sufficiently non-uniform, facilitating the development variable phase preferences in layer 4Cβ. The dynamics of the resulting network are such (as will be described in greater detail in section 4.2.2), that when the network is presented with a sequence of translated stimuli , the global spatial activation profile of neurons in both layers is stable during the sequence. However, locally, different neurons in the layer 4Cβ can respond differently to individual stimuli in the sequence (see figure 4.4). This means that during the presentation of such sequence of translating stimuli, Hebbian learning rule will cause nearby neurons in layer 4Cβ to adapt their RFs towards the same orientation while selecting one of the variety of phases.

4.2 Model description

Model architecture.

The model was built using the freely available Topographica simulator [22]. The model is an extension of the GCA-LISSOM architecture discussed in chapter 3. The main modifications are: addition of a new sheet of neurons corresponding to layer 2/3, decreasing the strength of lateral connectivity in the sheet corresponding to layer 4C, addition of feedback connectivity between the two cortical sheets, continuous network dynamics between input presentations, more realistic pre-natal and post-natal retinal and LGN processing, and additional sources of variability in the architecture and responses (see figure 4.3). This section will offer a detailed description of the model.

The simulator operates in discrete time steps. Retinal input changes every 20 time

steps (and during this period is kept constant), therefore afferent inputs to the layer 4Cβ sheet are effectively updated every 20 steps. Unlike in most previous LISSOM models, activity in the model is not reset at the beginning of each new retinal input presentation to allow learning of temporal correlations.

Previous LISSOM models computed the activity of a neuron at each time step based on the sum of incoming activities of all projections. This represents a discrete simulation of an otherwise continuous process of changes in membrane potential due to incoming spikes and consequent generation of spikes. Due to the recurrent connections, discrete simulation of this process can create or amplify oscillation in the network. The large number of recurrent connections in our model further amplify this undesirable behavior. Therefore, as will be described in greater detail below, in the proposed model we smooth out the neural dynamics, by computing the present activity of the model neuron as an interpolation between its previous activity, and the activity it would have under the former model. This process allows a lower time resolution to be used, making these otherwise intractable simulations feasible.

The Topographica simulator is based on 2D sheets of computational elements (neurons), referenced by a coordinate system we will refer to as sheet coordinates, where the central sheet element corresponds to coordinates (0,0). The number of units simulated in each sheet is determined by setting the density of units per unit length in both sheet dimensions. Both V1 sheets have nominal dimensions 1.0×1.0. The size of the RGC/LGN (2.0×2.0) and photoreceptor (2.75×2.75) sheets was chosen to ensure that each unit in the receiving sheet has a complete set of connections, thus minimizing edge effects in the RGC/LGN and V1. The density of units per 1.0×1.0 area is 48×48 for the photoreceptors and RGC/LGN ON and OFF, and 96×96 for both cortical sheets.

Units in the cortical sheets each receive up to three types of projections represented as matrices of weights: afferent, lateral, and feedback (figure 4.3). The contribution X_{jpl} to the activation of unit j in the layer 4Cβ sheet ($l = 4C\beta$) or layer 2/3 sheet ($l = 2/3$) from each projection p at time t is given by:

$$X_{jpl}(t) = \sum_{i \in F_{jpl}} \Psi_i(t-1)\omega_{ij} \tag{4.1}$$

where $\Psi_i(t)$ is the activation of unit i taken from the set of neurons in the input sheet of projection p from which unit j in sheet l receives input (its connection field F_{jpl}), and ω_{ij} is the connection weight from unit i in the input sheet of projection p to unit j in the sheet l. All connection field weights are initialized with 2D Gaussian profiles

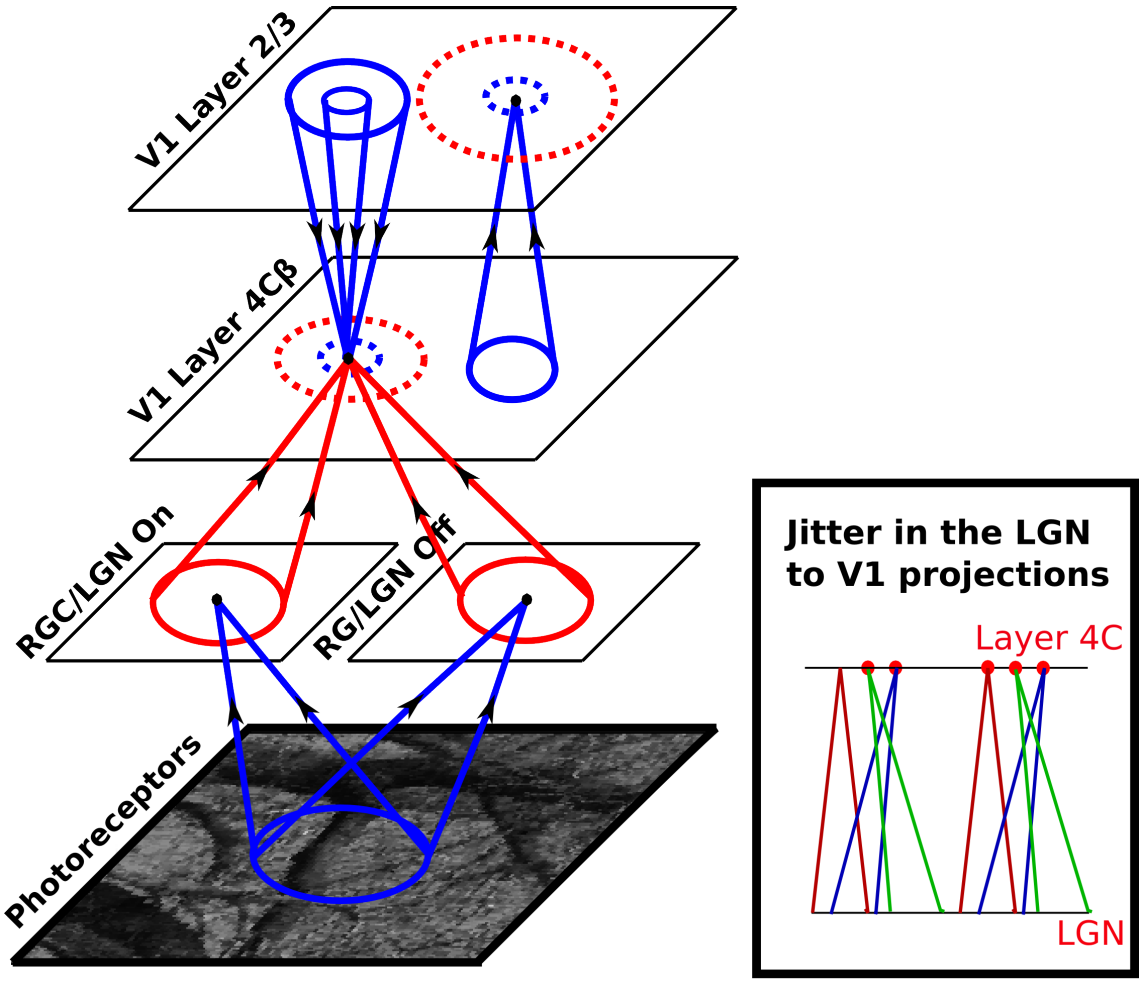

Figure 4.3: The model architecture. Each circular dot in this diagram represents a single unit in the indicated sheet. The cones indicate the incoming projections between layers, and the dashed circles indicate the lateral connections within a layer. Arrows on the projections cones indicated the flow of information and red color indicates plastic connections whereas blue indicates connections that are not modified during development. The activity propagates from the photoreceptors to LGN ON and OFF sheets. From there the activity arrives to the cortical layer 4Cβ. Within layer 4Cβ, activity spreads laterally via short-range excitatory and medium-range inhibitory lateral connections. Activity from layer 4Cβ further propagates via narrow afferent connectivity to layer 2/3, where it can again spread laterally via short-range excitatory and long-range inhibitory lateral connections. Finally, activity propagates back from layer 2/3 to layer 4Cβ via narrow excitatory and wider inhibitory connections, in a recurrent loop that (in combination with lateral connections in layer 4Cβ and 2/3) settles activity into stable 'bubbles' in layer 2/3. In layer 4Cβ activities settle into regions co-localized with the 'bubbles' in layer 2/3, but in which only some neurons are activated. This difference between the activation patterns in layer 2/3 and 4Cβ is mainly due to the weaker lateral connectivity in layer 4Cβ, which does not force nearby neurons to be co-activated. See section 4.2.2 for more detailed description of the network dynamics.

multiplied with uniform random noise, and cut off at the distance specified below. Contributions from each projection are weighted and summed to form the overall input of unit i in layer l:

$$Y_{il}(t) = \sum_p \gamma_p X_{ipl}(t) \tag{4.2}$$

where γ_p is a constant determining the sign and strength of projection p. Table 4.1 shows the strength, initial Gaussian kernel spatial extent, and the cut-off distance values for all projections. The final output of unit i is computed as:

$$\Psi_i(t) = \lambda f(Y_i(t)) + (1-\lambda)\Psi_i(t-1) + \sigma_n \omega \tag{4.3}$$

where

$$f(x) = \begin{cases} \varepsilon x & \text{if x}> \theta \\ 0 & \text{if x}<= \theta \end{cases} \tag{4.4}$$

and where $\lambda = 0.5$ is a time constant parameter that defines the strength of smoothing of the recurrent dynamics in the network. ω is a normally distributed random variable, which corresponds to firing rate fluctuations, and ε is the gain. For simplicity we implement homeostatic plasticity for neurons in layer $4C\beta$ only, and therefore θ is a constant for neurons in layer 2/3. For neurons in layer $4C\beta$, θ is adapted according to equation 3.3.

The initial connection weights from the RGC/LGN neurons to neurons in layer 4Cβ sheet have a 2D Gaussian profile multiplied with uniform random noise. Thus, initially, neuron will respond strongly when a stimulus is presented in the center of its RF. If the retinotopic ordering of RF centers is perfect, activities of nearby neurons will be very highly correlated, preventing the development of disordered phase in the model. Instead we assume that the initial activity of neurons will be more variable, because the initial retinotopic wiring between LGN and V1 is locally imperfect. Therefore, we alter the perfect retinotopic wiring from RGC/LGN to V1 by offsetting the afferent connection fields of each V1 neuron by a random factor drawn from a Gaussian distribution with variance σ_j (see figure 4.3 and table 4.1). RF position scatter of similar magnitude has been reported by experimental studies [43, 197].

Learning

The connection fields' weights for all the projections to V1 sheets are initially random within a Gaussian envelope and are spatially restricted to a specified radius. Table

4.1 shows the standard deviation of the Gaussian envelope and the radius of each projection. Only four projections in the model are being modified during development: the afferent projections from the two RGC/LGN sheets to the layer 4Cβ sheet, and the inhibitory lateral connections in both cortical sheets. In order to save computational resources, connection weights in these projections are adjusted only every 20 time steps (at the end of each input presentation). Weights are adjusted by unsupervised Hebbian learning with divisive normalization:

$$\omega_{ij}(t) = \frac{\omega_{ij}(t-1) + \beta_p \Psi_j(t) \Psi_i(t)}{\sum_k \left(\omega_{kj}(t-1) + \beta_p \Psi_j(t) \Psi_k(t)\right)} \tag{4.5}$$

where β_p is the Hebbian learning rate for the connection fields in projection p. Learning rate parameters are specified as a fixed value ι_p for each projection, and then the unit-specific values used in the equation above are calculated as $\beta_p = \frac{\iota_p}{\upsilon_p}$, where υ_p is the number of connections per connection field in projection p. We apply an exponential decay to the learning rates for the four modified projections throughout the simulation, simulating the decrease in plasticity of maturing V1. The reader can see the initial values of learning rate parameters and corresponding rates of decay in table 4.1.

Input patterns

In the simulation we consider both the pre- and post-natal stages of development (see figure 4.4) , each lasting 50000 time steps. In the first stage the input patterns correspond to spatially correlated spontaneous visual system activity such as the retinal waves generated in the retina of young animals [208]. We model these patterns as large moving rings of constant diameter convolved with white noise, representing the moving edge of retinal wave analogously to how cortical waves have been modeled in reference [79] (see figure 4.4 top panel). In the second stage natural images are presented as stimuli (see figure 4.4 bottom panel). The natural images are retina-sized patches from images of natural objects and landscapes from a dataset by Shouval et al. [169]. The pictures were down-sampled to a 256×256 pixels, with no other preprocessing of the images. For each natural image presentation, a random sub-image of the same dimensions as the photoreceptor sheet was selected. Each pixel value in the sub-image has been converted into a real value in the range of 0 to 1.0 and the corresponding units in the photoreceptor sheet have been set to these values. Also, all measurements at different contrast levels in this chapter involve full-field gratings and follow the Michelson contrast definition.

Input patterns are presented to the model at each time step by activating the retinal photoreceptor units according to the gray-scale values in the chosen pattern or image. For each input pattern to be presented, a random initial position is set. Then this input pattern is presented 15 times for 20 time steps, each time modified by a small factor relative to their initial position (see figure 4.4). In the case of retinal waves the initial retinal wave is always expanded by a constant factor of 0.02 (in retinal coordinates) per iteration (see figure 4.4 top panel). Natural images are always translated from the initial position in a random direction, for a distance picked from a uniform random distribution between 0 and 0.3 (in retinal coordinates) (see figure 4.4 bottom panel). This way the same input pattern with small differences in translation is presented for 80 time steps of the simulation overall. Each set of 15 presentations of the input pattern is followed by a single presentation of constant zero stimulus to the retina (see figure 4.4), which causes a decrease of activity in the network, and thus helps the network to form a different initial pattern of responses to the next stimulus. This blank input correspond to the periods of silence between retinal waves during prenatal development, or to the overall inhibition known to occur during saccades [63] during postnatal development.

4.2.1 ON and OFF RGC/LGN channels and eye-opening

Because it is known that retinal waves activate both ON and OFF RGC cells at the same time [113], in the first stage we bypass the processing that happens in the RGC/LGN sheets, as we cannot assume that activations in RGC/LGN ON and OFF sheets are anti-correlated before eye-opening as they are in adult animals. Having correlated ON and OFF channels during pre-natal developmental in the model means that at the end of the first developmental stage, neurons in layer 4C have developed similar connection fields in both the ON and OFF channels. However, this means that after the normal RGC/LGN processing is enabled (corresponding to eye opening in animal), neurons lose their orientation selectivity, which would hinder the continual development of orientation maps. To see why orientation selectivity is lost, imagine a V1 neuron with a connection field twice as long vertically as it is horizontally, connecting equally to both ON and OFF LGN inputs. A vertical grating aligned with this connection field will activate about half of the incoming connections, either all from the ON or OFF channel. A horizontal grating will activate similar number of connections, some from the light bars overlapping the ON connections and some from the dark bars overlapping the OFF LGN channels. Thus the response of the cell will be essentially unselective

for orientation.

One way to ensure sufficient orientation selectivity of layer 4C neurons after eye opening is to assume that either the ON or the OFF RGC/LGN channel is stronger, which increases the response difference from aligned and orthogonal stimuli. Interestingly, experimental studies have shown that individual V1 neurons have highly variable ratio between the strength of ON and OFF RF subfields, and are on average biased towards the OFF channel [104, 209]. Therefore in the model we randomize the ratio of the connection strength from the ON and OFF LGN sheets to layer 4C sheet neurons according to following formula:

$$\gamma_{AEONi} = \gamma_{\mathtt{AE}} 0.9 - X\gamma_{\mathtt{AE}}$$

$$\gamma_{AEOFFi} = \gamma_{\mathtt{AE}} 1.1 + X\gamma_{\mathtt{AE}}$$

where $\gamma_{\mathtt{AE}}$ is the average strength of the LGN to layer 4C projection (see table 4.1), X is a random variable drawn from uniform distribution from the interval $[-0.5, 0.5]$, and γ_{AEONi} and γ_{AEOFF} are the resulting ON and OFF projection strength for neuron i. We found this randomization to be sufficient to preserve selectivity. Note that the overall results do not depend on this randomization; merely making the OFF channel uniformly stronger yields similar orientation maps and range of complexity values, but it results in an unrealistic bias towards OFF-center receptive fields.

4.2.2 Network dynamics

Finally, let us briefly explain the dynamics that the discussed architecture imposes on the model, and how these dynamics ensure that the model can develop maps of complex cells. Let us assume the model is in the early stage of development and therefore neurons in layer 4C have only very weakly, if at all, orientation-selective RFs. Further, for the sake of simplicity, let us assume that previously the network has been presented with blank stimuli ensuring that both cortical layers have zero activity. Let us now present a new input to the network, for example a retinal wave. Given the unselective nature of RFs of layer 4C neurons at this stage and their high gain, in the time step when the new input arrives from RGC/LGN to layer 4C many neurons will stay silent but some will have elevated activities (see figure 4.4). The population activity will be largely random (see figure 4.4: activity at time 0). In the next time step the activities from layer 4C arrive to layer 2/3, which will produce output generally following the activation pattern in layer 4C, but with a smoother profile due to the summation of

afferent connection fields (see figure 4.4: activity at time 1). Because of the relatively unspecific activation of L2/3 at this time point, the feedback pathway from layer 2/3 to layer 4C will not significantly shape the activity of layer 4C. However, because of the strong lateral interactions in L2/3, a few time steps later the activity in layer 2/3 will converge into a more selective activity profile with the 'blobby' distribution typical for Mexican-hat like lateral interactions (see figure 4.4: activity at time 20). Similarly to the LISSOM model, during this period, the areas in L2/3 which are more activated relatively to their surrounding area via the feed-forward connections will gradually become more active, while the surrounding areas of neurons will become more and more inhibited, resulting in the typical 'blobby' activity pattern (see figure 3.1). Once the 'blobby' activity pattern is established, the feedback to layer 4C will have a very specific effect — the areas in layer 4C corresponding to activity blobs in layer 2/3 will be mildly excited, whereas the areas in layer 4C in the surround of activity blobs formed in layer 2/3 will be inhibited. The overall effect of these activations will be that neurons in layer 4C and layer 2/3 will be activated in the same areas, the difference being that in layer 2/3 the blobs of activity are smooth due to the strong lateral interactions, whereas activity in layer 4C in the elevated areas will stay sparse because of the higher input gain of the neurons and lack of strong lateral contributions.

Let us now consider one specific blob of activity formed in L2/3, surrounded by unactivated neurons, and a corresponding spot of sparsely activated area in layer 4C, also surrounded by unactivated neurons. At the end of the settling phase, Hebbian learning will ensure that the neurons in layer 4C that are activated will adapt to the current input pattern. Now let us consider presenting the same stimulus in the next step, but shifted slightly in spatial position. This means we can assume that the neurons in the area that we are discussing will see a stimulus with the same orientation but with a different phase. The dynamics in the network are not reset after each stimulus presentation, therefore when the new stimulus arrives at layer 4C, the layer will have generally the same activation profile as at the end of previous input presentation. However, because the new input is slightly different and because of the sources of variability in the model (the randomly shifted receptive fields of layer 4C neurons and the additive noise) it will activate a different subset of neurons within the discussed area. Note there will still be strong feedback from L2/3, which means that only neurons within the same area will be activated. The result is that at the end of settling, the same blob of neurons will be activated in L2/3 as in the previous step. Additionally, the same area of layer 4C will have elevated activities, but the subset of neurons activated will be different.

In summary, the dynamics in the model maintain a stable activity profile in both cortical layers over time, unless the input changes dramatically. Importantly, however, the activity profile in layer 4C is stable only at a large scale, but locally the network allows different subsets of neurons to be activated for subsequent input presentations. This ensures that at large scale L4 will become organized in the same manner as L2/3, but locally it can capture the changes that occur over short time scales. If we assume the input is typically translated (either in one direction or in a random manner) over short periods of time, we can conclude that it should be this translation (e.g., change in phase) that will be locally captured by L4 neuron RFs. Overall, this process leads to map development in both layers 4C and 2/3, and at the same time to disordered phase representation in layer 4C. This explanation also underlines the importance of the difference between the strength of lateral activity in the two cortical layers — strong Mexican–hat–like activities in layer 4C would not allow nearby neurons to have significantly different activities, and consequently would not allow neurons with different phase preference to develop.

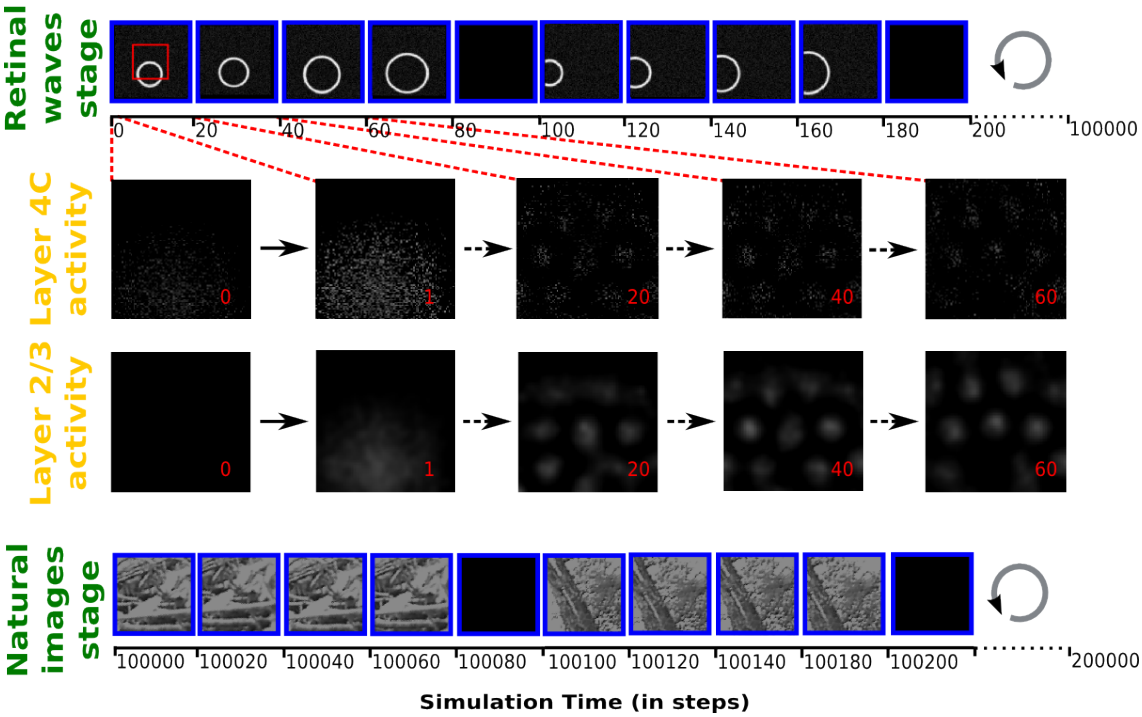

Figure 4.4: The protocol of input pattern presentation to the model, and the evolution of activity in the cortical the sheet after presentation of a retinal wave to an untrained network. Each input pattern is presented 15 times (4 shown in the diagram for illustration), each time somewhat transformed (in the case of retinal waves expanded and in the case of natural images translated in a random direction) relative to its initial position, followed by a blank stimulus. Each presentation lasts 20 time steps, during which the activity of the retinal sheet is kept constant. The input pattern presentation has two stages: 5000 iterations of expanding retinal waves, followed by 5000 iterations of natural images with randomly jittered positions. Over the 80 time steps that a given stimulus is presented, the layer 2/3 sheet activation gradually forms a pattern of blobs while the layer 4 sheet pattern has local disorder that persists only within the overall pattern of blobs matching the layer 2/3 sheet activity. These differences in activity patterns lead to different map organizations in 2/3 and 4 sheets, with the layer 2/3 sheet developing smooth maps for orientation and phase (see figure 4.6). The red rectangle outlines the region of the retinal sheet corresponding to the cortical 2/3 sheets.

Table 4.1: Model parameters

EqSymbol	Description	Value
	RGC/LGN	
γ_A	Strength of afferent projection from retina	7.0
γ_L	Strength of lateral projection	0.63
c	Slope of the gain function	0.11
	Layer $4C\beta$	
$\gamma_{\mathtt{AE}}$	Strength of afferent excitatory projection	4
$\gamma_{\mathtt{LE}}$	Strength of lateral excitatory projection	0.0
$\gamma_{\mathtt{LI}}$	Strength of lateral inhibitory projection	0.0
$\gamma_{\mathtt{FE}}$	Strength of feedback excitatory projection	0.14
$\gamma_{\mathtt{FI}}$	Strength of feedback inhibitory projection	-4.6
$\sigma_{\mathtt{AE}}$	Kernel size of afferent excitatory projection	0.2
$\kappa_{\mathtt{AE}}$	Cut-off distance of afferent excitatory projection	0.2
$\sigma_{\mathtt{LE}}$	Kernel size of lateral excitatory projection	0.04
$\kappa_{\mathtt{LE}}$	Cut-off distance of lateral excitatory projection	0.12
$\sigma_{\mathtt{LI}}$	Kernel size of lateral inhibitory projection	0.46
$\kappa_{\mathtt{LI}}$	Cut-off distance of lateral inhibitory projection	0.4
$\sigma_{\mathtt{FE}}$	Kernel size of feedback excitatory projection	0.01
$\kappa_{\mathtt{FE}}$	Cut-off distance of feedback excitatory projection	0.0025
$\sigma_{\mathtt{FI}}$	Kernel size of feedback inhibitory projection	2.5
$\kappa_{\mathtt{FI}}$	Cut-off distance of feedback inhibitory projection	0.2
$\iota_{\mathtt{A}}$	Learning rate of the afferent projection	0.5
$\tau_{\mathtt{A}}$	Learning rate decay time constant of the afferent projection	16000
	Layer 2/3	
$\gamma_{\mathtt{AE}}$	Strength of afferent excitatory projection	2.5
$\gamma_{\mathtt{LE}}$	Strength of lateral excitatory projection	1.5
$\gamma_{\mathtt{LI}}$	Strength of lateral inhibitory projection	1.5
$\sigma_{\mathtt{AE}}$	Kernel size of afferent excitatory projection	0.05
$\kappa_{\mathtt{AE}}$	Cut-off distance of afferent excitatory projection	0.075
$\sigma_{\mathtt{LE}}$	Kernel size of lateral excitatory projection	0.04
$\kappa_{\mathtt{LE}}$	Cut-off distance of lateral excitatory projection	0.12
$\sigma_{\mathtt{LI}}$	Kernel size of lateral inhibitory projection	0.46
$\kappa_{\mathtt{LI}}$	Cut-off distance of lateral inhibitory projection	0.4
$\iota_{\mathtt{L}}$	Learning rate of the lateral projection	0.2
$\tau_{\mathtt{L}}$	Learning rate decay time constant of the afferent projection	16000
	Other	
σ_n	The magnitude of the additive noise applied to all model neurons	0.025
$\theta_{2/3}$	The threshold of neurons in layer 2/3	0

4.3 Results

4.3.1 Development of maps of complex cells

In this section we present post-developmental results from the model. All results shown are from the same simulation run for 200000 iterations, unless otherwise specified. The only components of the model that undergo adaptation during development are the afferent connection from RGC/LGN to layer 4Cβ and the lateral inhibitory connections in both cortical sheets. One of the most important novel features of the model is that we assume strong lateral connections to be present in layer 2/3 and only weak ones in layer 4C. For the sake of simplicity, results presented in this section are from a model that completely lacks lateral connection in layer 4C. However, the effects of layer 4C lateral connectivity are addressed in section 3.3.

As can be seen in figure 4.5, the projections from both the RGC/LGN On and the RGC/LGN Off sheets to layer 4Cβ developed oriented profiles, giving rise to orientation selectivity for units in layer 4Cβ. The lateral projections developed connections between regions with similar orientation preferences, as expected from physiological evidence [36].

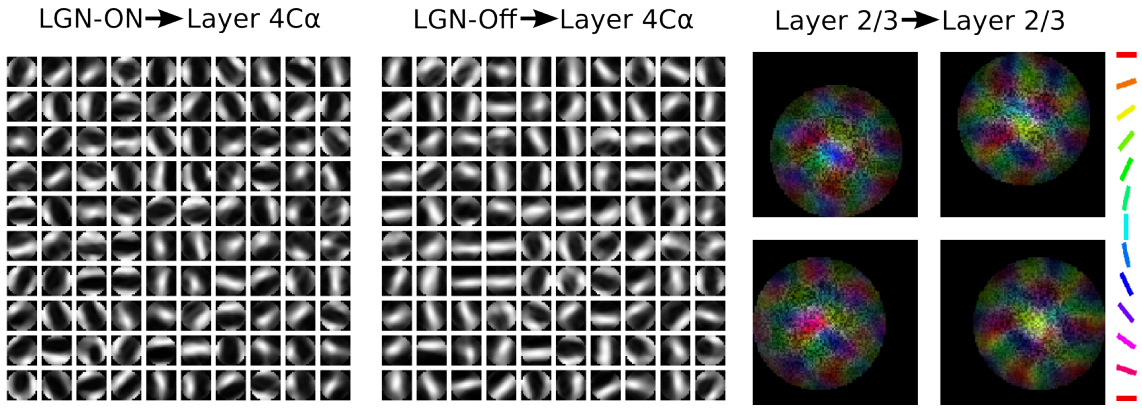

Figure 4.5: Sampling of final settled connection fields after 10000 input presentations. Only projections that are modified during development are shown: every 20th neuron in the projection from the On RGC/LGN layer to layer 4Cβ (left), similarly for the projection from the Off RGC/LGN layer to layer 4Cβ (middle), and sample lateral inhibitory projections in layer 2/3 (right). The color in the lateral inhibitory projection connection fields follow the color key on the right and indicates the orientation preference of the source neurons (see figure 4.6).

One of the most important aspects of the model is its topographical organization.

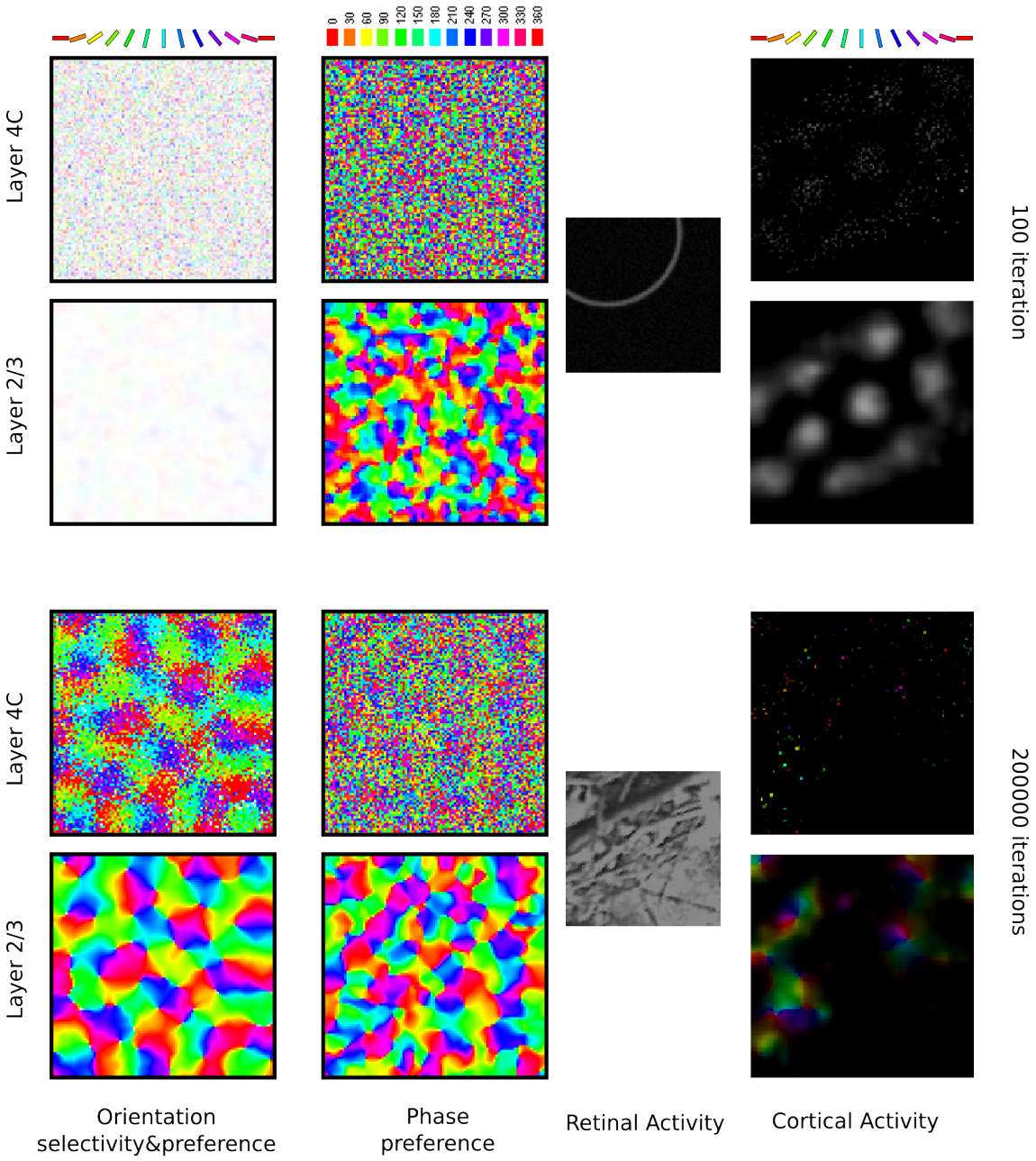

Figure 4.6: Orientation selectivity maps, phase preference, and activity in the two cortical sheets of the model, at 0 and 200000 iterations. In the orientation selectivity and activity plots, each unit is color coded according to the orientation it prefers (as shown in the color key), and the saturation of the color indicates the level of orientation selectivity (how closely the input must match the unit's preferred orientation for it to respond; unselective neurons appear white). Similarly, in the phase preference map each unit is color coded according to the phase it prefers (as shown in the color key). The first two rows show these measures in the model before development, and the bottom two rows show the final measurement after the network was trained for 200000 iterations by presenting stimuli as described in figure 4.4.

In order to assess the topographic properties we measured orientation and phase preference maps in both cortical sheets (figure 4.6). We did this in a way analogous to the procedure used in optical imaging experiments [33]. The network was presented with sinusoidal gratings of varying phase and orientation and neuronal activity was recorded as the parameters of the stimulus were varied. The activity values were used to compute the orientation and phase preference of each unit by a vector averaging procedure [132].

As can be seen in figure 4.6, layer 2/3 developed a smooth orientation map, containing the known signatures of cortical orientation maps (such as pinwheels, linear zones, saddle points and fractures). Furthermore, at a coarser scale, orientation maps in layer 4Cβ match those in layer 2/3 (figure 4.6). The orientation preference maps in layer 4Cβ contain some level of scatter, which although not previously reported, does not contradict any experimental evidence to the best of our knowledge. For instance, two-photon imaging studies [145] have only shown that scatter is low for orientation preference in superficial layers such as layer 2/3, which is also the case in the model. The existence of some orientation preference scatter in cortical layer 4C is therefore one of the predictions of the model.

The second column of figure 4.6 shows the phase preference of individual neurons. Phase preference is measured as the phase of the optimally oriented sine-grating that evoked the maximal response of the neuron. This is a measurement of absolute phase and depends both on the absolute position of the neuron's RF in retinotopic coordinates and the position of the On and Off subfields within its RF. In the phase preference maps measured in layer 4C, one can see a very small level of clustering, but the overall appearance is much more disordered than that of the orientation preference map from the same layer. On the other hand, the phase preference maps formed in layer 2/3 of our model look radically different from those formed in layer 4C, with large iso-phase patches and overall smooth characteristics. It is important to note that the phase preference of units in layer 2/3, which (as we show below) behave like complex cells, is very weak. However, the existence of weak phase selectivity in complex cells is in line with experimental studies [59, 155, 138]. Currently we are not aware of any experimental study measuring the relationship between the (weak) phase preference of complex cells and their topography. The most common technique for measuring topographic maps in layer 2/3 in cortex — optical imaging — might simply not be sensitive enough to capture weak, though well-organized, phase preference maps within the population of complex cells. This result represents a second prediction which could in principle be

tested in a detailed study of phase preferences in layer 2/3.

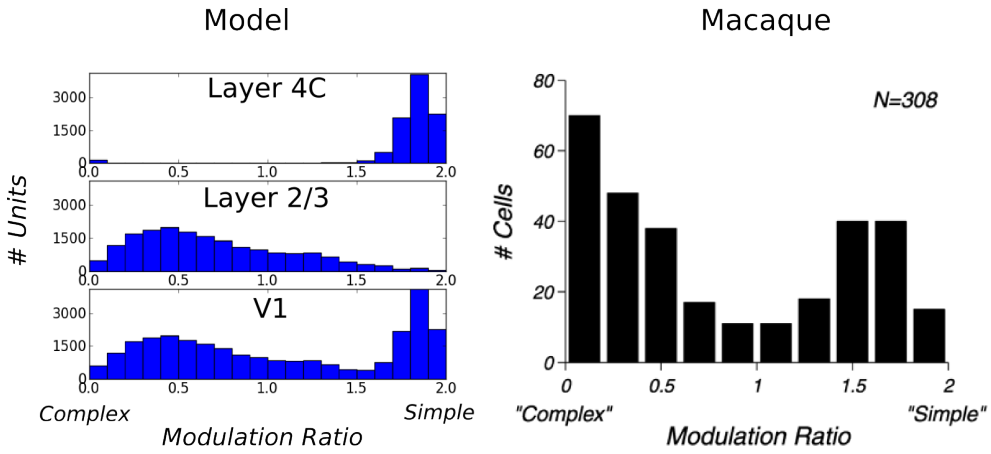

Figure 4.7: Comparison of the modulation ratio distribution in the model and in monkey V1. Data from the model (left), and data from Old World monkey reprinted from [155] (right); both show a bimodal distribution.

Finally, to assess whether the model cells behave like experimentally measured complex cells, we have calculated the modulation ratio (MR) index for all units. The MR index is a standard technique for classifying V1 neurons into simple and complex categories [138]. This value is computed as the F1/F0 ratio, where F1 is the first harmonic and F0 the mean of the response of the neuron to a drifting sinusoidal stimulus. The MR index classifies a neuron as complex if its value is below 1 and as simple if it is above 1. The histograms of the MR index of all cells in layers 4Cβ and 2/3 can be seen in figure 4.7. As expected, according to the MR measure, the majority of neurons in layer 4C are classified as simple cells (96%), whereas most neurons in layer 2/3 are classified as complex cells (65%). When cells from layer 4Cβ and layer 2/3 are pooled together as in the Ringach study, one can observe the typical bimodal distribution (figure 4.7).

One discrepancy between the experimental data and the model is the relative lack of model neurons with modulation ratios close to zero (i.e., neurons that are almost perfectly insensitive to phase). Given the large number of free parameters in our model and the limited ability to fine tune them because of the high computational complexity of the model, it is possible that one could find a parameter combination that would make the model match the experimental results more closely in this respect. However, it is more likely that one will need to simulate a larger (higher density) version of the model to see a qualitative improvement in the number of low-modulation-ratio neurons. In order to make the simulations practical, currently we set our model to have the

lowest densities that still provide a reasonable match to experimental data. The actual density of neurons in cortex is several-fold higher in cat than in the implementation of the model. A higher density of neurons per model cortical area means that neurons in layer 2/3 pool information from larger number of neurons in layer 4Cβ, which makes it more likely that they will receive input from wide range of phases, and consequently should lead to more neurons that are relatively insensitive to phase. Future increases in computational power or parallel implementation of the simulation software should allow such higher density models to be tested.

4.3.2 Single-cell properties

So far we have only discussed maps and population-level results. In order to compare the properties of the model to experimental data at the single cell level, we measured orientation tuning curves and phase responses of example neurons in layer 4Cβ and layer 2/3 (figure 4.8). This was done by presenting the model with orientation gratings of optimal spatial frequency and varying phase and orientation while recording the activations of neurons. Identical parameters of the receptive fields of all LGN filters in the model mean that the spatial frequency of the model neurons is virtually constant across the population. In order to save computational resources we used this single known value of spatial frequency preference as the optimal spatial frequency for all neurons. The response of a neuron for a given orientation is defined as the strongest response of that neuron to the sine gratings of given orientation, across all phases. As illustrated in figure 4.8, in layer 4C all examined neurons had narrow orientation tuning with realistically shaped tuning curves [6]. Similarly, in layer 2/3, many neurons have realistic tuning properties, although some neurons have elevated responses to a wide range of orientations and are overall less well tuned. On average, we observed that neurons in layer 2/3 were more broadly tuned to orientation compared with neurons in layer 4Cβ, which follows observations from some experimental studies [155]. Furthermore, we also observe that all neurons in layer 4Cβ and the well-tuned neurons in layer 2/3 achieve very good contrast invariance of orientation tuning width (compare contrast=30% with contrast=90% in figure 4.8).

Finally, we also show the responses of neurons with respect to the phase of an optimally oriented sinusoidal grating. As can be seen in figure 4.9, the responses of layer 4Cβ cells, which develop high modulation ratios, are very selective to phase, with zero response for most phases and a sharp peak around their preferred phase. In contrast

to the selective response of simple cells, complex cells in the model generally show significantly elevated activity for most phases as expected given their low modulation ratios (see figure 4.7): for the example neurons in figure 4.9 one neuron shows significant response for all phases, while the other neuron does not respond at all only for a single presented phase. On the other hand, both example neurons show a clear preference for some phases, further explaining the weak phase preference maps that we observe in layer 2/3 in the model.

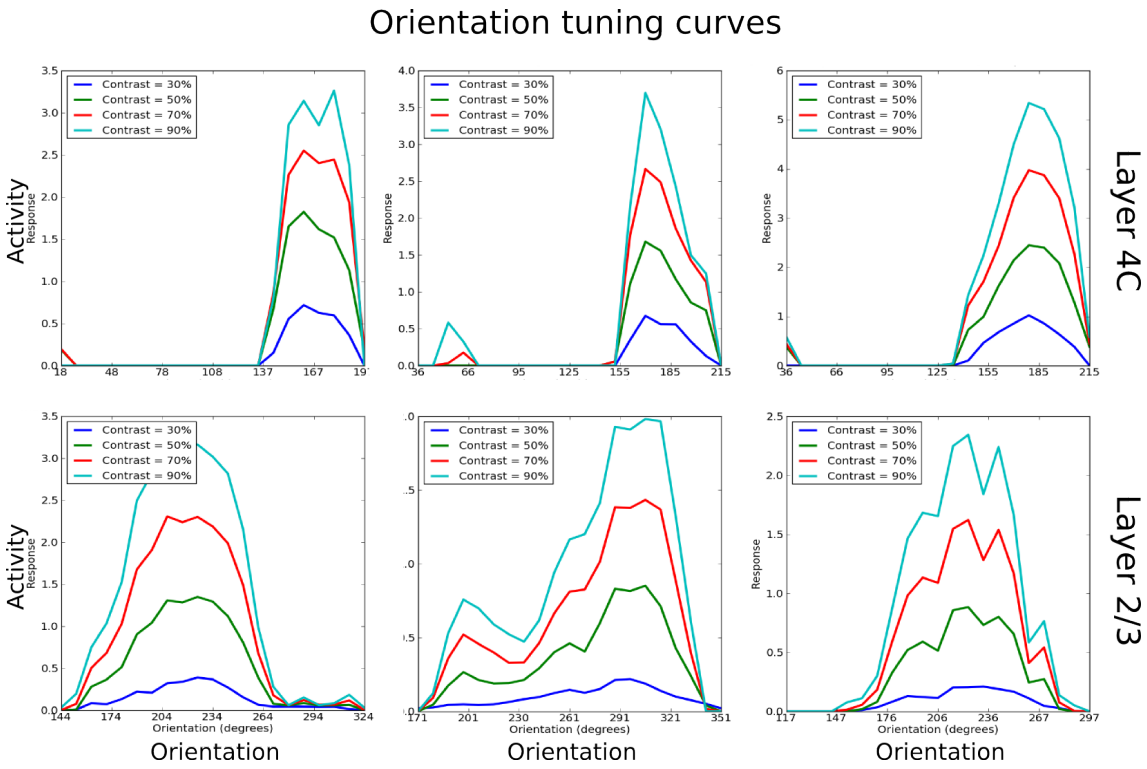

Figure 4.8: Orientation tuning curves of six representative cells, three from layer 4Cβ and three from layer 2/3. As for these examples, nearly all model neurons show contrast-invariant tuning. I.e., the shape of the tuning curve is similar across a wide range of contrasts.

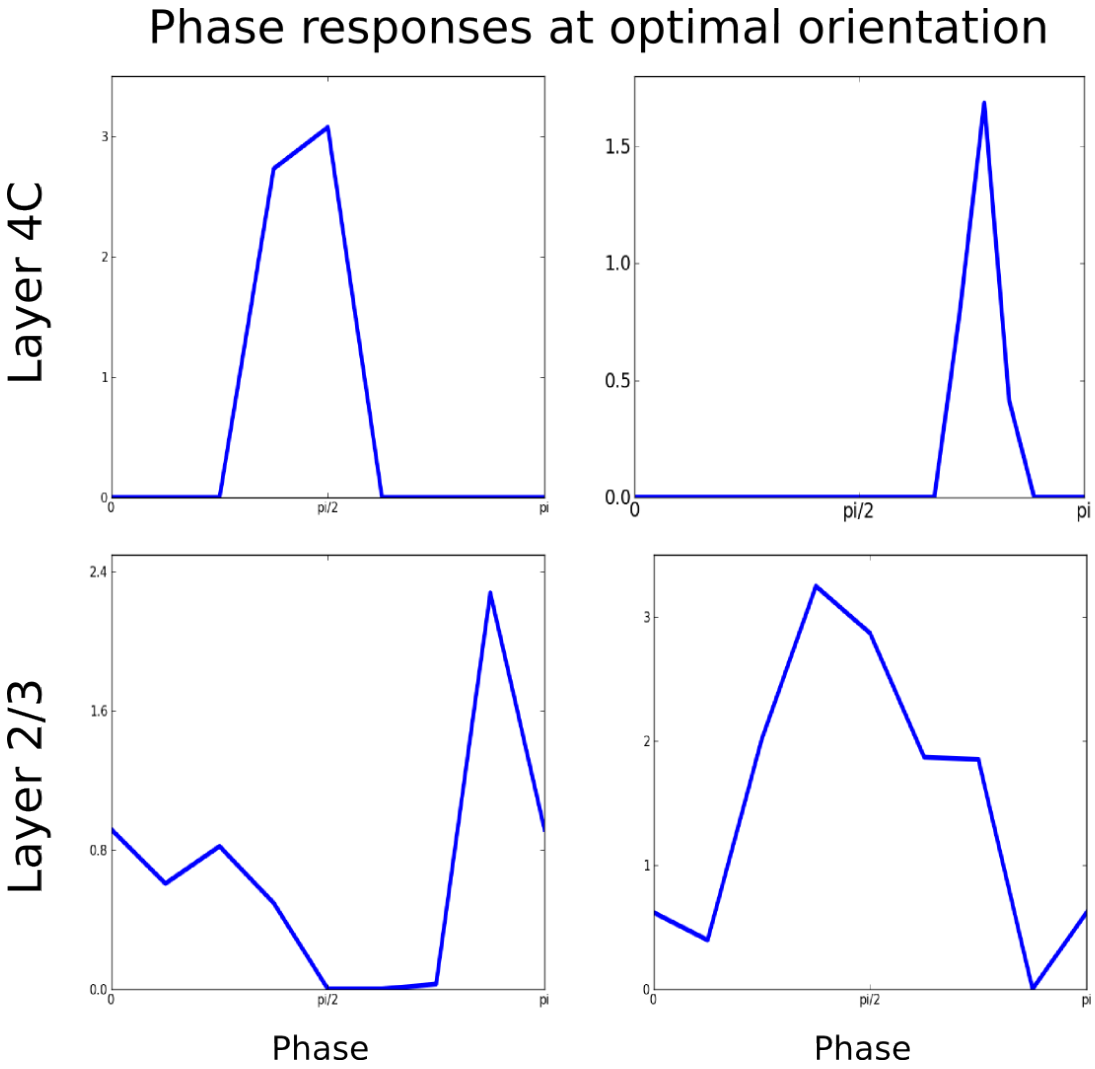

Figure 4.9: Responses of four representative cells, two from layer 4Cβ and two from layer 2/3, to the varying phase of an optimally oriented sine grating.

4.3.3 Influence of relative strength between lateral connections in layer 4$C\beta$ and layer 2/3

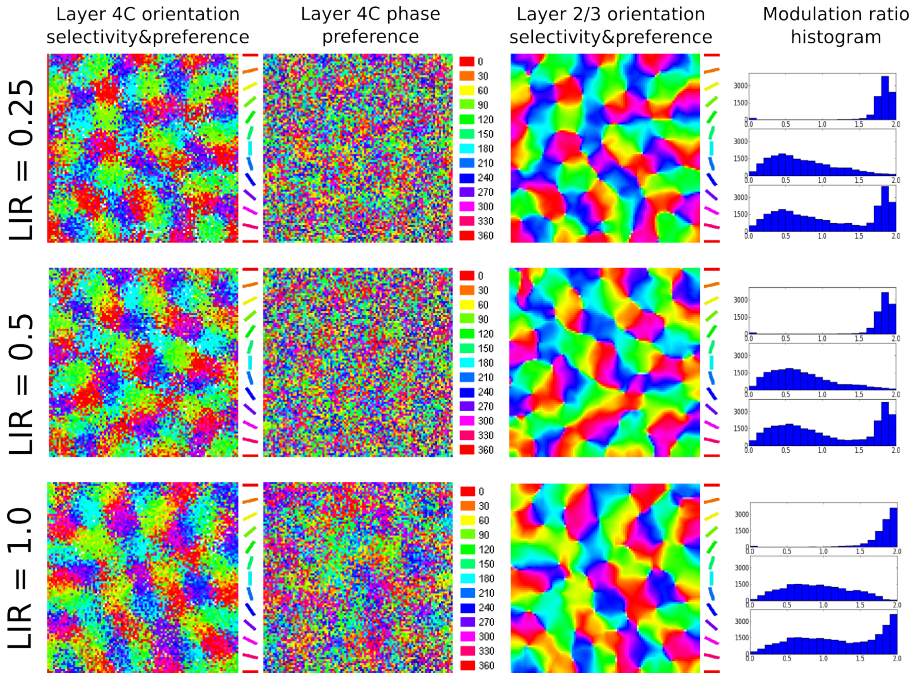

Figure 4.10: This figure demonstrates the influence of the strength of the lateral interaction in layer 4C relative to the strength of lateral interaction in layer 2/3 (the LIR). Each row shows the results of a simulation run with a different LIR. The main properties of the model do not change if we add weak lateral connectivity to layer 4C, but adding strong lateral connectivity to layer 4C causes phase clustering in layer 4C and more phase selective neurons in layer 2/3.

One of the key differences of the model from previous models of development is moving strong lateral interactions from the simple cell layer, to the complex cell layer. Layer 4C, however, does contain lateral connections, albeit about 4 times less dense than layer 2/3 (based on data from Binzegger et al. [28]). In order to test the effect of lateral connections in layer 4C, we ran several simulations with both short-range excitatory and long-range inhibitory lateral connections of identical parameters as those in layer 2/3 present in layer 4C. We varied the ratio between the strength of the lateral interaction in layer 4C and layer 2/3 (we will refer to this ratio as LIR) in order to examine the relative influence of these connections onto the model. Figure 4.10 shows that inserting weaker lateral connections to layer 4C does not significantly influence the results of the model, indicating the the model is compatible with the known weaker lateral connectivity in layer 4C. However, with increasing strength of

layer 4C lateral connections one can observe increasing clustering of phases in layer 4C and consequently layer 2/3 neurons becoming more sensitive to phase. This shows the importance of weaker lateral interactions in layer 4C as proposed.

4.3.4 Relationship between orientation map position and modulation ratio

Having a model of orientation map development with a realistic distribution of modulation ratios puts us in the unique position of being able to examine the relationship between these two features. In order to quantify the map position of a given neuron, we use the local homogeneity index (LHI) introduced by Nauhaus et. al. [142]. This index approaches 1 as the local region of the map is occupied by more similar orientation preferences, and approaches 0 as the local region is occupied by diverse orientation preferences. As figure 4.11 shows, the model exhibits a slight but clear trend of higher modulation ratios in regions with low LHI and lower modulation ratios in regions with high LHI, as confirmed by the weak but highly significant correlation ($r=-0.21$, $p<0.01$). This indicates that model neurons in the center of orientation domains tend to have lower modulation ratios than those located near singularities or fractures in the orientation map, and represents a clear prediction for future experiments.

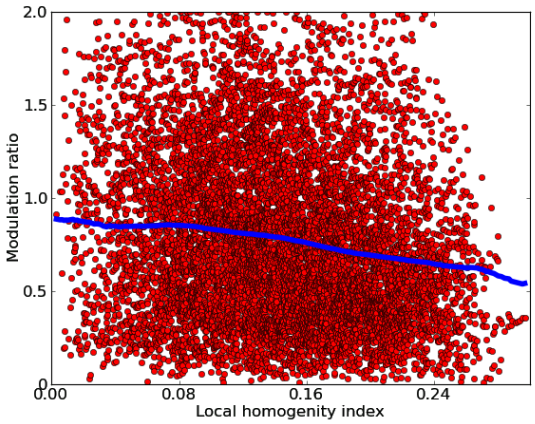

Figure 4.11: The relationship between local homogeneity index and modulation ratio. Each red point in this graph corresponds to a single neuron in layer 2/3 of the model. The x axis shows the LHI at the given neuron's position and the y axis shows its modulation ratio. The blue dots show the sliding average of the distribution. A clear trend of decreasing modulation ratio with increasing LHI index is apparent, as confirmed by the weak but highly significant correlation ($r=-0.21, p<0.01$).

4.4 Discussion

The majority of models of functional map development use a Mexican-hat profile of lateral interactions as the main driving force for map development [79, 132, 198, 149, 41]. These lateral interactions ensure that throughout development, the activity in the network is strongly correlated at short ranges and is anti-correlated at medium ranges. This results in identical or very similar RFs develop among proximate neurons, whereas neurons at medium ranges develop different RFs. This description of map development shows the conflict of such mechanisms with the existence of disordered phase representation in V1: cells with increasingly different phase preference should have increasingly anti-correlated activities, but Mexican-hat lateral connectivity leads to neurons in a local vicinity being correlated. Hence such models, in the absence of additional features, will develop a smooth phase representation, contrary to the experimental evidence.

Here we propose a model that provides a resolution to this conflict. The first key idea is to weaken the lateral interactions in the layer that is, after development, predominantly occupied by simple cells and receives direct thalamic input, and introduce them to the layer that is occupied by complex cells and does not receive direct thalamic input. This makes our two model cortical sheets a homologue of cortical layer 4C (which does receive the direct thalamic input and has weaker lateral connections) and layer 2/3 (which does not receive direct thalamic input, but rather its afferent input comes from layer 4 and has stronger lateral connections). The second essential ingredient of the model is the feedback connectivity from layer 2/3 to layer 4C, which ensures that matching maps can develop in both layers. This type of connectivity is supported experimentally, with evidence of a strong feedback pathway from layer 2/3 via layer 5 and 6 back to layer 4C [27, 5].

Finally, we introduce several realistic sources of variability in the model, which ensure that the initial responses of neurons in layer 4C are sufficiently non-uniform. As the results from the simulations show (see figure 4.6), these changes are sufficient to allow for disordered phase representation to develop in layer 4C. Once layer 4C has a disordered phase representation, complex cells are constructed very simply by pooling across a local area of simple cells.

As we discussed before, there is experimental evidence that layer 4C contains predominantly simple cells, and that layer 2/3 contains predominantly complex cells. However, experimental studies also clearly show that this difference is not as clear cut

in macaque as in the model, where almost all cells in layer 2/3 are classified as complex and nearly all cells in layer 4C are classified as simple (figure 4.7). In the model, the relative contributions of the different projections to a given neuron are fixed across each sheet. One obvious way to make the MR index of neurons in both simulated sheets more varied would be to introduce some variability in the projection strength for individual neurons. This would ensure that both in layer 4C and 2/3 the ratio between the contribution from lateral and afferent connections would become more variable, which in turn would induce more variable final MR indexes of individual neurons. However, this additional variability of projection strength among individual neurons would have to stay within the overall large-scale architecture proposed here, as this architecture is crucial for proper development of all the functional properties discussed here.

Another simplification we introduced to the model is the use of homeostatic plasticity described in chapter 3 only for neurons in layer 4C. This both simplifies the model, making the reasoning about its dynamics easier, and also saves computational resources. Note that because the only input to layer 2/3 is from layer 4C, the homeostatic control in layer 4C implicitly also controls the average firing rates of layer 2/3 neurons, and can thus ensure that their activity remains in linear region of their f-I curve. However, at the same time the average firing rates in layer 2/3 need not be the same as in layer 4C and are rather dependent on the other layer 2/3 parameters, such as the strength of afferent or lateral connections. At the same time, it is likely that homeostatic mechanisms are present in animal layer 2/3 cells, as they need to compensate for changing inputs from other sources not included in our model or because the statistics of firing need to be controlled in greater detail than just at the level of average firing rate as in our model. However, our results show that the simple homeostatic mechanism in layer 4C is sufficient to explain the development of all the V1 properties demonstrated in this chapter. Further studies will have to be undertaken to fully understand the underlying mechanisms and role of homeostasis across different cortical layers and areas before more accurate models of this type of plasticity can be constructed.

All previous models of complex cell map development, including the one presented in this chapter, depend on a locally disordered representation of phase to ensure phase invariant response of the complex cells, that pool from a local region of simple cells. The details of phase preference organization in V1 are controversial, with some studies showing that nearby neurons tend to have similar phase preference [16], whereas others have shown that nearby neurons tend to prefer opposite phases [122]. Furthermore,

a study by DeAngelis showing that relative phase preference of nearby neurons is random has added to the confusion, as it has been often incorrectly cited as evidence of random absolute phase representation. Randomness in relative RF shape, i.e. relative phase randomness, is not useful for constructing complex cells; only variety in absolute phase preference is helpful.

Despite these controversies, all these studies show that spatial phase is much less organized than orientation and one can thus find a range of phases represented in a local region of V1. Furthermore, limited clustering of phase in V1 can still lead to cells that have elevated activities in response to all phases of an optimally oriented sinusoidal grating, which in turn will ensure they are categorized as complex cells based on the F1/F0 ratio. On the other hand, even many complex cells will thus respond stronger to some phases — those over represented in their local pool of simple cells — than to others, giving them phase preference (albeit weak). Note that this is perfectly consistent with the F0/F1 categorization, as only cells with 0 MR will have 'perfectly invariant' response to phases, as demonstrated in references [59, 155]. A second consequence of such limited clustering of phase preferences of simple cells is that nearby complex cells — pooling from overlapping sets of simple cells — will also have correlated phase preference. The model in this chapter is in line with all the above predictions stemming from limited local clustering of phase preference.

In stark contrast to the highly disordered phase representation in layer 4C, the model predicts that nearby neurons in layer 2/3 develop strongly correlated phase preference, again a phenomenon predicted by clustering of phase preference among simple cells and local activity pooling by complex cells. It will be interesting to see whether future two-photon imaging experiments or advances in optical imaging techniques will be able to confirm this strong local correlation of (weak) phase preference among complex cells that our model predicts. Note that the predicted layer 4C and 2/3 organization differs markedly from the patterns predicted by Hyvärinen et al. [99] and Olson et al. [149] models. Due to the squaring of negative activities, the Hyvärinen et al. model predicts perfectly random phase preference of simple cells, as confirmed by the phase preference map shown in the paper. Even though Olson et al. do not directly show the phase preference maps, it is reasonable to conclude their model will also not predict clustering of phase preference of simple cells, due to the enforcement of pairs of simple cells to develop opposite phases.

An interesting characteristic of the model is that the formation of complex-cell-like RFs in layer 2/3 of the model assumes the existence of simple cells in layer 4Cβ.

On the other hand, the strong lateral connectivity that is the driving force not only of map but also of RF development is situated in layer 2/3, meaning the receptive field development of simple cells in layer 4Cβ is largely driven by feedback from complex cells in layer 2/3. To put it simply, the model uses a form of bootstrapping, where the development of complex cells requires the development of simple cells, and vice versa. The simulations show that with the correct parametrization, the dynamics of the model allow for such bootstrapping to work. In the model, sufficiently strong lateral interactions are required not only for orientation preference map formation but also RF development. Because the model assumes only relatively weak lateral interaction in layer 4C, removing the feedback from layer 2/3 to layer 4C in the model prevents the neurons in layer 4C from developing oriented receptive fields, which in turn will prevent these properties appearing in layer 2/3. Therefore, the model predicts that the development of simple and complex cells cannot be decoupled and has to take place over the same time period.

Another interesting aspect of the model is the feedback connectivity from layer 2/3 to layer 4C. There are relatively few previous modeling studies looking at feedback from higher-level areas to earlier visual areas [161] or the role of intra-areal feedback. The model shows that one role of the strong (albeit indirect) feedback pathway from layer 2/3 to layer 4C can be to ensure that similar selectivity for various features of the input (such as orientation) develops across the cortical layers. Furthermore, in the future, the model can provide insight into how the intra-areal feedback influences the properties of individual neurons in adult cortex, by measuring various properties of layer 4C neurons with feedback from layer 2/3 switched off.

As discussed in detail at the end of section 2, the dynamics in the network ensure a relatively stable activity profile on a larger scale in both layer 2/3 and 4C if the input pattern does not change dramatically, but at the same time, they allow layer 4C neurons to locally change activations in response to smaller changes in input. This behavior allows neurons in layer 4C to respond to changes of phase as the input pattern is translated over short periods of time, while on a larger scale, activity profile in the whole network is kept stable. These dynamics, together with Hebbian learning, can locally lead to development of cells selective to variety of phases in layer 4C and at the same time — on a larger scale — orientation maps can develop in both cortical layers, with neurons in layer 2/3 becoming phase invariant. One can see that in this way the model exploits the temporal correlations in the input to achieve the above properties. It is thus possible to relate the model to learning algorithms such as slow feature analysis

[207] or the trace rule [73]. In the latter case, Földiák's model uses a layer of oriented filters (spanning full range of orientations and phases), and a second layer of neurons initially fully connected with the fixed layer of filters. He defines a temporal learning rule — the trace rule — that performs the Hebbian update of the weights based on not only the current but also previous input activities (with decreasing weighting of activities in the past), that governs the development of these feed-forward connections. When such a network is presented with a series of sweeping bars of various orientations, due to the temporal correlations between inputs of the same orientation but various phases, and due to the trace rule, the afferent connections between the two model sheets develop such that each neuron in the second sheet receives strong inputs from filters of the same orientation but different phases, causing neurons in the second sheet to obtain phase invariant response. Note that this final configuration corresponds to the one developing in our model — e.g. neurons in L2/3 in our model will generally at the end of development receive inputs from neurons in L4C of the same orientation but variety of phases. This shows that one can potentially substitute a more elaborate learning rule with an appropriate combination of dynamics in the network and a simple Hebbian learning rule, explaining how one can implement these advanced learning rules in a more biologically plausible framework.

To the best of our knowledge, all previous developmental models of visual cortex that include lateral interactions place them in the layer containing simple cells. Although anatomical studies show that layer 4C contains lateral connections, they are significantly weaker [27, 92, 55] and shorter [173, 157, 28] than those present in layer 2/3. Also, the lateral connectivity in layer 4C does not express the orientation specific daisy pattern characteristic of the layer 2/3 lateral connections [173, 157], which have been implicated in a number of functional properties of neurons in V1 such as orientation-selective surround modulation [107, 117]. Although the previous models of cortical circuitry with strong lateral interactions between simple cells are not directly in conflict with experimental evidence, the experimental data highlight the need to explore models that consider layer 2/3 and complex cells as the main source of lateral interactions. In this respect, the model shows that it is possible to develop orientation maps in both layer 4C and layer 2/3 without any (or only weak) lateral connectivity within layer 4C. This result is largely due to feedback from layer 2/3 to layer 4C. Furthermore, neurons in layer 4C exhibit properties (for example the orientation specific surround modulation) which are linked to the daisy-like pattern of lateral connections in layer 2/3 that is lacking in layer 4C. The proposed feedback mechanism could ex-

plain the missing link between these functional properties of layer 4C neurons and the anatomical features in layer 2/3 that are often believed to be responsible for them.

Another important advance from previous modeling studies of V1 map development is that the model has realistic single-cell responses in both simulated cortical layers, as demonstrated in figure 4.8. Previous developmental studies have paid little attention to the more detailed properties of single cells such as the shape and sharpness of orientation tuning curves. In the model, individual simple and complex cells develop realistic orientation tuning curves. Also, neurons in both categories achieve realistic contrast invariance of the width of the orientation tuning curves. Replicating these features is crucial for explaining how the neurons actually operate for visual inputs. Finally, in accordance with the experimental evidence, the model correctly predicts broader orientation tuning for complex cells than for simple cells. The fact that the model follows these additional constraints imposed by experimental studies, and that we have not intentionally sought them when designing the model, make us even more confident that the important new features of the model (the strong lateral connectivity in layer 2/3 with weak lateral connectivity in layer 4C, and feedback from layer 2/3 to layer 4C) reflect V1 architecture.

The large number of V1 properties that the model can demonstrate and the possibility to relate the model directly to anatomical properties of V1 comes at a cost. The model is complicated, both analytically and computationally, and contains a large number of free parameters. Where possible, we constrained these parameters to values known from experimental studies, but for most parameters the values of their biological counterparts are not known. These free parameters have been set through extensive empirical search, where the criterion was to find a model parametrization that follows all the constraints from experimental studies that we focus on in this study, i.e. variable phase preference development in layer 4C, complex cell development in layer 2/3, and realistic orientation map shape. Due to the large number of free parameters and the high computational requirements of each simulation run (about 48 hours on a modern CPU with 8GB of memory), it is not possible to perform a rigorous parameter search to outline the region of parameter combinations in which we can achieve all the presented results.

The limited empirical parameter search that was possible to perform does suggest that there are parameters to which the model is sensitive particularly the balance between the various projection strengths. It is unrealistic to assume each V1 neuron will have precisely balanced strength of connections from the different projections, but it is

reasonable to assume this to be true on average for a local population of neurons. It is also likely that these and other free parameters of the model are actively regulated in animal V1.

Overall, our work diverges from the more common approach to build the simplest possible model that explains only a few properties of a system, but rather trades simplicity for the ability to explain a large number of properties in single model. Because the brain is a significantly non-homogeneous and non-linear system, we believe such a modeling approach is inevitable, if we want to have a single consistent explanation for how the cortex works. At the same time, however, the approach highlights the importance of simple models, as it builds on top of many insights obtained from them. Our work also shows that constructing such more complex models has the advantage of bringing insight into interactions between the various properties of V1, as demonstrated by the predictions we have formulated in this chapter. Particularly, we predict limited but measurable clustering of the strong phase preferences in layer 4C, clear and smooth clustering of the weak phase preferences of complex cells in layer 2/3, and a tendency for neurons located at non-homogeneities in the orientation maps to have higher modulation ratios.

Chapter 5

Surround modulation in V1

5.1 Introduction

Natural vision is a complex process where the perception of local visual features can depend on the spatial arrangement of the surrounding visual stimuli. This context dependence is evident even in the earliest stages of the visual system, including the retina, LGN and V1. By definition, presentation of a visual stimulus outside the RF will not elicit a response in the neuron. Experimental studies have shown, however, that if we present a stimulus to the RF of a neuron in V1, by itself eliciting a certain firing rate, that firing rate can be enhanced or suppressed by presenting a second stimulus in the RF surround [32, 60, 195]. I.e., visual stimuli outside a neuron's RF can modulate its firing rate. This phenomenon is referred to in the literature as **contextual modulation**, **surround modulation**, or in some conditions **surround suppression**.

Surround modulation in the early visual system of cat and macaque has been studied extensively with systematic effects consistent across species found. Surround modulation has been implicated in a number of important perceptual phenomena, such as contour integration, figure-ground segregation, and attention [7, 117, 156]. Surround modulation might, therefore, represent an important link between early- and high-level vision, which highlights the importance of a detailed understanding of its function and the neural substrate and mechanisms underlying it. For a comprehensive review of literature on surround modulation in the early visual system, see ref. [11].

As discussed in section 2.1.4, an important potential substrate for the surround modulation effects in V1 are the short and long range lateral connections in the superficial cortical layers (2/3). Interestingly, lateral connections are also implicated in the formation of functional maps in V1, being the source of Mexican-hat lateral interac-

tions as illustrated in previous chapters [200]. Thus lateral connectivity binds two very different V1 phenomena, operating at different time scales yet to our knowledge, long-term map development and short-term surround modulation have not been yet studied in a single model. The main goal of this chapter, therefore, is to create a model that shows how orientation and position preference maps with functionally specific lateral connectivity can develop, and at the same time show that these specific connection patterns in the developed model replicate the SM properties of adult V1 known from experimental studies.

5.2 Background

The most common experimental paradigm for studying surround modulation, which we have also adopted in this study, is to use sine-grating stimuli to stimulate the RF and RF surround of a neuron. Experimental studies have so far mainly focused on describing whether the surround modulation has a facilitatory or suppressive effect, depending on the various configurations of the center and surround stimulating sine gratings, and on identifying the spatial extents at which these effects occur. In the following paragraphs we will discuss this literature in greater detail.

The earliest studies of surround modulation employed the simplest stimulation paradigm, using a single sine-grating patch with variable aperture. In a typical experiment, the optimal orientation and spatial frequency for a given neuron are determined, and subsequently the neuron's responses are measured for a sequence of sine gratings of optimal orientation and spatial frequency, but variable spatial extents (see figure 5.1a). In this way, the neuron's size tuning curve (STC) is measured. A schematic example of a representative STC of a V1 neuron is shown in figure 5.2. This curve characterizes the behavior of a typical V1 neuron at high contrast: its firing rate initially increases as the extent of the stimulating sine grating increases up to certain extent, at which point it starts to decline and eventually asymptotes. The extent at which the firing rate of the neuron stops increasing is referred to as the high-contrast summation RF (hsRF) [12] illustrated in figure 5.1b. If we perform the same experiment but with a low contrast sine grating, we will obtain a similar tuning curve, except that, in a typical cell, the peak shifts to the right. The peak of the low contrast STC is referred to as the low-contrast summation field (lsRF) [12] illustrated in figure 5.1b. The region between the hsRF and lsRF is also often referred to as the 'near surround', and the region beyond the lsRF as the 'far surround'.

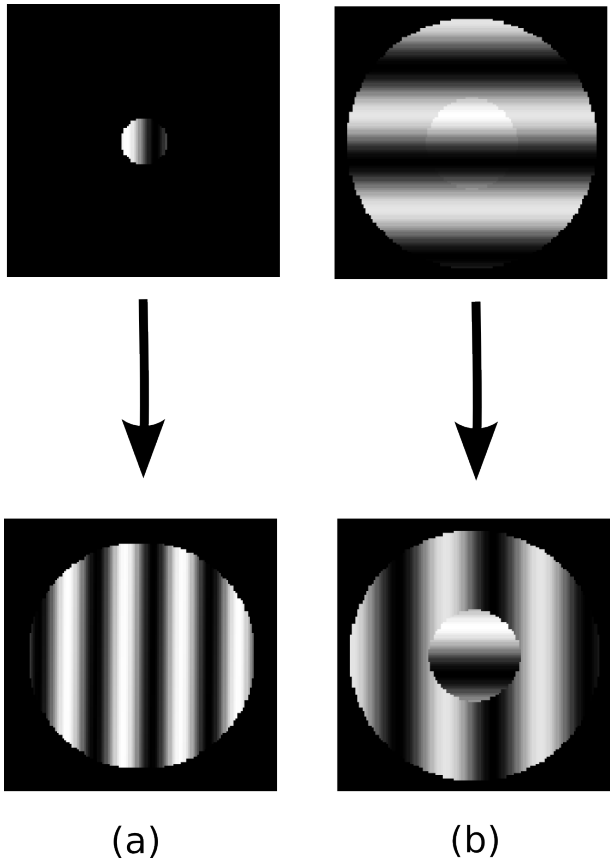

Figure 5.1: Example visual stimuli used to probe surround modulation properties of V1 neurons. (a) The STC is measured with sine grating patches of optimal orientation and spatial frequency and increasing size. (b) Orientation contrast response is measured by fixing the central sine-grating patch to have optimal orientation, size and spatial frequency for the given neuron, while varying the orientation of the surrounding sine grating disk (which has the same spatial frequency).

To further quantify the properties of the STC, a suppression index (SI) has been defined:

$$SI = \frac{R_{opt} - R_{sup}}{R_{opt}}$$

where R_{opt} is the response of the neuron at optimal grating extent and R_{sup} is the response of the neuron once it asymptotes [49, 196, 184]. We also define the contrast dependent summation shift (CSS) as:

$$CSS = \frac{\delta_{opt}^{low}}{\delta_{opt}^{high}}$$

where δ_{opt}^{low} is the radius of the optimal sine-grating patch at low contrast and δ_{opt}^{high} is the radius of the optimal sine-grating patch at high contrast. Both the SI and CSS parameters have been quantified for macaque and cat in several studies. The average SI over the V1 neuron population reported are 0.16 [184] and 0.44 [196] for cat, and 0.33 [184] and 0.38 [49] for macaque. CSS has been measured as 1.33 [196] and 1.36 [184] in cat, and 2.3 [160] in macaque.

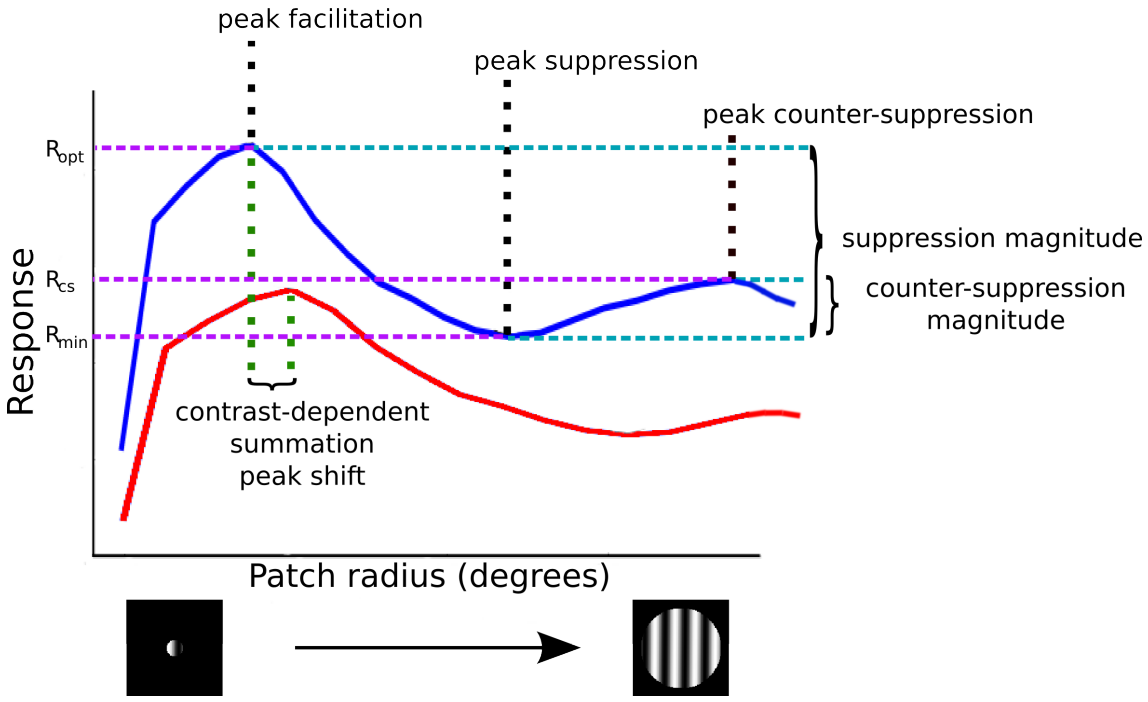

Figure 5.2: A stereotypical STC, overlaid with a description of the measures that we compute in this study.

Recently it has been shown that this relatively simple description of size tuning must be further extended to account for additional phenomena. It has been noted that

in many neurons the surround suppression is reduced at certain extents, as shown in figure 5.2. This reduction can be quantified by the counter suppression index (CSI):

$$CSI = \frac{R_{cs} - R_{min}}{R_{opt}}$$

where R_{opt} is defined as above, R_{min} is the minimal response of the neuron after R_{opt}, and R_{cs} is defined as the maximum response after R_{min} [196]. The existence of counter suppression was first pointed out in a modeling study by Schwabe et al. [161]. After counter suppression was observed in their model, Schwabe et al. identified it in the data of several existing studies. This phenomenon was overlooked probably because of the relatively coarse sampling of the sine-grating patch size in most studies, and also the use of a difference-of-Gaussians model for fitting the STC, which is not able to capture the counter-suppression component. We are aware of only two experimental studies that have so far investigated counter suppression in greater detail, the first by Ichida et al. [100] and the second by Wang et al. [196]. The latter study found the average CSI to be 0.19 in cat.

So far we have discussed aspects of surround modulation that can be revealed by using only a single sine grating to stimulate the RF and RF surround of the neuron. Many previous experimental studies of surround modulation have extended this paradigm by using two sine-grating stimuli: one (of optimal orientation) to stimulate the center, and a second (whose parameters are typically varied) to stimulate the surround (see figure 5.1b). A distinctive property of surround modulation that can be revealed by this stimulation paradigm is the orientation specificity of the surround. Although the results of these studies have been less clear than in the case of size tuning, the general effect is that if one stimulates the RF center with a sine-grating patch of optimal parameters, presentation of a second grating of the same orientation in the surround will suppress the response of the neuron but a cross-oriented grating will elicit less suppression, or even facilitation [107, 117, 115, 32] (see figure 5.3). Finally let us note that generally, no significant differences in surround modulation between simple and complex cells have been found [106, 160, 165, 184, 196, 107, 49].

So far we have only discussed the functional aspects of surround modulation. However, another important question is what the underlying substrate is that is responsible for this phenomenon. Three main sources are implicated in surround modulation in V1: feed-forward, lateral, and feedback. Surround modulation has been identified by a number of studies at the earliest stages of visual processing, both in retinal ganglion cells [174] and LGN [35, 159]. These surround-modulation effects can therefore be

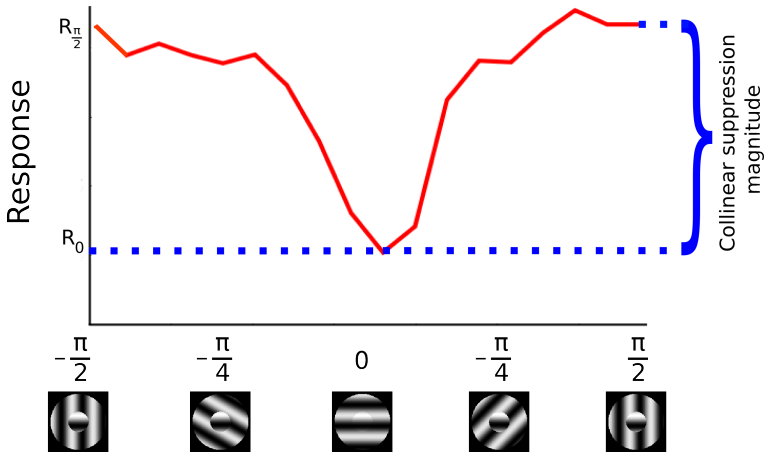

Figure 5.3: A stereotypical orientation contrast tuning curve (ORTC), overlaid with the description of the main measure that we compute in this study. The x axis shows the relative orientation of the surround with respect to the central sine-grating patch.

passed onto V1 via feed-forward connections. There is, however, substantial evidence that these areas cannot be the sole source of surround modulation in V1: the surround modulation in LGN does not seem to be sufficiently strong or sufficient in spatial extent, and the orientation dependence of surround modulation in V1 is not compatible with the orientation un-selective cells in the LGN [166].

The most obvious candidate for the underlying substrate of surround modulation in V1 is the intra-areal lateral connectivity. The extent of long-range lateral connections in V1 layer 2/3 is known to be sufficiently spatially extended to account monosynaptically for most of the spatial extent of surround modulation. Furthermore the known orientation preference specific bias of this connectivity offers an obvious explanation for the orientation dependent aspects of surround modulation.

There is a longstanding debate about the role of feed-back connections from higher level visual areas (such as area V2 or V4) in V1 surround modulation. Cortical cooling studies have shown that deactivating higher-level visual areas leads to a decrease in the magnitude of surround modulation effects [98]. Furthermore, another line of evidence based on the timing of surround modulation onset in V1 suggests that feed-back connections are required: the onset of surround modulation, even if only the far surround is stimulated, is very fast [18]. Several studies have examined the speed of propagation of action potentials along lateral and feed-back cortical connections, showing that lateral connectivity is significantly slower [40] than feed-back connectivity [97]. Together with the fast onset of far-surround modulation, this indicates that

the far-surround modulation is at least partially mediated via feed-back connections. In this chapter we focus on the lateral connections, but in future work the model can be extended to include feedback.

The first large scale model to show how surround modulation could arise from the lateral connectivity in V1 was by Somers et al. [177]. This model works with a two dimensional grid of both excitatory and inhibitory neurons, interconnected via short range and long range lateral connections. The afferent receptive fields of individual neurons, and the strength of the long range lateral connections are determined by their position in an overlaid experimentally measured orientation map. The main contribution of this study is that it shows how the lateral connectivity in V1 can lead to size tuning. It correctly predicts the expansion of the summation at low contrast, and it also replicates the dependence of the magnitude of surround suppression on the orientation of the surround.

Wielaard et al. [204] proposed a model of similar architecture with a two dimensional grid of neurons initialized with an orientation map. The most important architectural difference from the Somers et al. study is that it explicitly assumes only local lateral connectivity. An advantage of this study was that the individual neurons in the model showed a number of basic functional properties such as orientation preference and a realistic distribution of modulation ratios. With this architecture Wielaard et al. were able to show basic size tuning properties including the expansion of summation at low contrast. However, without orientation-specific long range lateral connectivity, this model cannot explain the orientation-specific surround modulation.

The most recent model of surround modulation comes from Schwabe et al. [161]. Unlike the two previously discussed studies, the Schwabe et al. model is only one dimensional, representing orientation columns along a hypothetical line lying along the V1 surface. For the previously described studies, this model simulates a single layer of both excitatory and inhibitory neurons, laterally interconnected via both short and long range lateral connections. As for the Somers et al. model, the authors do not demonstrate the basic realistic functional properties of neurons such as orientation tuning or phase invariance. The main novelty of this study is the addition of extra-striate feedback connections. The model replicates the basic size tuning properties of V1 neurons, but without orientation-specific neurons the model cannot replicate the orientation contrast effects, as in Wielaard study. Unlike both previous studies, this model predicts counter suppression. The main contribution from Schwabe et al. is to demonstrate how surround modulation effects, at very large distances (beyond the

monosynaptic reach of long range lateral connections), can be explained by inclusion of extra-striate feedback into the model.

As discussed above, the lateral connections in layer 2/3 are implicated in both surround modulation and the development of V1 orientation preference maps [194]. Previous modeling studies have shown that lateral short range excitatory and long range inhibitory connections, in combination with Hebbian learning of afferent connections, can explain the development of oriented RFs and the self-organization of orientation preference maps in V1 [132]. As discussed in previous paragraphs, models of V1 surround modulation in the adult animal also rely on V1 lateral connectivity. We are not aware of any computational modeling study that tries to reconcile these two different roles of lateral connectivity in a single model. The main aim of this study is to address this issue, by constructing a single computational model of V1, based on known connectivity, that shows both how orientation maps in V1 can develop and at the same time how individual neurons in the model acquire surround modulation properties, through the same developmental mechanisms. Furthermore, a developmental model of orientation maps and surround modulation manifests various in-homogeneities stemming from the orientation maps and patchy lateral connectivity, allowing us to link some of the experimentally observed variation in SM properties to the position of neurons within the orientation maps. Finally, neurons in our model express realistic basic functional properties while replicating the orientation-specific properties of surround modulation. Thus, we unify previous modeling approaches while showing how their combination can explain the diversity of effects observed experimentally.

The model presented in this chapter is an extension of the complex cell map development model introduced in chapter 4. Until recently, all previous models of map development that are dependent on lateral connectivity, used short-range excitatory and long-range inhibitory connections. However, this configuration is in contradiction with the anatomical evidence showing that most inhibitory neurons have only short-range axonal arbors, and the long-range lateral connections originate in layer 2/3 pyramidal neurons and primarily target other excitatory neurons [91, 200, 76]. Judith Law has recently overcome this discrepancy, by designing a new model — LESI [119] — which extends the cortical sheet into two layers, one with excitatory neurons and one with inhibitory neurons. The lateral connectivity of this model follows the anatomical evidence, and at the same time this model shows how orientation preference maps and patchy lateral connectivity can develop. Here, we extend the model from chapter 4 such that the lateral connectivity in layer 2/3 follows the realistic architecture

of the LESI model. The resulting model of V1 development has realistic lateral connectivity in layer 2/3, explains how orientation maps can develop both in layer 4Cβ and layer 2/3, and exhibits realistic surround modulation properties after development. This model thus unifies all of the modeling results in this thesis as well as those in many previously described models.

5.3 Model Description

The surround modulation model is derived from the complex cell model described in chapter 4. The dynamics of the model are defined by the same equations as those governing the model in chapter 4, described in section 4.2. The architecture of all layers other than layer 2/3 is identical to the complex cell model. In order to implement more realistic architecture of lateral connections, we have replaced layer 2/3 of the previous model with the architecture described by Law [119]. Thus we split layer 2/3 of the previous model into two layers, one simulating excitatory and the other inhibitory neurons, and add short range excitatory and inhibitory, and long range excitatory connections, as described in ref. [119]. The diagram of the resulting model can be seen in figure 5.4. The added feedback connectivity from layer 2/3 to layer 4 alters the dynamics of the whole model, and therefore we need to adjust parameters throughout the model to compensate for these changes. See table 5.1 listing the new parameter values, together with additional parameters due to the layer 2/3 modification.

5.4 Methodology

In this study we present a number of results on SM. We have attempted to replicate the experimental measuring methodology of the SM effects, namely the STC and orientation contrast curve, as closely as possible, in order to be able to compare our results with those from animal models. Although the existing studies of surround modulation use similar general principles to measure and quantify these two surround modulation curves, they differ in many details, which prevents us from devising a single paradigm that would be identical to those in all studies. However, several studies have compared some of the different measurement techniques on the same data and have found them to yield qualitatively similar results. At the same time, when one compares the reported means of various parameters of surround modulation across the existing experimental studies, one finds significant variations. Thus it is not possible to precisely

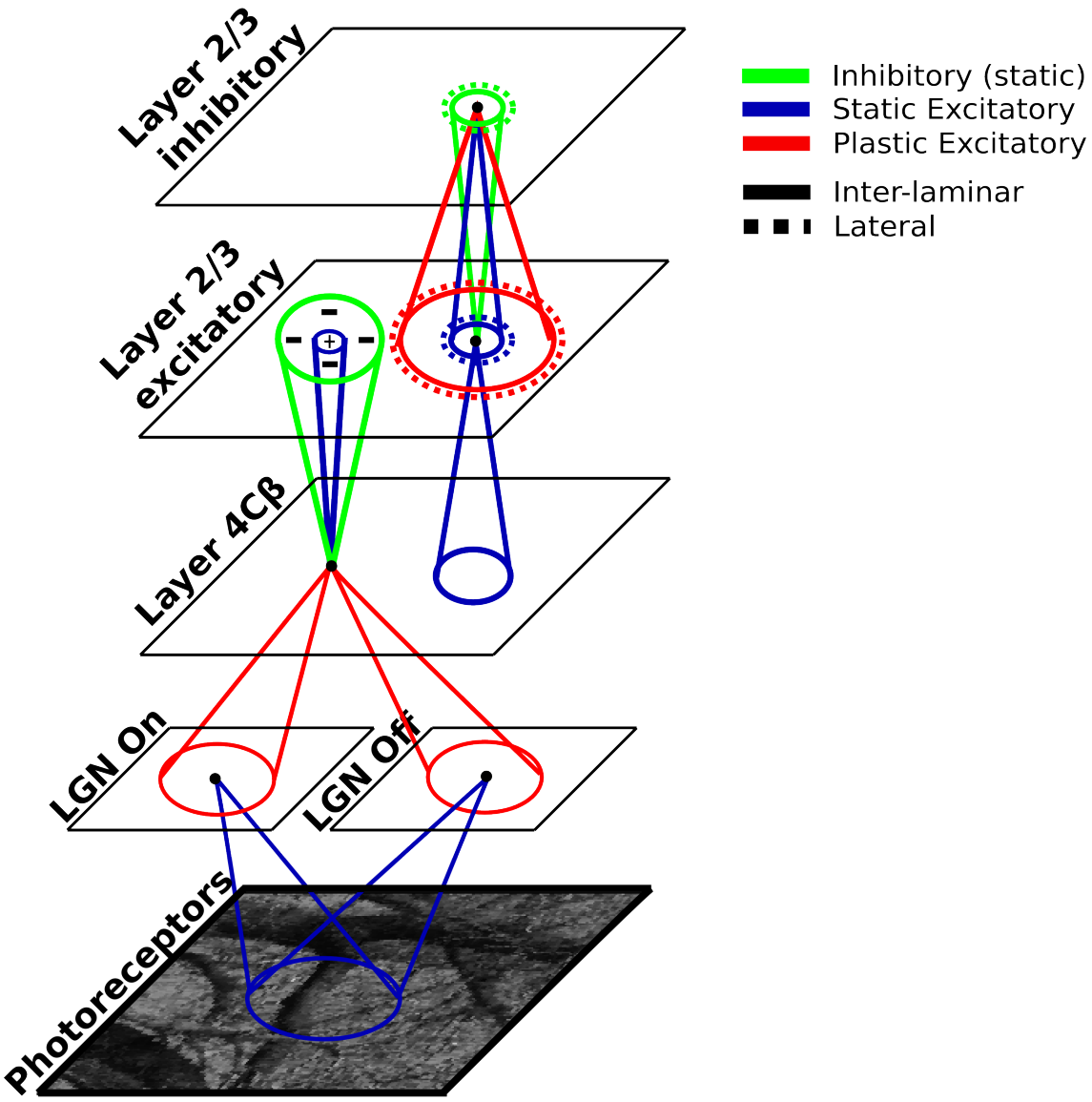

Figure 5.4: The model architecture. Each dot in this diagram represents a single unit in the indicated sheet. Each cone indicates a projections between layers to one of these neurons, and each circle indicates a set of lateral connections to that neuron within a layer. The activity propagates from the photo-receptors to the LGN On and Off sheets. From there the activity arrives at the cortical layer 4Cβ. From layer 4Cβ activity further propagates via narrow afferent connectivity to layer 2/3 excitatory neurons, where it can again spread laterally via short- and long-range excitatory lateral connections. At the same time, the activity is passed from layer 2/3 excitatory neurons to local inhibitory neurons that in turn inhibit nearby excitatory and inhibitory neurons in layer 2/3. Finally, activity also propagates back from layer 2/3 to layer 4Cβ via narrow excitatory and wider inhibitory connections.

Table 5.1: Model parameters

Symbol	Description	Value
	RGC/LGN	
γ_A	Strength of afferent projection from retina	2.33
γ_L	Strength of lateral projection	0.5
c	Slope of the gain function	0.2
	Layer $4C\beta$	
$\gamma_{\mathtt{AEOn}}$	Strength of afferent excitatory projection	-2.22
$\gamma_{\mathtt{AEOff}}$	Strength of afferent excitatory projection	5.18
$\gamma_{\mathtt{FE}}$	Strength of feedback excitatory projection	0.1
$\gamma_{\mathtt{FI}}$	Strength of feedback inhibitory projection	-2.5
$\sigma_{\mathtt{AE}}$	Kernel size of afferent excitatory projection	0.8
$\kappa_{\mathtt{AE}}$	Cut-off distance of afferent excitatory projection	0.3
$\sigma_{\mathtt{FE}}$	Kernel size of feedback excitatory projection	0.01
$\kappa_{\mathtt{FE}}$	Cut-off distance of feedback excitatory projection	0.0025
$\sigma_{\mathtt{FI}}$	Kernel size of feedback inhibitory projection	2.5
$\kappa_{\mathtt{FI}}$	Cut-off distance of feedback inhibitory projection	0.15
$\iota_{\mathtt{A}}$	Learning rate of the afferent projection	0.5
	Layer 2/3 excitatory	
$\gamma_{\mathtt{AE}}$	Strength of afferent excitatory projection	3.0
$\gamma_{\mathtt{LES}}$	Strength of short range lateral excitatory projection	1.5
$\gamma_{\mathtt{LEL}}$	Strength of long range lateral excitatory projection	0.1
$\gamma_{\mathtt{LEL}}$	Strength of inhibitory projection	0.6
$\sigma_{\mathtt{AE}}$	Kernel size of afferent excitatory projection	0.05
$\kappa_{\mathtt{AE}}$	Cut-off distance of afferent excitatory projection	0.075
$\sigma_{\mathtt{LES}}$	Kernel size of short-range lateral excitatory projection	0.08
$\kappa_{\mathtt{LES}}$	Cut-off distance of short-range lateral excitatory projection	0.12
$\sigma_{\mathtt{LEL}}$	Kernel size of long-range lateral excitatory projection	2.0
$\kappa_{\mathtt{LEL}}$	Cut-off distance of long-range lateral excitatory projection	2.0
$\sigma_{\mathtt{LEL}}$	Kernel size of inhibitory projection	0.8
$\kappa_{\mathtt{LEL}}$	Cut-off distance of inhibitory projection	0.12
$\iota_{\mathtt{L}}$	Learning rate of the lateral projection	0.3
	Layer 2/3 inhibitory	
$\gamma_{\mathtt{AE}}$	Strength of excitatory projection from layer 2/3	2.6
$\gamma_{\mathtt{LI}}$	Strength of lateral inhibitory projection	1.3
$\sigma_{\mathtt{AE}}$	Kernel size of excitatory projection from layer 2/3	0.08
$\kappa_{\mathtt{AE}}$	Cut-off distance of excitatory projection from layer 2/3	012
$\sigma_{\mathtt{LI}}$	Kernel size of lateral inhibitory projection	0.8
$\kappa_{\mathtt{LI}}$	Cut-off distance of lateral inhibitory projection	0.12
	Other	
τ	Learning rate decay time constant	160000
σ_n	The magnitude of the additive noise applied to all model neurons	0.025
$\theta_{2/3}$	The threshold of neurons in layer 2/3	0.1

fit all these parameters to accommodate all or even most experimental studies. Also, the small possible differences due to details of the alternative measurement techniques lie well within the variability observed between studies. Therefore, while assessing the plausibility of our model, we will only require the measured SM parameters to lie in the interval outlined by the experimental studies, and we will ignore the various details in which some of the measurement methodology varied between studies.

5.4.1 Size tuning analysis

In this study we focus on two different surround modulation curves, the first being the size tuning curve (STC). We measure size tuning in line with the protocols used in the experimental literature. First, in order to determine the optimal parameters of sinusoidal grating for each neuron, we measure the orientation preference and position preference of all neurons within model. Identical parameters of the receptive fields of all LGN filters in the model mean that the spatial frequency of the model neurons is virtually constant across the population. In order to save computational resources we therefore use this single known value of spatial frequency preference for all neurons. Subsequently, for each measured neuron, we present the network with a set of sine gratings of optimal orientation, position, and spatial frequency, confined to a variable aperture. For each aperture size we present the sine grating with 10 phases then pick the highest response of the neuron across these phases as the response of the neuron to the given aperture size. We can then construct the STCs, an illustration of which is in figure 5.2.

After measuring the STC we quantify a number of parameters of the curve. First we have to determine the radii at which the peak summation, the peak suppression and the peak counter suppression occurs. The exact definition of these points between different studies has varied slightly, the most important difference being that in some studies it has been computed directly from the raw tuning curves [165, 49, 106], whereas in others authors have first fit the STCs with models (of various kinds) and then derived these points from the fitted model parameters [100, 160, 184, 196]. Because the studies testing both approaches found very good agreement between the parameters derived in these two ways, and also because we can measure the STCs in our model with as great a precision as necessary, we have decided to automatically identify these points directly from data based on these criteria:

1. The summation peak δ_{max} is defined as the radius where maximum response is

achieved, across all aperture sizes.

2. The suppression peak δ_{min} is defined as the radius at which the minimum response is achieved, in the interval from δ_{max} to the maximum aperture size.

3. The counter-suppression peak δ_{cs} is defined as the radius at which the maximum response is achieved, in the interval from δ_{min} to the maximum aperture (see figure 5.2) .

The identification of these three points now allows us to define the peak summation response R_{max}, peak suppression response R_{min} and peak counter-suppression response R_{cs} as the neuron's responses at the corresponding aperture sizes. In turn, we can define the suppression index (SI) analogously to the experimental studies [196] as:

$$SI = \frac{R_{max} - R_{min}}{R_{max}}$$

and the counter suppression index [196] as:

$$CSI = \frac{R_{cs} - R_{min}}{R_{max}}$$

We also define the contrast dependent shift as

$$CSS = \frac{\delta_{max}^{low}}{\delta_{max}^{high}}$$

where δ_{max}^{low} and δ_{max}^{high} are the summation peaks at low and high contrast, respectively.

5.4.2 Orientation contrast analysis

The second aspect of surround modulation that we study is its orientation specificity, by measuring the orientation contrast tuning curve (see figure 5.3). The stimulus used to measure this curve consists of a central sine grating patch and a surrounding sine-grating ring of variable orientation (see figure 5.1b). As for the STC, we identify the optimal parameters of the sine-grating for the measured neuron. The central sine grating patch is set to have the optimal spatial frequency, orientation and position. The size of the central sine-grating patch is derived from the previously measured STC of the given neuron, as the summation peak δ_{max}. All parameters of the central sine grating except phase are kept constant during the measurement. The surrounding sine-grating ring is set to have the optimal spatial frequency and position, but its orientation is varied during the measurement. For each orientation, phase is varied such that both the

central and surrounding sine grating have the same phases ensuring they are collinear when both center and surround have the same orientation. The response of the neuron for a given orientation of the surrounding sine grating is taken as the maximum over the presented phases. We calculate the orientation contrast suppression index as:

$$OCSI = \frac{R_0 - R_{\frac{\pi}{2}}}{R_0}$$

where R_0 is the response of the neuron in the collinear condition and the $R_{\frac{\pi}{2}}$ is the response of the neuron at the orthogonal condition.

5.5 Results

The two main V1 properties that we have examined in this model are the development of orientation maps and the surround modulation properties of individual neurons after development. In this section we will present post-development results from our model. We will start by discussing the functional topological properties that have to be re-evaluated for the new model presented in this chapter. This will be followed by an examination of the qualitative properties of the two surround modulation curves we measure in this study (STC,OCTC). Next we will examine the population statistics of the surround modulation properties and compare them with experimental evidence. Finally we will present the most important predictions of this model: the various relationships between surround modulation and position in the cortical maps.

All results are from a single simulation instance run for 100000 iterations. The measure of surround modulation properties of individual neurons has to be made separately for each neuron, due to the need to center the stimuli on the neuron's receptive field. Because the computational time required to measure SM properties per neuron is very large due to the size of our model, for this study we have measured the surround modulation properties of limited set of excitatory neurons (43) in layer 2/3. Furthermore, given that the model represents only a small section of V1, edge effects can occur, which can have particularly detrimental effects on properties dependent on the long-range lateral connections, such as surround modulation. Therefore we selected the 43 measured neurons to lie in the central part (0.35×0.35) of the model layer 2/3 sheet, evenly spaced on a lattice to avoid further selection bias.

The only components of our model that undergo adaptation throughout the development are the afferent connection from LGN to layer 4Cβ and the long-range lateral excitatory connections in layer 2/3. The other lateral connections are short range and

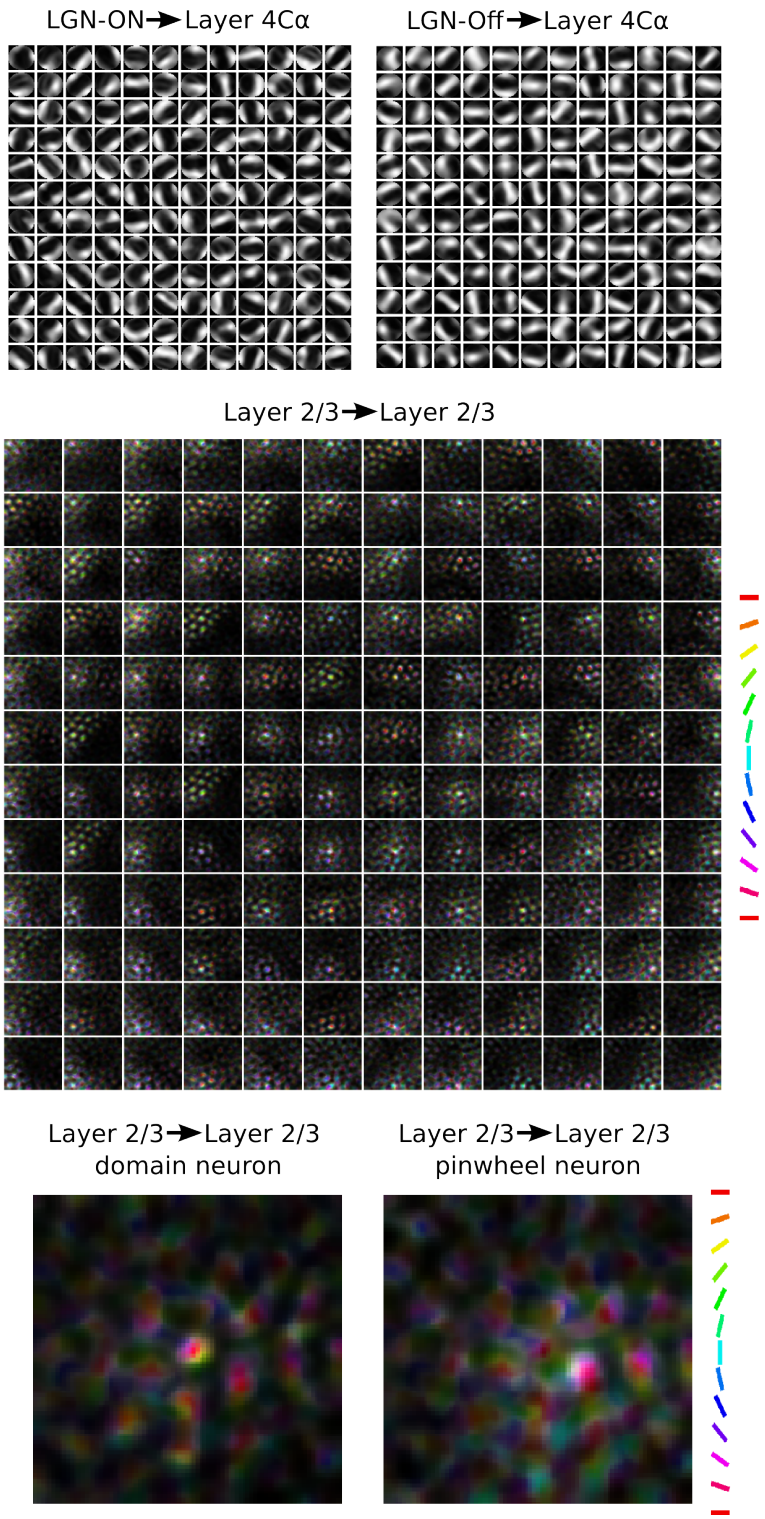

Figure 5.5: Sampling of final settled connection fields after 10000 input presentations. Top row: Weights to every 20th neuron in the projection from the On RGC/LGN layer to layer 4Cβ (left), and from the Off RGC/LGN layer to layer 4Cβ (right). Middle row: Weights to every 20th neuron in the lateral excitatory projection between excitatory neurons in layer 2/3. Bottom row: connection fields of two neurons enlarged, one located in the center of an iso-orientation domain (left) and one located at a pinwheel (right), illustrating less orientation-specific lateral connections in neurons located at map discontinuities than in iso-orientation domains. The color in the lateral excitatory projection connection fields follows the color key on the right and indicates the orientation preference of the source neurons (see figure 5.6).

remain isotropic throughout development. As can be seen in figure 5.5, the projections from both the LGN On and the LGN Off sheet to layer 4Cα developed oriented profiles, giving rise to the orientation selectivity of units in layer 4Cβ. On the other hand, the long-range excitatory lateral projections developed connections between regions with similar orientation preferences, as expected from physiological evidence [36, 173]. Furthermore, figure 5.5 illustrates that neurons located at map discontinuities after development have less orientation-specific lateral connections than neurons located in iso-orientation domains.

5.5.1 Functional topological properties

The model presented in this chapter was derived from the model discussed in chapter 4 by adding a new layer explicitly modeling inhibitory neurons, and consequently changing the architecture of lateral connections in model layer 2/3. Therefore it is important to check that the various properties of the previous model are still present.

We measured orientation and phase preference maps in both cortical sheets (figure 5.6). As can be seen in figure 5.6, the model has maintained all the functional topological properties of the complex cell model presented in chapter 4. Both sheets representing layer 2/3 developed a smooth orientation map, containing the known signatures of cortical orientation maps (such as pinwheels, linear zones, saddle points and fractures). Furthermore, at a coarser scale, orientation maps in layer 4Cβ match those in layer 2/3 (figure 5.6).

In the phase preference map measured in layer 4*C*β, one can see a very small level of clustering, just like in our model discussed in chapter 4, but the overall appearance is much more disordered than that of the orientation preference map from the same layer. This means that the new model has maintained this V1 property.

Finally, to assess whether the model cells behave like experimentally measured complex cells, we have calculated the modulation ratio index for all units. The histograms of the MR index of all cells in layers 4Cβ and in the excitatory layer 2/3 sheet can be seen in figure 5.7. As expected, according to the MR measure, the majority of neurons in layer 4Cβ are classified as simple cells whereas the majority of neurons in layer 2/3 are classified as complex cells. When cells from layer 4Cβ and layer 2/3 are pooled together one can observe the typical bimodal distribution measured in experimental studies (figure 5.7). Overall, we conclude that all the basic properties of the model introduced in chapter 4 that are relevant to this study have been maintained in

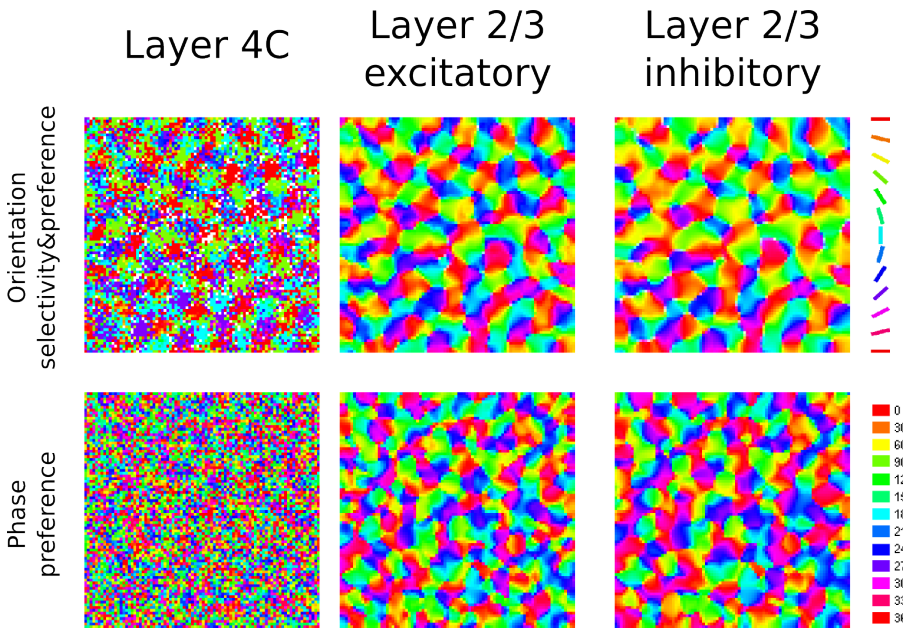

Figure 5.6: Orientation preference maps and phase preference maps in the three cortical sheets of our model after development. In the orientation selectivity plots each unit is color coded according to the orientation it prefers (as shown in the color key), and the saturation of the color indicates the level of orientation selectivity (how closely the input must match the unit's preferred orientation for it to respond). Similarly, in the phase preference map, each unit is color coded according to the absolute phase it prefers for a grating at the center of the retina, as shown in the color key.

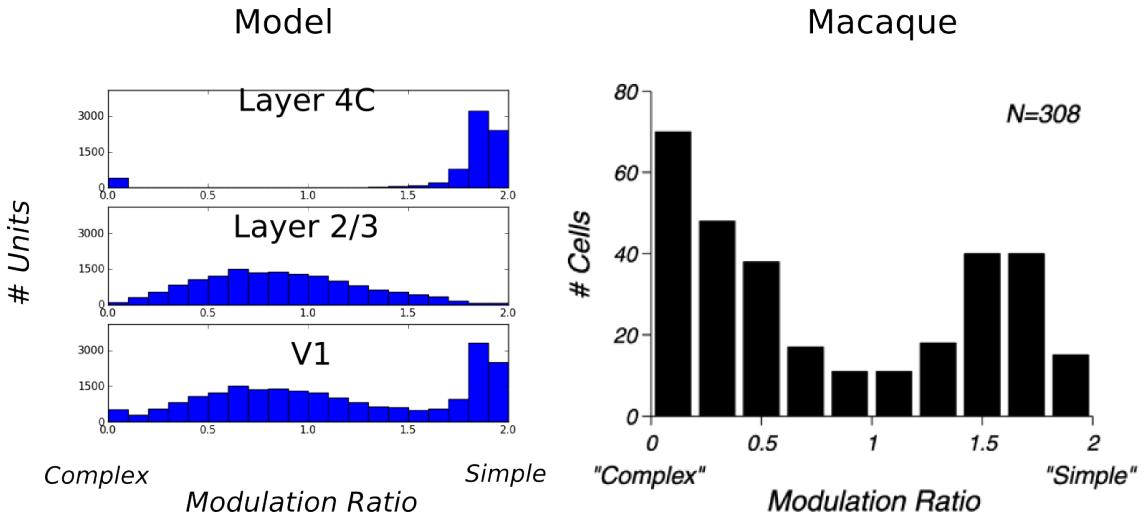

Figure 5.7: Comparison of the modulation ratio distribution in the surround modulation model and in monkey V1. Data from our model (left), and data from Old World monkey reprinted from [155] (right).

the new model.

5.5.2 Size tuning

In this section we will discuss the size tuning properties of individual neurons in the model after development. In figure 5.8 the reader can see surround modulation curves from six example neurons. The top row in figure 5.8 shows curves from three neurons that correspond well to the stereotypical STC described in experimental studies. We can see that for these neurons, the STC initially rises monotonically to its maximum response (peak summation response, δ_{max}), marked in the figure by a green arrow. After the peak, the STC monotonically drops to its minimum (the peak suppression response, δ_{min}), marked in the figure 5.8 with a red arrow. Finally, after the peak suppression, the STC rises somewhat to an eventual secondary peak (the peak counter-suppression response) marked with a blue arrow. The pattern of an initial rise followed by suppression is the stereotypical STC found in the model and is exhibited by the largest group of model neurons (16 neurons; 37%). Furthermore, if one compares the STC measured at low and high contrast, one can see a systematic shift of the summation peak to the right, another phenomenon found in many experimental studies [160, 49, 196].

In figure 5.9, we illustrate the network interactions leading to a typical STC, by showing the view of the population activity in layer 2/3 corresponding to the STC of the central neuron. The figure shows the response of the layer 2/3 neurons to a small grating barely eliciting activity in layer 2/3 (left), to an optimally sized grating eliciting maximal response in the central neuron (middle), and a grating size that elicits maximal suppression in the central neuron (right). This figure demonstrates that even tiny stimuli will elicit activity in relatively large area of model cortex, approximately 3 orientation columns across, which is due to the size of the afferent connection fields of layer 4C and layer 2/3 model neurons and due to the scatter of the centers of the connection fields. It is clear that the optimal sized grating elicits strong response across a large cortical area, indicating that strong lateral interactions are present in the model even when stimuli sizes that have been in the past associated with the afferent RFs are used [11]. Finally, the figure demonstrates that increasing the grating size further eventually recruits enough neurons across cortical space that the response of the central neuron is suppressed.

Although experimental studies tend to talk about the size tuning phenomena in terms of the stereotypical STC, it is clear from the published data that there exist con-

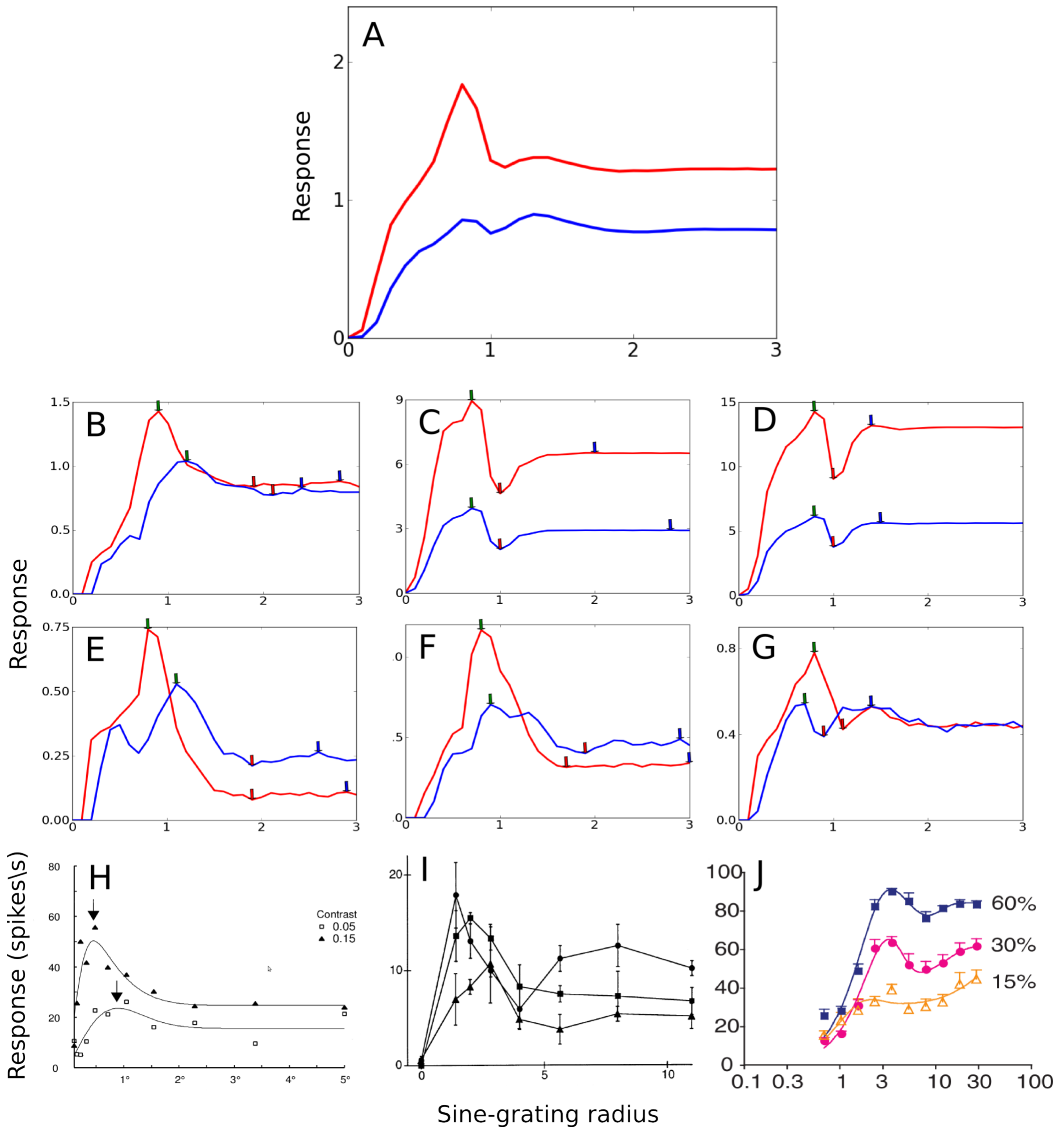

Figure 5.8: Average STC from the sample of 43 measured cells (A). An example of STCs from six neurons in our model (B-G) and 3 neurons from cat and macaque (H-J). The curves in the top row (B-D) represent the most common STC observed in our model (37%), and correspond well to the stereotypical STC described in experimental studies. The middle row (E-G) shows three STCs that in various ways diverge from the stereotypical STC. The blue line is contrast 50% and the red line is contrast 100%. The bottom row (H-J) shows three STC curves from cat and macaque that show similar deviations from the typical STC as the corresponding STCs in the middle row. (H) STC measured in macaque showing the non-monotonous rise to the summation peak [160] as demonstrated in model neuron D. Note that raw data (squares corresponding to low-contrast grating, triangles corresponding to high-contrast grating) show this property but it disappears when fitted with a difference-of-Gaussian model (full lines). (I) STC measured in cat [165] demonstrating that certain grating patch sizes of higher contrast can elicit a lower response from the neuron than corresponding patches of lower contrast (filled circles 5% contrast, unfilled circles 10% contrast, unfilled triangles 40% contrast), as found in model neuron E. (J) STC measured in cat showing that summation peak can decrease with decreasing contrast [196] as demonstrated in model neuron F. The radius of the sine-grating patch is measured in linear retinal sheet coordinates for the model neurons, whereas in experimental studies it is measured in degrees of visual field, on a logarithmic axis in (J).

siderable deviations from this stereotypical STC in many neurons. One of the contributions of this modeling study is the examination of these variations, and their link to other functional and anatomical properties of the model neurons. Let us therefore discuss some of the systematic variations of STCs that we observe. In the middle row of figure 5.8, we show STCs of three example neurons that represent these variations. The STC labeled D shows the case where the initial rise to the maximum is not monotonic, which is also common in our model (10, 23%). Interestingly one can observe this property in example STCs presented in various experimental studies [100, 160]. Another common deviation from stereotypical tuning curves, also found in published data [165], is demonstrated by the STC labeled E. This example shows that in the presence of a large surround stimulus, some neurons can express lower activity in the high contrast condition that in the low contrast condition. Finally, the STC labeled F shows that the shift of the summation peak at low contrast does not always have to be towards larger diameters, a fact that is clearly present in many neurons in published data [100, 160, 196]. Previously these effects were ignored, usually considered as noise or even discarded from further analysis by fitting the data with idealized STCs. We predict that at least some of these 'imperfections' of the experimentally measured STCs are not noise but systematic deviations from the ideal STC that arise due to inhomogeneities of individual neurons, patterns of connectivity and their position in the functional topological cortical maps.

5.5.3 Orientation contrast tuning

The second surround modulation effect that we have systematically examined in the model is orientation contrast tuning. Figure 5.10 shows the orientation tuning curves for six neurons, including the response of the neuron to the center grating patch alone (red curve), and the orientation contrast tuning curves at two surround contrast (green & blue curves). The low 50% contrast (blue curve) matches the contrast of the center patch, while we use double the low contrast as the high contrasts (green curve). All further population results are computed from the 50% condition, where the surround and center contrasts are matched.

The top row of figure 5.10 shows three example neurons that exhibit a stereotypical orientation contrast tuning curve, with strong collinear suppression that gradually becomes weaker as the surround grating shifts towards an orthogonal configuration, sometimes even leading to facilitation, as observed in ref. [107]. This type of ORTC

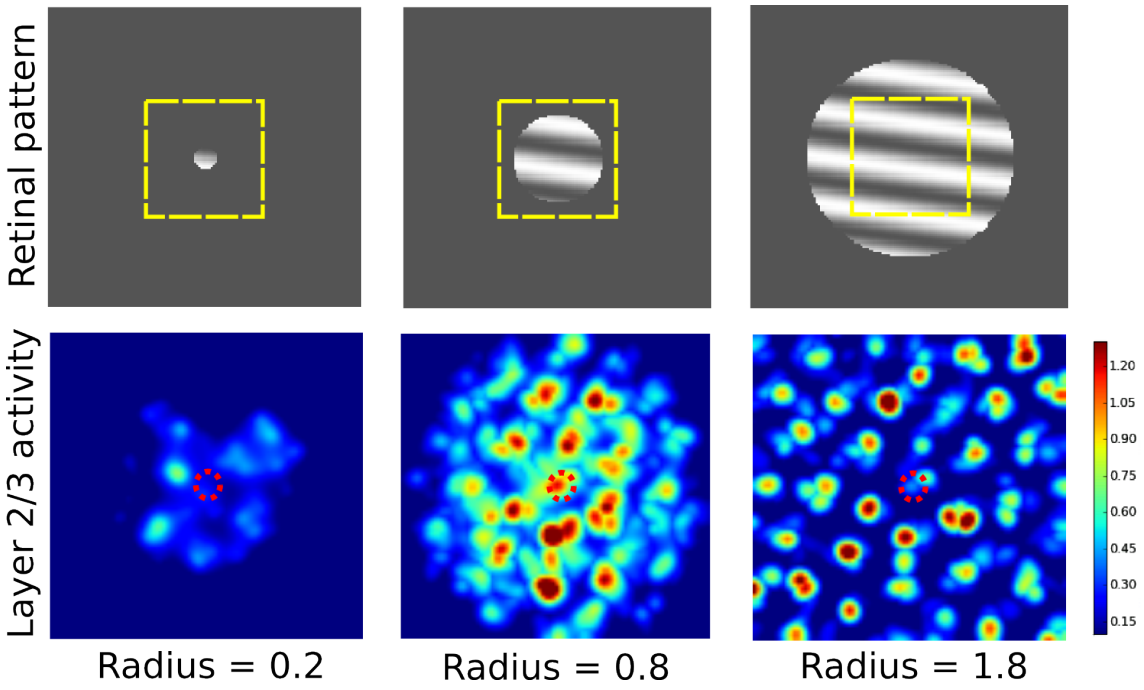

Figure 5.9: The activity patterns in the model photoreceptor and layer 2/3 sheets in response to sine gratings of different diameters. The sine grating is centered over the RF of the central layer 2/3 neuron (located at the center of the red circle), and its orientation corresponds to the orientation preference of the central neuron. The small grating on the left barely elicits activity in the network. The diameter of the sine grating in the middle corresponds to the peak of the size-tuning curve of the central neuron (0.8 in sheet coordinates). The diameter of the sine grating on the right corresponds to the peak suppression of the size-tuning curve of the central neuron (1.8 in sheet coordinates). The size tuning curve of the central neurons is shown in figure 5.8E. The size of the retinal sheet is 2.75$\times$2.75 and the size of the layer 2/3 sheet is 1.0$\times$1.0 in sheet coordinates. The yellow rectangle outlines the region of the retinal sheet corresponding to the layer 2/3 sheet.

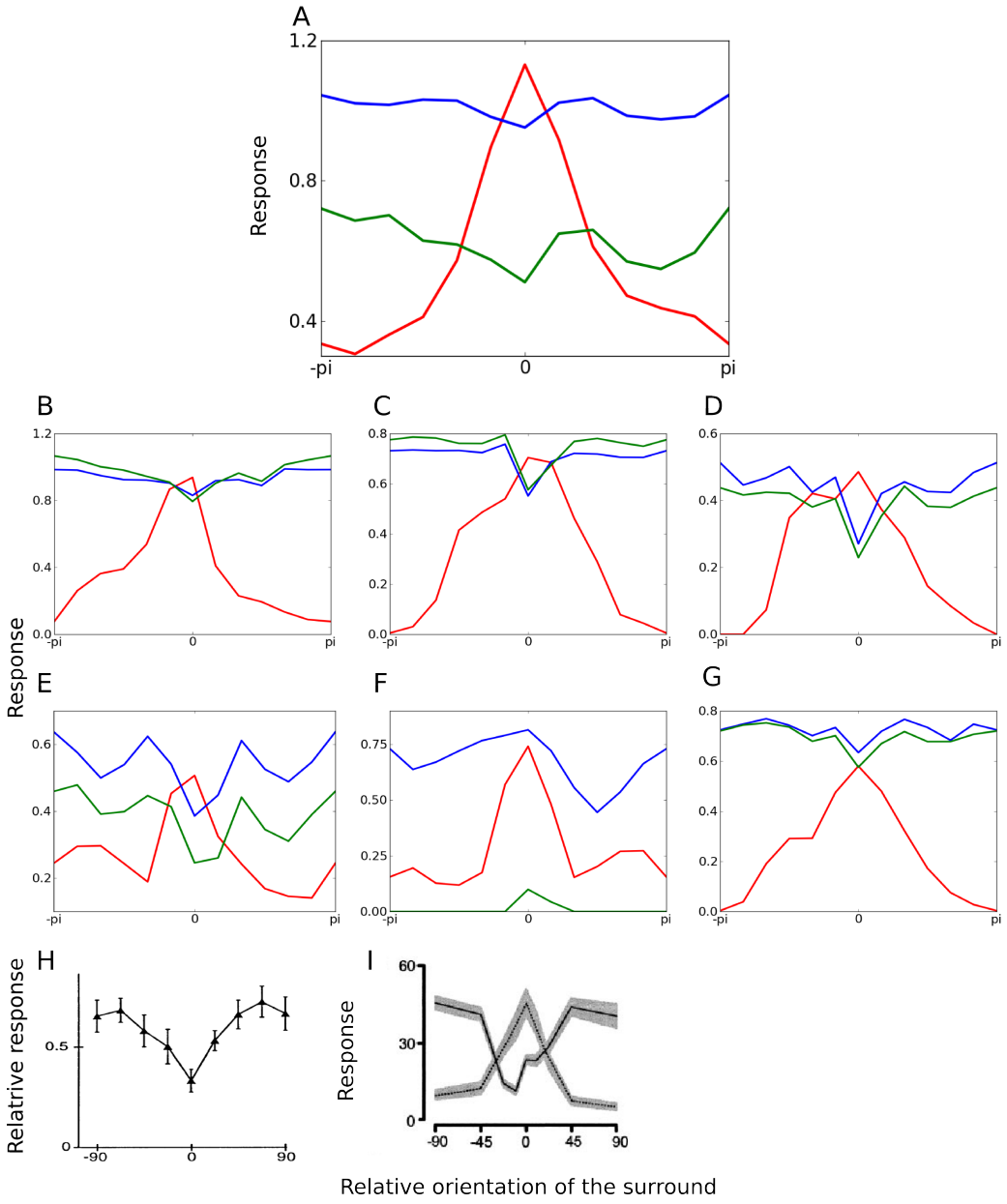

Figure 5.10: Average OCTC from the sample of 43 measured cells (A). An example of OCTCs from six neurons in our model (B-G) and 2 neurons from cat and macaque (H-I). The three curves in the top row (B-D) represent the most common ORTC observed in the model (22; 51%) and correspond well to the stereotypical ORTC described in experimental studies, with strongest suppression at the collinear configuration that decreases as the surround approaches an orthogonal configuration. The middle row (E-G) shows three OCTCs that in various ways diverge from the stereotypical OCTC. The red line is center alone, the blue line is surround contrast 50%, and the green line is surround contrast 100%. (G) OCTC measured in cat showing the strongest response at a diagonal configuration [165], as demonstrated in model neuron D. (I) OCTC measured in macaque showing the strongest suppression not at the collinear configuration [107], as demonstrated in model neuron E. The orientation in the graphs is relative to the orientation preference of the given neuron; the 0° point corresponds to the collinear configuration, and 90° corresponds to an orthogonal configuration of the surround sinusoidal grating stimulus relative to the central grating. The relative orientation in the model neurons is marked in radians, whereas in the experimental data in degrees.

is exhibited by the majority of measured neurons (22; 51%). However, just as for the STC, a significant number of neurons show different shapes of ORTCs. Some of the ORTCs have maximum facilitation or release of suppression at a diagonal orientation (9; 20%) (figure 5.10D), as found experimentally in ref. [165]. Another example of deviation from the stereotypical ORTC are neurons expressing strongest suppression clearly away from the collinear configuration (figure 5.10E). Several such orientation tuning curves where the maximal suppression does not align with the maximal response to the central grating patch can be observed in ref. [107]. Finally, we observe a few neurons (2; 5%) that do not exhibit suppression to any orientation of the surround grating, but instead express facilitation tuned to the orthogonal configuration (figure 5.10F). We could not find examples of the latter type of tuning curve in the literature, but given the small number of published orientation contrast tuning curves, it is possible such tuning curves can be found also in animal V1. Note that all of this variability comes from the variations in connection patterns that develop through Hebbian learning, in the context of map structure that itself is emerging through Hebbian learning. Thus the model predicts that Hebbian learning is sufficient to explain much of the functional variability between V1 neurons.

5.5.4 Population characteristics of surround modulation

The great advantage of this model over previous single-cell models of surround modulation or over multi-cell surround modulation models with isotropic connectivity is that it allows us to explore the population characteristics in the model as well, and compare them with experimental findings. As a first approximation, we can examine the means and variance of the various measures we applied to the size tuning and orientation contrast curves, and compare them to those obtained in the experimental studies. As discussed previously, the published experimental surround modulation measures vary significantly between studies. Table 5.2 shows how our model compares to the experimental studies in this respect.

The magnitude of the mean suppression index matches well the range of mean suppression indexes outlined by the experimental studies both in cat and macaque. The counter-suppression index has so far been quantified only in cat and has been found to be weak in both cat (0.19) and the model (0.1). Given the variability in the other measures where data is available from multiple studies, the model value appears to be in reasonably good agreement, which can be verified once additional experimental

Table 5.2: Model parameters

Measure name	Cat	Macaque	Model
Suppression index	0.16[184] 0.44[196]	0.33 [184] 0.38[49]	0.35
Counter-suppression index	0.19[196]		0.1
Contrast dependent summation peak shift	1.33[196] 1.36[184]	2.3[160] 2.1[100] 2.5[49]	1.29
Orientation-contrast suppression index	-0.25[165]∗	-1.7[107]†	-0.24

∗ This value was approximately derived from the graph shown in figure 6D in ref. [165].

† This value was computed from statistics presented in table 1 in ref. [107].

data is available. The contrast-dependent shift of summation peak has been found to be considerably larger in macaque than in cat. A similar pattern appears in the case of orientation contrast suppression, which has been found to be several fold stronger in macaque than in cat. As table 5.2 shows, on the latter two measures, our model very well matches the values measured in cat and, consequently, not in macaque. Overall, our model is in good agreement with the measurements of these three parameters in cat, suggesting that our model captures important aspects of the dynamics of V1 surround modulation.

As a next step, we examine the population histograms of the four measures, at high and low contrast, and compare them with analogous histograms from experimental studies where available (figure 5.11). In the case of the suppression index (figure 5.11 first row), the most marked difference between the model and the two experimental studies is the lack of neurons showing weak or no suppression in our model — our model shows the weakest suppression greater than 0.1, whereas studies show significant numbers of neurons with suppression weaker than 0.1 in both cat and macaque. On the other hand, our model correctly predicts the shift of distribution of suppression index at high contrast to higher values. The distribution of counter-suppression index in our model seems to be considerably narrower than in cat, with only a very few neurons showing stronger counter-suppression than 0.2 (figure 5.11 second row). Similarly, the distribution of contrast-dependent summation peak shifts spans a significantly narrower range than the experimentally measured one (figure 5.11 third row). We do not observe many neurons where the radius of the summation peak decreases with decreasing contrast, and those that do exhibit only a small decrease, unlike in the experimental results. At the same time, we do not observe increase of the summation peak distance beyond $\approx$1.8, unlike the experimental results. Overall, the model shows less variability in these parameters than is evident in the animal data, which is likely

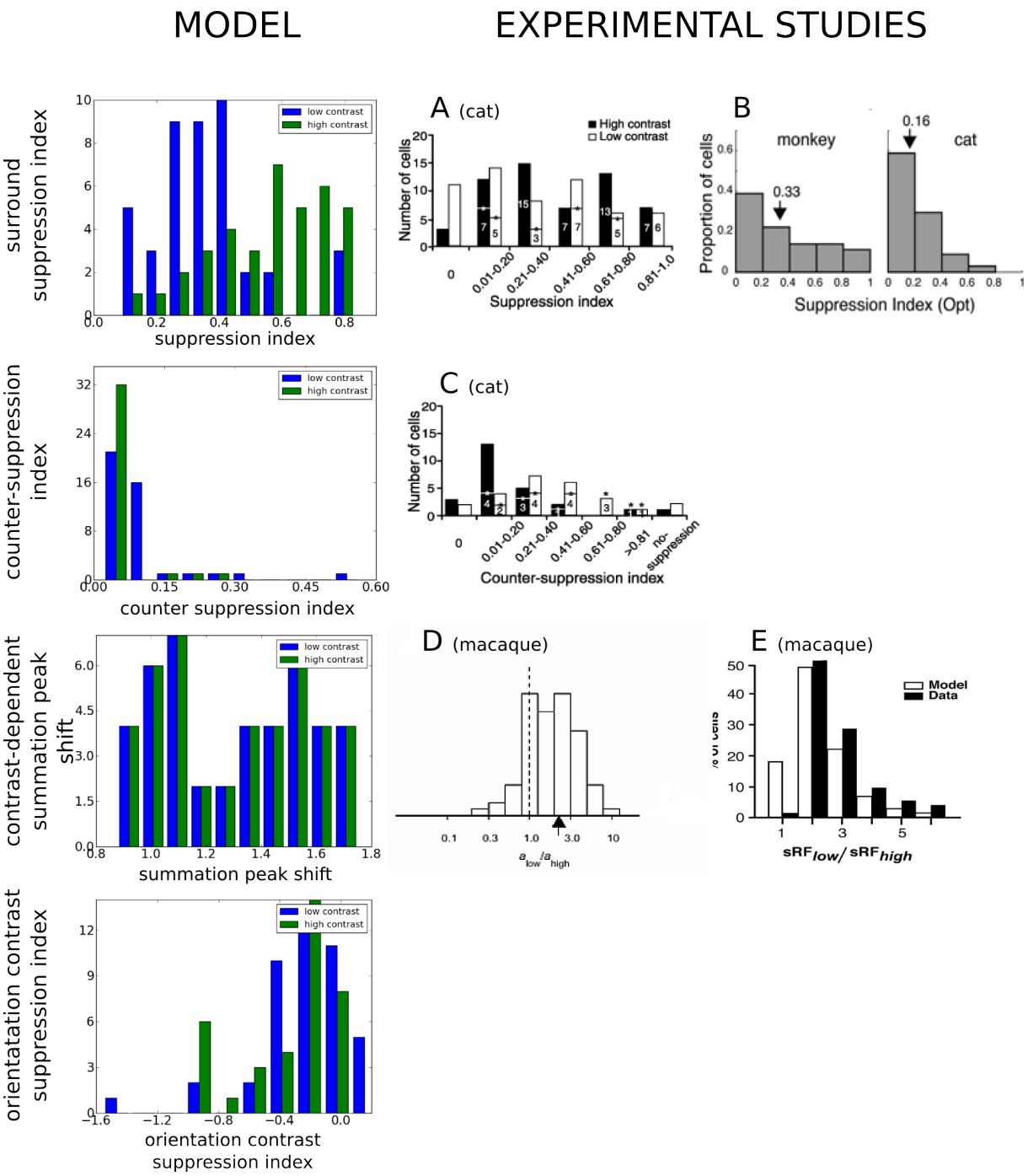

Figure 5.11: The histograms of the four main surround modulation measures, as indicated at left. First column shows the results from our model, second and third columns show corresponding data in cat and macaque (where available). The experimental data have been obtained from refs. [196] (A,C), [184] (B), [160] (D),[100] (E). The means of the distribution match those in cat well (see table 5.2), but the distributions are generally narrower in the model than observed in the experimental data.

partly due to the deterministic nature of the simulations and partly to the many possible additional sources of variability not included in the model.

5.5.5 Relationship between map position and surround modulation

The fact that our study shows the development of maps and surround modulation properties of adult neurons in a single model gives us a unique and unprecedented opportunity to link the positions of neurons in the maps with the surround modulation properties of the neurons. It is reasonable to expect that such systematic relationships might exist, because the development of maps is due to the development of afferent and lateral connectivity and thus one can expect that the pattern of connections (both lateral and afferent) should vary in a systematic way with the position in the map. This type of phenomenon has been demonstrated in V1 with orientation-specific clustering of lateral connections [36, 173]. Because it is the afferent and lateral connectivity of a given neuron that are the main determinants of its functional properties in general and surround modulation in particular, one can expect that these will also systematically vary with position in the map to some degree.

As a measure of relative position of a neuron in a map, we use the local homogeneity index (LHI) introduced in ref. [142]. The LHI for a cortical location x is defined by the expression:

$$LHI(x) = \frac{1}{2\pi\sigma^2}\left|\int exp(-\frac{\|x-y\|^2}{2\sigma^2})exp(i2\theta_y)\,dy.\right|$$

where x and y are 2D vectors corresponding to cortical locations, θ_y is the orientation preference at location y, and the parameter σ determines the spatial scale of analysis. The LHI reflects whether given neuron sits in a region of the map with great variation of orientation preference (such as a pinwheel or fracture), where it yields values close to 0, or in a region of the map with uniform orientation distributions (such as the center of an iso-orientation domain), where it yields values close to 1.0.

As a first exploratory study, we have examined the various surround modulation measures calculated in this study against orientation selectivity, LHI and modulation ratio indexes, and calculated the linear regression to estimate the correlation factor in each case (totalling 18 potential relationships). Here we describe 5 strongest relationships (based on the correlation coefficients) as potential candidates to be examined experimentally. This analysis is limited by the relatively small number of neurons

from which we have obtained surround modulation measures. Collection of surround modulation measures from a larger sample of neurons in future could reveal additional candidate relationships or make the relationships clearer.

First we will look at three relationship between local homogeneity index and surround suppression parameters, all of which had statistically significant correlations (p¡0.05). Figure 5.12A shows the relationship between the local homogeneity index and the suppression index, which defines the strength of maximal suppression relative to the peak facilitation. As can be seen, the suppression index increases with increasing homogeneity index, indicating that neurons located at singularities in the orientation map show less surround suppression overall than neurons that are in the middle of orientation columns.

An opposite relationship can be seen between the local homogeneity index and the orientation contrast suppression index (figure 5.12B), indicating that neurons located at fractures and singularities in orientation map show less collinear suppression than neurons that are in the middle of the orientation columns. This is not surprising, as we would expect the neurons sitting at singularities to be less selective over the course of development and thus developing less specific lateral connectivity (as illustrated in figure 5.5), which in turn should lead to smaller differences in activations of these neurons between the collinear and orthogonal surround conditions.

The last relationship between the local homogeneity index and surround suppression we found is that the stimulus size at which neurons reach summation peak decreases with increasing local homogeneity index (see figure 5.12C). The clumping along the x axis in the figure is caused by the narrow range in which the measured neurons reach the summation peak, and the limited number of sine grating patch diameters at which we measured the size tuning. The narrow range of size preferences indicated by this figure is not surprising, as the simulated LGN sheets in our model contain only a single size of On and Off channels, effectively constraining the selectivity of the V1 neurons into a narrow range of spatial frequencies, which in turn is likely to constrain the size tuning of neurons. This unrealistic behavior could be rectified by incorporating the subcortical pathway of the recent developmental model of frequency map development by Palmer [151], which considers variable sizes of LGN channels, and in turn shows how realistic frequency tuning emerges in a similar computational modeling framework as our model. However, the fact that neurons located at singularities in the orientation map have wider size tuning than those located in orientation columns is consistent with the previous two findings indicating weaker surround modulation in

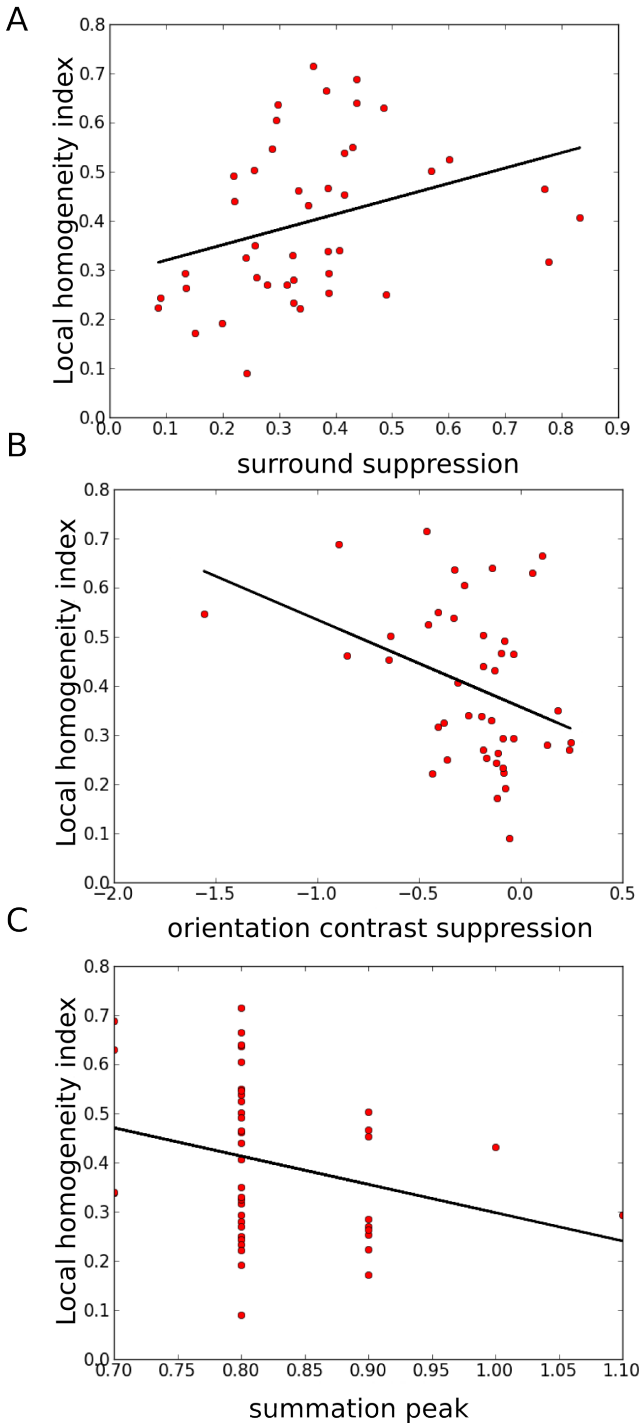

Figure 5.12: (A) The relationship between suppression index and local homogeneity index in layer 2/3 model neurons. Correlation coefficient = 0.327 (p¡0.05). (B) The relationship between orientation contrast suppression index and local homogeneity index in layer 2/3 model neurons. Correlation coefficient = -0.362 (p¡0.01). (C) The relationship between summation peak at high contrast and local homogeneity index in layer 2/3 model neurons. Correlation coefficient = -0.271 (p¡0.05).

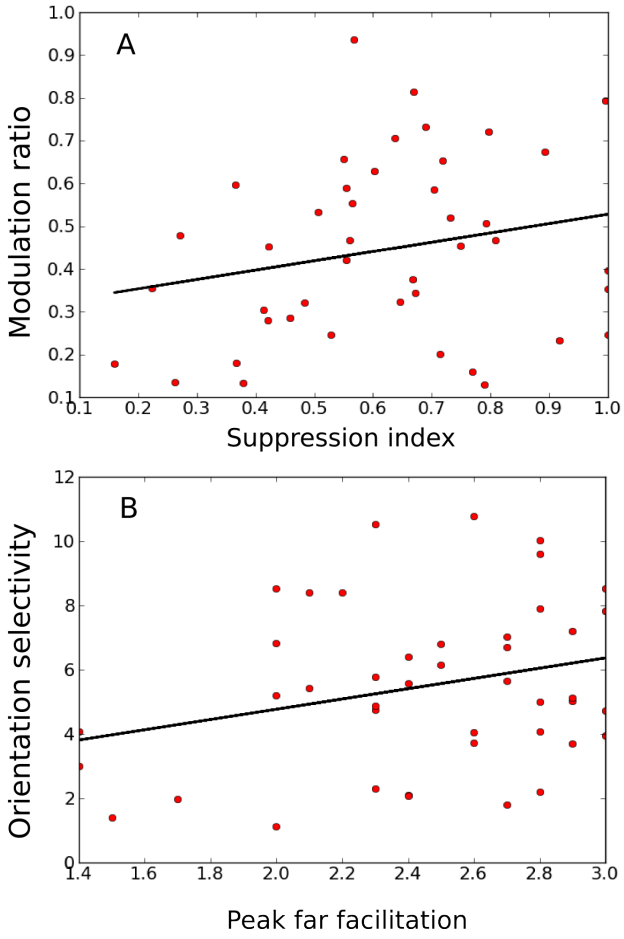

Figure 5.13: The relationship between suppression index and modulation ratio in layer 2/3 model neurons. Correlation coefficient = 0.226 (p=0.071) (A). The relationship between counter-suppression peak and orientation selectivity in layer 2/3 model neurons. Correlation coefficient = 0.270 (p¡0.05) (B).

the neurons at singularities. This is because weaker surround modulation should correspond to less inhibition impinging on the neuron from the predominantly inhibitory surround, which in turn should increase the diameter of stimulus at which inhibition overtakes excitation, as indicated by the peak of the STC. Therefore we believe this is qualitatively a correct prediction, although quantitatively it is likely to be biased by the unrealistically narrow preferred frequency range of our model.

So far we have concentrated on the relationship between surround modulation and the location of neurons in orientation maps. We have also examined two other properties of V1 neurons — orientation selectivity and modulation ratio — in relationship to their surround modulation properties. One of the relationships is between the suppression index and the modulation ratio, as demonstrated in figure 5.13A. This relationships was not statistically significant, but it was very close to being significant (p=0.072), therefore we decided to report it. Neurons with lower modulation ratios (and thus more simple-cell–like characteristics) tend to have weaker suppression indexes than neurons with higher modulation ratios (and thus more complex-cell–like characteristics). This is somewhat surprising, as we have shown above that model neurons with low suppression index tend to be at locations with lower homogeneity indexes (figure 5.12A). We have also shown in section 4.10 that neurons at low homogeneity index locations tend to have higher modulation ratios. Thus a simple prediction would follow: a neuron with a low suppression index will tend to have a higher modulation ratio — which is opposite to the relationship shown in figure 5.13A. However note that there is wide variability in all these relationships, and thus such findings are not necessarily inconsistent, however, as stated above, it is possible that due to the limited sample of neurons some of these relationships are not significant.

The last relationship we will discuss is between the orientation selectivity of a neuron and the distance at which the strongest counter suppression occurs (figure 5.13B) and was found statistically significant (p¡0.05). Neurons with low orientation selectivity tend to reach the counter-suppression peak earlier. It is not clear at the moment why such a relationship holds. One possible explanation — that needs to be verified in future — is that neurons with low selectivity tend to have shorter lateral interactions, which would explain why they express counter suppression at shorter distances, as counter suppression occurs at the largest distance of all the surround modulation effects we measure.

Finally, we have tested the robustness of the above relationships by excluding the extremal points (in both dimensions) from the dataset and reassessing the statistical

significance of correlations in the reduced datasets. It is important to note that as the original datasets are small (n=43) reduction by up to 4 extremal points is significant. Furthermore, for example in the case of homogeneity index, one can expect that the distribution of LHI values is highly uneven, as there are relatively few points in the map that lie on discontinuities in comparison to those that lie in relatively homogeneous areas. Thus removing extreme values from dataset can in fact eliminate important informative points rather than outliers. Nevertheless, after removing the extremal points we have found that for relationship between local homogeneity index and orientation contrast suppression and for relationship between modulation ratio and suppression index the correlation coefficient have increased and the relationships were statistically significant ($p_¡=0.05$). The correlation coefficients of the remaining three relationships have dropped and in all cases the relationships ceased to be statistically significant.

5.6 Discussion

In this chapter we presented a developmental model of V1 that exhibits realistic surround modulation properties after development. This is the first model showing that the role of lateral cortical connectivity during development as a driving force of functional map organization is consistent with the role of lateral cortical connectivity in adult animals as a substrate for surround modulation in individual neurons. In this way, the model represents an important advancement in our understanding of both the development of V1 and its function in adult animals, in a single computational framework.

We have shown that the model develops realistic receptive fields, which are organized in cortical space such that they form orientation maps. Furthermore, after development, the model contains both simple and complex cells, and individual neurons exhibit realistic orientation tuning curves. Overall, despite the changes introduced, the model expresses all the important V1 properties that we have demonstrated in the complex cell model discussed in chapter 4, which underscores the incremental design of our models.

When examining surround modulation, we focus on the two most-studied properties of V1 neurons: size tuning and orientation contrast tuning. We show that most neurons in model layer 2/3 express both realistic size and orientation contrast tuning. However, at the same time, we show that a considerable number of model neurons express size and orientation contrast tuning that deviate from the stereotypical tuning

curves described in experimental literature. Importantly, we have identified similar deviations in the published data, indicating that such systematic deviations might also be present in animals. This highlights the potential predictive power of our model, and at the same time stresses the need to analyze data from experiments in greater detail, focusing not only on formulating the simplest general principles, but also examining systematic deviations from the stereotypical average. As our study shows, these deviations are not necessarily measurement or intrinsic noise or malfunctioning neurons, but can be consequences of important general properties of V1 such as the functional and anatomical inhomogeneities resulting from functional maps and selective connectivity of individual neurons. Such variations can have important implications for population coding, as they can significantly reduce the redundancy of representation of visual information in V1.

Next, we have examined the distribution of three measured parameters — surround suppression index, counter-surround suppression index and contrast-dependent summation peak shift — and compared them with experimental evidence. The re-occurring pattern in the difference between the histograms of these three parameters in our model and the experimental studies is the lower variance and range in our model compared to the experimental studies (see figure 5.11). This is, however, not surprising for the following reasons. Even though we believe our study makes an important step in modeling the variability in V1, most of the variability in our model can be attributed to only two sources: the variability between the afferent receptive fields and long-range lateral connections after development as a consequence of Hebbian learning, and the position of the neurons within orientation maps (which are themselves defined by connections set by Hebbian learning). Even though, as shown in the previous and present section, these sources are sufficient to explain a considerable amount of variability in the cortex, it is reasonable to expect that additional sources of variability exist. For example, we set the strength of the individual projections in the model to fixed numbers. Due to the weight normalization enforced throughout development, this means that even after development, neurons within each model sheet will receive exactly the same proportion of input from the different projections. It is reasonable to assume that in animal cortex the relative strength of inputs from the different projections in individual neurons will be considerably variable. In a similar manner one can consider several other sources of variability in the cortex that, if implemented in our model, could explain the greater variance and range of the discussed parameters. Unfortunately, the quantitative parameters of these sources of variability is currently not known, but our model could be

used to formulate predictions on these values by evaluating which additional sources of variability and of what magnitude could account for the amount of variability of the discussed surround modulation parameters measured in animals.

Another important technical limitation of the current model could further explain the limited range of some of the surround modulation parameters. The model simulates only a limited region of V1, corresponding approximately to 4-5 hypercolumns in width. Given the known large spatial extent of surround modulation effects, corresponding to regions spanning considerably more than the simulated 4-5 hypercolumns, it is impossible for our model to account for surround modulation effects in their full spatial extent. For example, due to these constraints, the model in principle cannot show an increase of the distance of summation peak between low and high contrast that is 10 fold, as is sometimes observed in experimental studies (see figure 5.11). The current computational resource costs of the model do not allow us to increase its size. However, further advancement in the Topographica simulation software by parallelization and/or adoption of GPU computing could allow for simulations that would span a sufficient number of hypercolumns to account for the full extent of surround modulation in V1.

Finally, given the hypothesis that some of the surround modulation effects cannot be fully accounted by only long-range lateral connections within V1 [11], even a sufficiently large V1 model would fail to explain some of the extreme values of surround modulation parameters. The addition of feedback from higher-level visual areas might be necessary to fully account for the demonstrated discrepancies between the surround modulation measures in the model and V1.

The most important predictions formulated in this study come from examining the various functional parameters of individual neurons, and correlating them with their position in the orientation maps or with other parameters. In section 5.6.5 we formulate five such predictions for various surround modulation properties of layer 2/3 model neurons. In the model the local homogeneity index of neurons is positively correlated with suppression index and negatively correlated with both orientation contrast suppression index and the distance of summation peak, indicating that the suppression at singularities in the map is both less strong and less orientation specific than in the centers of orientation columns. At the same time, the weaker suppression in singularities causes the summation peak to shift to larger distances. All these results are consistent with the strongly orientation-specific lateral connectivity developing in the homogeneous areas of functional maps, and less specific lateral connectivity develop-

ing in areas near singularities. This way we combine the development of neurons in the context of functional maps, and consequently the development of their orientation specificity, with the surround modulation properties of adult neurons in a single model. These findings thus further improve our understanding of the dual role of lateral connections in the formation of functional cortical maps and in the expression of adult single cell properties such as surround modulation.

The incremental and inclusive design of our model has resulted in a model with rich dynamics. In this chapter we have examined only some of the known important properties of V1 that were the main focus of this thesis. A more detailed analysis could be performed in order to further constrain the model and formulate more predictions. For example, in this chapter we focused on examining the SM properties of neurons in layer 2/3. An immediate next step in the analysis would be to examine the various tuning properties of simple cells in model layer 4Cβ and compare them with the complex cells in layer 2/3. Some differences in contextual modulation both between cortical layers and between simple and complex cells have already been found in animals. For example, complex cells have been found to express stronger surround suppression than simple cells, and similarly cells in layer 2/3 have been found to express stronger suppression than neurons in other layers [3]. Note that these results support the theory of layer 2/3 being the primary source of surround modulation in V1. On the other hand, even though layer 4Cβ in our model does not contain lateral connectivity, the neurons can still express orientation-specific surround modulation due to the feedback connections from layer 2/3 to layer 4Cβ. Furthermore, a wide range of other parameters of surround suppression (and other V1 properties) could be compared between layers and functional cell types in the model, and predictions formulated.

In this thesis we have focused on examining only the overall output of neurons (e.g. firing rates). This could be complemented by analysis concentrating on the individual excitatory and inhibitory components of the incoming signals, or even further analysis that separates these individually for each projection in the model. Such analysis could offer further insight into the mechanics of surround modulation, particularly some of its properties which are less clear, such as the occurrence of counter suppression. In a similar manner, a more detailed explanation of the variability in the various surround suppression properties than we have described in this study could be found, relating it to more-specific features of the map or patterns of connectivity.

Previous studies examining these issues in cat V1 have found significant variability in the tuning of the excitatory and inhibitory components and their relationship to

the resulting spiking of the cells [136]. Monier et al. hypothesized that this variability could reflect inhomogeneities in functional intracortical connectivity regulated by correlation-based activity-dependent processes. Our model contains such processes (in the form of Hebbian learning) which we have shown lead in the model to development of systematic functional and structural inhomogeneities known to exist in V1 (orientation maps and development of patchy lateral connectivity). Because we have already linked these inhomogeneities to several V1 neuron properties, comparing our model with the work of Monier et al. [136] could in future lead to a single coherent explanation of all these V1 phenomena. Finally, taking the suggested analysis one step further, one could study the detailed time course of the onset of the excitatory and inhibitory components and relate them with existing studies which have examined these issues in V1 neurons, further extending the range of V1 phenomena covered by the model.

In this chapter we have presented a model of orientation map development that expresses a wide range of surround modulation effects, including realistic size tuning and orientation contrast tuning. This work offers a consistent explanation of wide range of V1 properties of different spatial and temporal scales in a single computational model, providing a rich platform for studying the interactions between these V1 properties. We demonstrate the advantage of our modeling approach by formulating predictions on how several parameters of surround modulation systematically vary in relation to the position of the neurons in the orientation maps.

Chapter 6

Overview and future work

6.1 Introduction

The main goal of this thesis was to create a comprehensive model of V1 development and function that explains how orientation maps in V1 can develop while individual neurons express realistic orientation tuning and surround modulation properties after development. We have approached this problem in three steps, each covered in one of the three results chapters. In this chapter I will discuss the extent to which the aims of each of these steps have been achieved, and how these aims could be further extended. Despite the single main goal of this thesis, the three results chapters in the thesis have covered a breadth of topics, each offering a number of possibilities for future research. Each individual topic is thus discussed in a separate section (chapter 3 in section 6.2, chapter 4 in section 6.3 and chapter 4 in section 6.4). Finally, we close the chapter by offering a more general discussion of the modeling paradigm employed in this thesis and ways to extend it further.

6.2 A robust self-organizing model with realistic contrast response

We decided to use the ALISSOM model [119] as the basis for our models, because it already reproduces number of experimental findings about development of orientation maps and is the first model that has shown development of orientation maps that is robust to the statistics of training stimuli, which make it an ideal starting point for our model. An important feature of surround modulation is that its properties are strongly

dependent on the contrast and orientation of the stimulus. Therefore, in order to study surround modulation, it is important that a model has realistic behavior with respect to contrast and orientation. Previous developmental models of functional maps in V1, including the ALISSOM model, have been highly unrealistic in this sense, not exhibiting contrast gain control and contrast-invariant orientation tuning. Before addressing the two main results of this thesis — the model of complex cell map development (chapter 3) and subsequent demonstration that with appropriate adjustment of lateral connectivity such model is consistent with surround modulation (chapter 4) — we first modified the ALISSOM model in order to obtain these important functional properties relevant to the subsequent models.

Specifically, we added a gain control mechanism and changed the transfer function of the V1 model neurons from sigmoid to linear threshold and found that the resulting model is a good fit to contrast responses in cat. As an additional benefit, these modifications allowed us to simplify the homeostatic rule used in ALISSOM, thereby eliminate the last parameter that had to be tuned in order to achieve stable development of orientation maps which was the focus of the ALISSOM model. The results is an improved version of the ALISSOM model called GCA-LISSOM.

As stressed in chapter 3, these modifications were required for our subsequent modeling steps, but were not the main focus of this thesis. Accordingly, we approached these problems from a practical standpoint, omitting deeper analysis that could be performed for each of them. In each case we strived for qualitative rather quantitative match with the experimental evidence, but in future work it would be worthwhile to establish quantitative match as well.

In particular, the LGN size tuning and gain control properties have been extensively experimentally measured, and can be fit directly since the LGN model is not developmental. Such a step would be necessary especially should one want to use the final surround modulation model described in chapter 5 to investigate the influence of the surround modulation effects present already in LGN on V1 surround modulation.

Similarly, the contrast invariant orientation tuning width has been extensively studied both experimentally and computationally, and enough data exists to constrain the model quantitatively rather than just qualitatively. Direct fitting of the data on a neuron by neuron basis in a large scale developmental model like ours is impossible due to the fact that the final properties of neurons can be only indirectly influenced by the various parameters of the model. However, it would be possible to attempt to achieve quantitatively more accurate orientation tuning properties on average across the simulated

population of neurons.

The GCA-LISSOM model exhibits contrast invariant orientation tuning across a wide range of contrasts. However, we have noticed that at very low contrasts the orientation tuning curves of many neurons become clumped to 0 at non-preferred orientations, breaking the contrast invariance of their width. This imperfection of the model at very low contrasts does not affect any conclusions based on the models discussed in this thesis, because none of the analysis is dependent on the behavior of the network at such very low contrasts. However, it represents an opportunity for further improvement of the model. One of the key differences between the ALISSOM and GCA-LISSOM model was the change of sigmoid transfer function for a linear threshold one. Although as discussed in section 3.3.3, such linear threshold transfer function represents a good approximation of the f-I curve of many V1 neurons, the relationship between the membrane potential and the firing rate in response to varying contrast of the stimuli exhibits a slight elbow shaped non-linearity at low contrasts due to the effects of random fluctuations of membrane potential [72]. Interestingly, it was also shown experimentally in ref. [72] that this transfer function changes its gain depending on the input contrasts. Altogether, this mechanism can account for the contrast invariant width of orientation tuning of V1 neurons [72]. Implementing this mechanism in our models should be straightforward, either by explicitly simulating the noise resulting from membrane potential fluctuations, or by hard-coding the change of slope of transfer function based on the contrast of the stimulus into the model and offers an opportunity to correct the imperfect orientation tuning of our models at very low contrasts.

Finally, despite our model exhibiting stable orientation map development through a range of input statistics, it is still possible that this property breaks down under more extreme conditions. Therefore, further analysis involving systematic parameter search is required to fully establish the region of input statistics in which our model develops stable, smooth, and selective orientation maps, and to compare this region to experimental results as they become available.

6.3 Development of maps of complex cells

As discussed in section 4.1.1, only a few models of complex cell map development exist and they all have limitations. The main goal of chapter 4 is to offer a new model of complex cell map development that rectifies the problems of previous models and thus subsequently allows us to model surround modulation in the context of complex

cells and patchy long-range connectivity in layer 2/3.

Starting from GC-ALISSOM, we were successful in designing a model of V1 that shows how orientation maps among simple cells in layer 4C and among complex cells in layer 2/3 can develop. Unlike the previous models of complex cell map development, it does not require any specific neuron-to-neuron connectivity before development [149] or implausible negative 'firing rates' of neurons [99, 198].

One of the assumptions of our model is the existence of two sources of initial variance in the responses of neurons: the intrinsic noise in neural activity and a degree of scatter in the retinotopy of layer 4C RFs prior to development. This variability is necessary to induce random phase preference development in our model and thus subsequent complex cell formation. It is known that — after development — V1 neurons exhibit local scatter of retinotopy [43, 197] at the order of magnitude used in our model, however, we are not aware of any current evidence that would show this to be true (or not) already prior to development. Although we believe that assuming variability in the undeveloped cortex is reasonable, this remains one of the assumptions of our model that needs to be verified experimentally.

Our model develops both simple and complex cells with a distribution of MR indexes similar to those measured in animal experiments (see figure 4.7). As discussed before, there is experimental evidence that layer 4C contains predominantly simple cells and that layer 2/3 contains predominantly complex cells. However, experimental studies also clearly show that this difference is not as clear cut as in our model, where almost all cells in layer 2/3 are classified as complex and all cells in layer 4C are classified as simple (figure 4.7). In the model, the relative contributions of different projections to a given neuron are fixed across each sheet. One obvious way to make the MR index of neurons in both simulated sheets more varied would be to introduce some variability in the projection strength for the individual neurons. This could ensure that some neurons would get a larger contribution from lateral connectivity than others, which in turn would affect their final MR index, and thus in turn induce more variability in the MR indexes of the population of neurons in both cortical layers.

The stereotypical model of V1 neurons receptive field — a Gabor filter — would predict that all neurons in V1 will respond preferentially to the strongly oriented stimuli such as bars or sinusoidal gratings. However, Hegdè & Van Essen [85] have shown that many neurons, even in early stages of visual processing like V1, exhibit maximal responses to more complex stimulus shapes, such as corners, stars or arcs. Even though the architecture of our model is based on the idealized complex cell, i.e., one

that pools responses from simple cells of similar orientation but different phases, due to the developmental nature of our model, one can assume a considerable deviations from such idealized model in many cells, for example due to their position in the map. If a cell in layer 2/3 is located at a discontinuity in the map, one can expect it will in fact pool information from simple cells preferring a more diverse range of orientations. The strong lateral interactions in our model could be another source of input contributing to selectivity of neurons to more complex shapes than predicted by the idealized Gabor filter RF. Overall, our model is an ideal candidate for investigating this intriguing property of V1.

As discussed in section 4.1.1, the most similar previous model of complex cell map development is the one by Olson et al. [149]. The main drawback of this model, which we have rectified in our model, is the requirement of very specific local neuron-to-neuron connectivity between pairs of layer 4C neurons, such that neurons are grouped systematically into mutually inhibited pairs. This, in combination with a BCM learning rule, ensures that the neurons in each pair develop opposite polarity of RFs. Such specific connectivity has not been demonstrated in young animals before development, and given that the goal of this model is to explain the development of specific connectivity itself (particularly between LGN neurons and layer 4C neurons), this assumption, in our opinion, leads to a inconsistent explanation.

However, functional properties of layer 4C neurons measured in adult animals suggest that similar local specific connectivity can exist [9, 70, 90], and it has been assumed by a number of models explaining a range of experimental data [118, 110, 189]. Furthermore, Kayser & Miller [111] have shown that such local connectivity can be explained by activity-based development if Hebbian learning is assumed to operate on excitatory synapses and anti-Hebbian like learning on inhibitory synapses. In their model, similarly to Olson et al., pairs of neurons that become mutually inhibitory develop similar orientations but opposite phase of RFs (see figure 6.1). However, as the authors discuss, this model is unlikely to explain orientation map development with any simple architecture of lateral interactions, as demonstrated by their simulations. Note, that their results also indicate that one cannot assume that such local connectivity development could precede the development modeled in Olson et al. model, as the orientation preference of neurons would already be determined by the first developmental phase. Therefore, the Kayser & Miller model cannot be considered as an explanation of the initial specific local connectivity assumed in Olson et al. study. However, as Kayser & Miller point out, some external factor, such as interactions be-

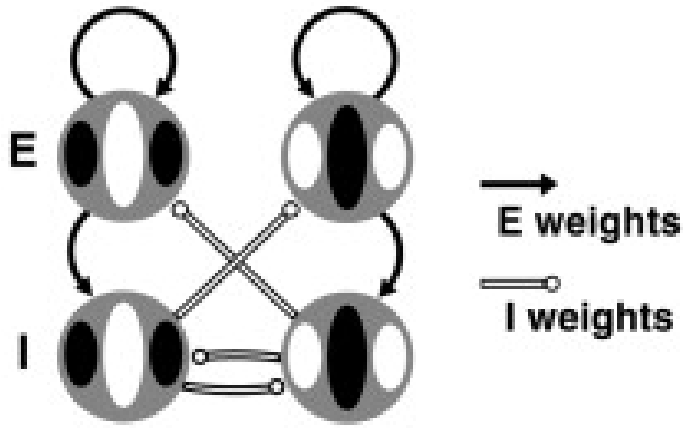

Figure 6.1: A schematic depiction of push-pull local connectivity among hypothetical neurons in V1. All four indicated RFs are meant to be centered on the same spatial position so that identical receptive fields represent cells with the same absolute spatial phase, while opposite receptive fields represent cells with opposite absolute spatial phase. Excitatory weights tend to link neurons of the same absolute spatial phase, while inhibitory weights tend to connect neurons of the opposite absolute spatial phase. The circuit model depicted here, excepting inhibitory-to-inhibitory connections, was previously shown to account for many experimental observations, including the contrast invariance of orientation tuning [118, 110, 189]. Reprinted from [111].

tween complex cells in layer 2/3, coupled with feedback to layer 4C, could provide a secondary pressure that could induce the development of orientation maps in their model of layer 4C.

We believe that this missing link between local layer 4C connectivity development and global orientation map (and other functional maps) development can be resolved by our model, because it incorporates both required mechanisms — map development primarily driven by layer 2/3 interactions, and feedback responsible for synchronization of map development between both cortical layers. Therefore, we propose a possible further extension of our model where our layer 4C architecture would be substituted with the one described by Kayser & Miller [111], while the layer 2/3 and feedback architecture would remain.

Besides unifying the Olson et al. and Kayser & Miller studies and our current work, the new model could demonstrate a number of additional functional properties of V1 neurons that have been attributed to the push-pull effects induced by the specific local layer 4C connectivity, the development of which has been demonstrated in the Kayser & Miller model. Furthermore, this change could improve the robustness of our model, as it would provide a second developmental mechanism that induces nearby neurons to develop a range of phase preferences. Such a model would not necessarily have to rely on the sources of initial variability (intrinsic activity noise and scatter of local retinotopy) as our current model does, and both mechanisms may be operating in animals.

6.4 Surround modulation in V1

In chapter 5 we finally reached the main goal of our thesis by extending the model of complex cell map development introduced in chapter 5 with realistic lateral connectivity, and showing that this model not only develops realistic orientation maps of simple and complex cells, but also exhibits realistic surround modulation after development. In this way we merge two families of computational models focused on different V1 phenomena — the models of V1 topological organization development and the models of surround modulation — into a single computational model via a unifying mechanism of lateral interactions. Furthermore, we believe that the range of V1 phenomena that this new model exhibits make it the most comprehensive models of V1 development and function to date.

When examining surround modulation in our model, we focused on the two most-

studied properties, the size tuning and orientation contrast tuning of V1 neurons. We show that most neurons in the model layer 2/3 express both realistic size and orientation contrast tuning. However, at the same time we show that a considerable number of model neurons express size and orientation contrast tuning that deviate from the stereotypical tuning curves described in experimental literature. Importantly, we have identified similar deviations in the published data, indicating that such systematic deviations might also be present in animals. This highlights the potential predictive power of our model, and at the same time stresses the need to analyze data from experiments in greater detail, not focusing only on formulating the simplest general principles but also examining systematic deviations from the stereotypical average.

To further facilitate the advantages of our modeling paradigm which does not rely on a single or homogeneous groups of neurons but rather exhibits a high degree of variability, we proceeded to examine this variation of single cell properties and identifying relationships between them. The most important predictions of this analysis come from correlating the surround modulation properties with the position of neurons in the orientation maps as discussed in section 5.6.5. In the model, the local homogeneity index of neurons is positively correlated with suppression index and negatively correlated with both orientation contrast suppression index and the distance of summation peak, indicating that the suppression at singularities in the map is both less strong and less orientation specific than in the centers of orientation columns. At the same time, the weaker suppression in singularities causes the summation peak to shift to larger distances. These findings represent predictions for future animal experiments.

In the present work we focused our analysis on the layer 2/3, mainly because it is the main contributor to the lateral interactions in the model that drive the surround modulation. However, the feedback pathway from layer 2/3 to layer 4C means that model neurons in this layer are likely to inherit the surround modulation properties of layer 2/3 cells. Therefore, an immediate next step in the analysis would be to examine the various tuning properties of simple cells in model layer 4Cβ and compare them with the complex cells in layer 2/3. Some differences in contextual modulation both between cortical layers and between simple and complex cells have already been found in animals. For example, complex cells have been found to express stronger surround suppression than simple cells, and similarly cells in layer 2/3 have been found to express stronger suppression than neurons in other layers [3].

Furthermore, previous studies in cat V1 have found significant variability in the tuning of the excitatory and inhibitory components and their relationship to the result-

ing spiking of the cells [136]. Monier et al. hypothesized that this variability could reflect inhomogeneities in functional intra-cortical connectivity regulated by correlation-based activity-dependent processes. Our model contains correlation-based activity-dependent processes (in the form of Hebbian learning) which we have shown lead to development of systematic functional and structural inhomogeneities known to exist in V1 (orientation maps or development of patchy lateral connectivity). Because we have already linked these inhomogeneities to several V1 neuron properties, comparing our model with the work of Monier et al. [136] could in future lead to a single coherent explanation of all these V1 phenomena. Finally, taking the suggested analysis one step further, one could study the detailed time course of the onset of the excitatory and inhibitory components and relate them with existing studies [136] which have examined these issues in V1 neurons and thus further extending the range of V1 phenomena covered by the model.

Another possible direction of investigation is the extension of our model into higher cortical areas. Because the main output of cortical areas originates in layer 2/3 and unlike most developmental models of cortical maps our model simulates layer 2/3 and complex cells, we are in an ideal position to build large scale developmental models of V2, with realistic input from V1. This in turn can further improve the study of contextual modulation in V1, as it would allow the inclusion of the second major anatomical substrate implicated in surround modulation (especially in the far surround and at short latencies [18]) — the feedback connections from higher cortical areas. Similarly, V1 sends feedback connections to LGN, which have been shown to modulate the responses of LGN neurons [11]. This thalamo-cortical loop is another mechanism that is hypothesized to influence the surround modulation properties of V1 neurons and could be studied in our model upon inclusion of the cortico-thalamic feedback connections.

The study of attention is another area where our model could be used as a test-bed for computational studies. It has been shown that attention modulates responses in V1 [137] and seems to influence the surround modulation properties of neurons [103]. Furthermore, it has been shown that acetylcholine influences the surround modulation properties of V1 neurons in an attention dependent way [88]. This might indicate that acetylcholine influences lateral interactions in V1 neurons and in turn change the surround modulation properties of V1 neurons. After the inclusion of higher level areas (such as V2) and corresponding feedback connections to V1 that are implicated in mediating the top-down attentional signals to V1, our model could be used to investigate the complex interactions of attention with the ongoing processing in V1.

Unlike most previous large scale developmental V1 models, this model demonstrates a wide range of realistic single cell properties. This advantage could in future be used to study the time course of development of such single-cell properties, leading to a formulation of additional modeling constraints and predictions. Currently, detailed data on the time course of the development of V1 neurons' properties is lacking and for this reason such study could be very useful to direct experiments in this area. On the other hand, there is substantial data comparing various V1 neurons' properties in young animals (mostly kittens) with those in mature animals. Although such studies typically lack the temporal precision to describe the whole time course of development, they could prove to be useful in constraining the model.

6.5 The modeling approach

The goal of this thesis was to create a comprehensive large-scale model of V1 that reproduces wide range of functional properties, while assuming only known connectivity. To a great extent, this goal determined the level of abstraction and modeling methodology we used to make the project practically feasible. Here we will discuss some of the main limitations that had to be accepted in the design of the models, and the potential implications on the results that stem from them.

One of the most important abstractions we made was the adoption of firing rate based representation. The nature of neural coding is one of the central questions of neuroscience. Unfortunately, even one of the most fundamental questions — whether the cortex (or the brain in general) primarily uses rate coding, or whether the timing of each single spike transmits important information — is still unanswered. Rate codes have obvious advantage of being robust to noise, a seemingly important property given the strong intrinsic noise observed in neurons, whereas the main advantages of temporal coding are that it can transmit more information per spike and responses can be decoded more quickly. There are examples of neural systems that clearly use a rate code, such as the neurons that innervate muscles [75], or a temporal code [48], such as the neurons in the early auditory pathway.

However, identifying temporal codes and especially showing that they are indeed used by the brain to encode information at the cortical level has proven difficult. Several studies have demonstrated millisecond precision timings for both awake and anesthetized animals [15, 186]. Note that, these studies were done under very specific stimulation paradigms, and it is not clear whether these findings transfer to normal vision.

In contrast, a recent study by London et al. [123] concluded that given the trial-to-trial variability present in cortex, the brain must be using rate code. It is unlikely that this controversy will be resolved soon.

The most important reason for choosing rate coding for this study was that all the functional properties that we attempted to reproduce in our models (orientation maps, orientation tuning, surround modulation effects, contrast response etc.), are measured in animals in a way that implicitly assumes rate coding. I.e., the measurement of these properties require recording of average firing rates over periods of tens to hundreds of milliseconds in response to various stimuli, and the rates are often further averaged across multiple trials. Thus, one can treat our model as a simplification of the neural processing where the time axis has been quantized into fixed-sized bins, each representing the number of spikes occurring in the given neuron during the corresponding time interval.

Naturally, even if the information in visual cortex is transmitted at the level of firing rates, such abstraction still leaves the possibility that despite reproducing the various functional properties correctly at a firing-rate level, the dynamics in our model leading to these specific firing rates are different from those we would observe if we assumed single spikes and more detailed models of single neurons. Consequently, one has to be cautious in interpreting the detailed temporal dynamics in our model and linking them directly to experimental data. In future we intend to extend the model with more realistic temporal properties, by assuming latencies of individual connections and direct modeling of single spikes. However, without doubt, should such transition be made, one can consider the current firing rate model as an important blueprint, which should significantly reduce the time of construction of such a more detailed model. At the same time it is unlikely that introduction of spiking would change the basic principles allowing our current models to achieve the various V1 properties, meaning that the main conclusions we draw from our simulations should still be valid.

In all models presented in this thesis, simple Hebbian learning was used as the underlying plasticity mechanism. A number of experimental studies have shown that activity-dependent, correlation-based synaptic adaptation is involved in neural plasticity [58, 87, 190], suggesting the Hebbian learning is a plausible abstraction of these mechanisms. Hebbian learning in its simplest form has an important disadvantage in that it causes connections weights to increase indefinitely, which is both computationally impractical and biologically implausible. The most common techniques for addressing this problem assume some form of normalization. The two most common

types are subtractive and divisive normalization. Subtractive normalization decreases each weight by an equal amount after the weights adapt, so that the total strength of weights remains constant. Divisive normalization instead decreases weights proportional to their original size. Over time, subtractive normalization tends to drive each connection weight towards zero or some maximum strength, which is biologically implausible, whereas divisive normalization allows for development of graded representations and drives the weights towards the eigenvector of the input correlation matrix [135]. Therefore, in our models we adopt divisive normalization as it is more biologically plausible and allows for finer control of synaptic weights. Furthermore, even though the normalization terms were originally introduced for computational and theoretical reasons, later experimental studies have found a number of biological mechanisms regulating the overall synaptic strength and intrinsic neural excitability during adaptation [153, 37, 140, 191], which could implement such normalization in biological neurons. For example, Turrigiano et al. [191] showed that a change in a synapse can cause an opposite change in the other synapses in the same neuron, in line with the synaptic adaptation implied by normalization.

An assumption that we have adopted from previous LISSOM models is that plasticity decreases over time, simulating the reduction of plasticity between critical periods in early development and adulthood. We implement this phenomena as an exponential decay of the learning rate over time, meaning that the plasticity will be close to 0 at the end of the simulation. Even though assuming a decrease of plasticity after early development is plausible, visual cortex does not become completely static after maturation and can adapt to retinal lesions or other changes in visual input. Due to the complexity and high computational costs of our models, it was out of the scope of this thesis to study in detail the stability of the development in the models with respect to the learning rate regime. However, as Law showed [119], one can achieve stable map development in LISSOM-type models even under non-decreasing learning rates, suggesting that it should be possible to adjust our models in future such that they remain stable under constant non-zero learning rates.

Hebbian plasticity of connections has not been applied to all projections in the model. In the final model presented in chapter 5, we model plasticity in the layer 4C afferent and layer 2/3 long-range excitatory connections, but we keep the sub-cortical pathways, short-range excitatory and inhibitory, and the narrow afferent and feedback excitatory connectivity between layer 4C and 2/3 static. The afferent connections to layer 4C and the long-range excitatory connections are widely believed to be highly

plastic during early development in line with our model. In this work we are mainly interested in activity-based development at the cortical level, and thus the sub-cortical pathways are assumed to have adult characteristics at the beginning of the simulations. There is substantial evidence that inhibitory neurons express broad tuning, indicating less selective pooling of information from neighboring neurons [112, 143]. Therefore our assumption of non-plastic inhibitory connectivity should be plausible. However, should future experiments find direct evidence of selective pooling in inhibitory neurons, plasticity in inhibitory neurons can easily be added to the model. Given that previous LISSOM models were assuming plastic lateral inhibition we believe, this should not interfere with the main properties of the model. This leaves the short-range excitatory and the narrow (and thus implicitly short-range) connectivity between layers 4C and 2/3. A recent study by Buzás [42] found that the distribution of lateral connections with respect to orientation maps is best described by superposition of a spatially extended orientation-specific and a local orientation-invariant component, indicating that the short range connectivity of pyramidal neurons in layer 2/3 is unselective. The functional specificity of the connections between layers 4C and 2/3 are currently unclear, however as they also correspond to short range connectivity and we do not want to add complexity to the model that is not confirmed experimentally, it is reasonable to assume these connections also static. Again, should future experiments reveal specificity, it is straightforward to assume plasticity also in these connections, and study its influence on the development.

The next important simplification we made in the model is that we have ignored the detailed temporal properties of the subcortical neural responses and of signal propagation along the various types of connections. Instead we assumed that the RGC/LGN neurons have a constant, sustained output, and that all connections in each projection have a constant delay, independent of the physical length of that connection. Modelling the subcortical temporal response properties and simulating non-uniform delays on the various model projections would have greatly increased the number of time-steps needed to simulate each input presentation. Given the size of our models and the number of input presentations required for simulation of development, modelling such phenomena is currently computationally infeasible. Once sufficient computing power is available, the Topographica simulator provides mechanisms for simulating the dynamics in more detail, and all the models presented in this thesis can in principle be extended in that direction. However, it is likely that such changes will change the dynamics in the model somewhat, so some of the parameters will have to be adjusted

in order to compensate for these changes and achieve the V1 properties reproduced by the current model. Because of these simplifications, one shoulld be cautious about over-interpreting the details of the dynamics observed in the models, which limits our ability to address some of the interesting questions in surround modulation that are critically dependent on timing [18, 101].

The last design step we do on the way to the final model in chapter 5 is to explicitly model excitatory and inhibitory neurons (instead of positive and negative connections as in the other presented models) and to introduce short-range inhibitory and long-range excitatory lateral connections in layer 2/3. As we have shown in chapter 4, assuming realistically weak lateral connections in layer 4C (about one fourth of the strength in layer 2/3) does not change the behavior of our model significantly compared to the case when we remove the lateral connectivity from layer 4C altogether. Therefore, in order to save computational resources, for our final model we decided to omit lateral connectivity in layer 4C, and consequently also avoided explicitly modeling excitatory and inhibitory neurons in this layer. However, in future it would be desirable to study the model with lateral connectivity present also in layer 4C, especially should one want to perform a detailed comparison between various properties of neurons in the two model cortical layers.

In the cortex, excitation elicited by a stimulus is followed a few milliseconds later by inhibition [199, 205], thus possibly limiting the window for integration and preventing explosion of activation. This idea is supported by studies showing that pharmacologically blocking inhibition leads to cortical activity becoming epileptic [64]. Overall, the current experimental evidence suggests that co-activation of inhibition and excitation is a basic functional principle in cortex, but the exact balance between them can change in specific conditions [86]. Reflecting these general principles, we set lateral inhibitory and excitatory connections to have opposite values for the model in chapter 4, ensuring that the excitation and inhibition at cortical level is on average approximately balanced. Empirical tests during the tuning of the model showed that small changes to the strength ratio of these connections (on the scale of 10%) do not disrupt the model dynamics, but that larger changes can have very significant effects. However, due to the high computational costs of the model, a detailed parameter search and analysis of this issue has not been done. The final model in chapter 5 simulates inhibitory and excitatory neurons separately and two types of lateral connections (short range and long range), and thus the balance between excitation and inhibition is not directly defined only by the strength of the connections. However, again during the tuning of the

model, we set the strengths of the lateral connections such that the inhibition and excitation is approximately balanced, ensuring stable network dynamics. During the tuning of the model we observed that this model is more sensitive to the precise strength of the various connections, which is not surprising given the higher complexity and larger number of recurrent pathways than in the somewhat simpler model introduced in chapter 4. Overall, all of the models operate under the general principle of co-activation of inhibition and excitation that are on average approximately balanced, and are sensitive to any changes of parameters that disrupt this balance. It is likely that this relatively precise balance between excitation and inhibition, which in our model was achieved by deliberate tuning of the connection parameters, must be maintained via active mechanisms in animal brains. However, currently there is little specific evidence what these hypothetical mechanisms might be and how they operate. Once more details become known in the future, our model would represent an interesting context for the study of these mechanisms.

6.6 The big picture

In the first chapter we expressed our belief that one of the main problems with the current state of the field of neuroscience is that it is rapidly producing huge amounts of findings, with relatively little effort in reconciling all this accumulated evidence into a comprehensive theory of brain development and function. Following this belief, instead of focusing this thesis on formulating even more detailed explanation of specific cortical phenomena or addressing those that had received little attention before, we decided to focus on bringing numerous well-studied V1 phenomena into a single model. Pursuing such goals is not trivial, because not all previously proposed explanations for the different V1 phenomena are mutually compatible, and one not only has to select those that can potentially work together but also further modify them in order to integrate them into a single model. We believe that this study shows that by doing so, one not only creates a description of V1 development and function that is more comprehensive (a goal that we believe should be pursued in every scientific discipline) but it also allows for examination of V1 properties that would not be accessible in simpler models and can produce novel predictions that can be used to guide future V1 experiments. Naturally, this study still represents only a small step towards a model that can explain V1 development and function in totality, and a lot of work remains to be done. In the reminder of this chapter, we will discuss some of the more general topics that

stem from this study and outline directions of future work that we would like to pursue.

One interesting phenomenon that we have encountered several times when building the models described in this thesis is a duality relationship between plasticity rules and the architecture of the underlying network in which they operate. As discussed in chapter 3, the Triesch rule is a homeostatic plasticity rule that should achieve an exponential distribution of firing rates of a pre-defined mean for a given neuron. This rule was derived under the general conditions that the neuron is embedded in a arbitrary neural network. However, neural networks in the brain are highly structured, and as demonstrated in the GCA-LISSOM model, even simpler homeostatic mechanism in the context of such structured network can account for the same properties (eg. in our case achieving exponential distribution of firing rates of desired mean).

Another example of this principle come up in our complex cell model introduced in chapter 4. As explained in detail in section 4.2, the architecture of the complex cell model, and consequently the resulting temporal dynamics of activations in the model, allow it to exploit the temporal correlations in the input, such that when combined with simple Hebbian learning rule the model forms cells that are insensitive to the exact phase of the stimulus. It is thus possible to relate the model to learning algorithms such as slow feature analysis [207] or the trace rule [73]. This again shows that one can potentially substitute such elaborate learning rules with an appropriate combination of dynamics in the network and a simple Hebbian learning rule, explaining how one can implement these advanced learning rules in a more biologically plausible framework.

To summarize, it is possible to encode properties that are traditionally assumed to take forms of various advanced plasticity rules into the architecture of the network and thus allow for implementing these advanced properties even with simpler plasticity mechanisms already identified in the brain. This further supports our proposal to work with more elaborate models, as it shows that concentrating purely on simple models lacking the structure of cortical networks can lead to a formulation of increasingly elaborate learning rules that could be avoided should the structure of the cortical network be taken into account.

One of the main contributions of this thesis is that the presented models adhere more closely to the known anatomy of V1 than previous developmental models, by explicitly modeling both layer 4C and layer 2/3 and assuming only known connectivity between these layers and LGN. Furthermore, in chapter 5 we take one step further by explicitly modeling inhibitory neurons in layer 2/3. A natural progression in this direction would be to continue covering other anatomical features of cortex, notably layer 5

and 6, that are responsible for sending major projections back to the thalamus and receive the input from other cortical areas. Even further, one could consider the different morphological cell subtypes, such as dividing the excitatory neurons into pyramidal and spiny stellate cells. The major difficulty in including these features is the fact that relatively little is currently known about their specific role in cortical function. Perhaps the most promising immediate project of this kind would be considering the feedback connections from layer 6 to LGN and examining the influence of this additional loop in information flow on the various functional properties already present in the model both at the level of LGN and V1.

Instead of increasing the detail at which we model the primary visual cortex, another direction of future work we are particularly excited about is extending the scope of the model to other cortical areas. One of the major contributions of this work towards future models is the addition of layer 2/3 — the main layer in cortex sending projections to other cortical areas. This makes our model ready to be extended with higher level visual areas such as V2 or MT which receive strong input from V1. Because our model exhibits a large number of V1 properties, both at the population and single cell level, such an endeavor could be particularly fruitful, as previous models of higher level areas had to rely on much less realistic output from V1. Again, the main difficulty is that relatively little is known about processing in V2. However, because our model expresses already significantly realistic functional properties, we could instead attempt to simply replicate the architecture used to simulate V1 in the present models to model V2 and look for properties that emerge. These emerged properties could then be compared to the existing experimental results and tested in new experimental studies.

Another natural progression from the current work is to extend the temporal level of detail by simulating individual spikes rather than just working at the level of average firing rates. This would allow the simulation of the network dynamics at finer temporal scales, making it possible to investigate such phenomena as the detailed temporal evolution of the surround modulation effects, which have been described experimentally [18], or the evolution of orientation tuning after stimulus onset. Given the high non-linearity and strong recurrence of the model, the finer temporal dynamics after implementation of spiking should prove rich, giving ample opportunity to further constraining the model against the known experimental evidence.

The proposed model builds on a rich heritage of the numerous variants of the LISSOM model architecture. One particular strength of this model family is the high num-

ber of different known functional cortical maps that have been developed using these models, including maps of ocular dominance, orientation, disparity, spatial frequency, motion direction, and color. Furthermore, several LISSOM variants have shown development of not only single map but combinations of maps in a single model. Because our model builds on top of the LISSOM architecture, it should be relatively straightforward to replicate these results in the present model using proven techniques from the previous work. Another interesting contribution of the previous LISSOM model family is that it is possible to explain the tilt after effect and other illusion with them [24]. The improvements of the surround modulation model over previous LISSOM models suggest that it would be worthwhile to examine whether we can now explain some of the wide range of illusions believed to be induced in early vision [65]. This would further extend the explanatory power of the model, as it would allow us to link its dynamics with behavior.

However, most of the above proposals would certainly come at a great computational cost. It became evident throughout the work on this thesis, that before significant advances from the current models can be done, a fundamental revision of the modeling software will have to be undergone. The most complex model presented in the chapter 5 occupies up to 8 GB of memory and it takes about 24 hours to run the 100000 iterations required for the development of the model on a modern desktop machine. Clearly this performance is on the edge of practical usability. During the work on this thesis we have encounter a several situations where it would have been beneficial to be able to run more simulations or larger models. A common issue is the need to explore more thoroughly the parameter space in order to establish the region of parameter space in which the models exhibit certain properties (as we have discussed, for example, in chapter 3). Another common requirement is the need to run the models with higher density to increase number of neurons per cortical column to improve certain model features, such as a more even distribution of phase preference as pointed out in chapter 4, or running simulations representing larger regions of cortical space, so as to model the full extent of lateral connections as discussed in chapter 5. Finally, the subsequent analysis of the networks can prove to be even more computationally demanding. This was encountered in chapter 5 where we had to limit the number of neurons for which we have measured detailed surround modulation tuning curves to about 30, because it took more than a week of CPU time to perform this analysis even with this limited number. In any case, it is clear that before any significant advancement of these models can be done, the simulation software will have to be able to exploit distributed com-

putational resources. The two most promising solutions are via parallel computing on clusters or using GPU acceleration. Luckily, the nature of the computations required for these models are ideally suited for parallelization, and there is ongoing work in the Bednar lab examining both of these options. Therefore, we hope that in the near future we will be able to address at least some of the above issues.

6.7 Conclusions

The holy grail of computational neuroscience and artificial intelligence is to achieve a single comprehensive and unifying theory of the brain expressed as a runnable computational model. At the beginning of this study we expressed our belief that the current state of neuroscience in general and computational neuroscience in particular is such that the knowledge in this field is largely fragmented, with a lack of concerted effort to unify it. The main overarching contribution of this thesis is that it addresses this problem in the narrower context of V1 cortex, by merging properties usually studied in two different groups of models — models of V1 map development and models of adult function — into a single model. This way, we believe we have achieved the most comprehensive model of V1 function and development today. Even more importantly, we demonstrate that creating such comprehensive model does not purely serve the goal of unification, but by examining the interactions between the different V1 properties represented in the model, allows us to explore aspects of V1 that has been largely overlooked in previous experimental studies or abstracted away in computational models. Finally, the inclusion of many features of V1 into a single model, makes it an ideal candidate for future models of cortex that will step beyond V1, as it can provide them with realistic input from this cortical area.

Bibliography

[1] L. F. Abbott, J. A. Varela, K. Sen, and S. B. Nelson. Synaptic depression and cortical gain control. *Science (New York, N.Y.)*, 275(5297):220–224, January 1997.

[2] B. Ahmed, J. C. Anderson, R. J. Douglas, K. A. Martin, and D. Whitteridge. Estimates of the net excitatory currents evoked by visual stimulation of identified neurons in cat visual cortex. *Cereb. Cortex*, 8(5):462–476, 1998.

[3] T. Akasaki. Suppressive effects of receptive field surround on neuronal activity in the cat primary visual cortex. *Neuroscience Research*, 43(3):207–220, 2002.

[4] D. M. Alexander, P. D. Bourke, P. Sheridan, O. Konstandatos, and J. J. Wright. Intrinsic connections in tree shrew V1 imply a global to local mapping. *Vision Research*, 44:857–876, 2004.

[5] H. Alitto. Corticothalamic feedback and sensory processing. *Current Opinion in Neurobiology*, 13(4):440–445, 2003.

[6] H. J. Alitto and W. M. Usrey. Influence of contrast on orientation and temporal frequency tuning in ferret primary visual cortex. *J Neurophysiol*, 91(6):2797–2808, 2004.

[7] J. Allman, F. Miezin, and E. McGuinness. Stimulus specific responses from beyond the classical receptive field: Neurophysiological mechanisms for local-global comparisons in visual neurons. *Annual Review of Neuroscience*, 8(1):407–430, 1985.

[8] J. M. Alonso, W. M. Usrey, and R. C. Reid. Rules of connectivity between geniculate cells and simple cells in cat primary visual cortex. *J Neurosci*, 21(11):4002–4015, Jun 2001.

[9] J. S. Anderson, M. Carandini, and D. Ferster. Orientation tuning of input conductance, excitation, and inhibition in cat primary visual cortex. *J Neurophysiol*, 84(2):909–926, 2000.

[10] I. M. Andolina, H. E. Jones, W. Wang, and A. M. Sillito. Corticothalamic feedback enhances stimulus response precision in the visual system. *Proceedings of the National Academy of Sciences of the United States of America*, 104(5):1685–1690, January 2007.

[11] A. Angelucci and P. C. Bressloff. Contribution of feedforward, lateral and feedback connections to the classical receptive field center and extra-classical receptive field surround of primate V1 neurons. *Prog Brain Res*, 154:93–120, 2006.

[12] A. Angelucci and J. Bullier. Reaching beyond the classical receptive field of V1 neurons: Horizontal or feedback axons? *J Physiol Paris*, 97(2-3):141–154, 2003.

[13] A. Angelucci, J. B. Levitt, and J. S. Lund. Anatomical origins of the classical receptive field and modulatory surround field of single neurons in macaque visual cortical area V1. *Progress in Brain Research*, 136:373–388, 2002.

[14] A. Angelucci, J. B. Levitt, E. J. Walton, J. M. Hupe, J. Bullier, and J. S. Lund. Circuits for local and global signal integration in primary visual cortex. *Journal of Neuroscience*, 22:8633–8646, 2002.

[15] E. Arabzadeh, S. Panzeri, and M. E. Diamond. Deciphering the spike train of a sensory neuron: Counts and temporal patterns in the rat whisker pathway. *J. Neurosci.*, 26(36):9216–9226, September 2006.

[16] D. Aronov, D. S. Reich, F. Mechler, and J. D. Victor. Neural coding of spatial phase in V1 of the macaque monkey. *J Neurophysiol*, 89(6):3304–3327, 2003.

[17] R. Azouz, C. M. Gray, L. G. Nowak, and D. A. McCormick. Physiological properties of inhibitory interneurons in cat striate cortex. *Cereb. Cortex*, 7(6):534–545, 1997.

[18] W. Bair, J. R. Cavanaugh, and J. A. Movshon. Time course and time-distance relationships for surround suppression in macaque V1 neurons. *J. Neurosci.*, 23(20):7690–7701, 2003.

[19] C. Bardy, J. Y. Huang, C. Wang, T. FitzGibbon, and B. Dreher. 'Simplification' of responses of complex cells in cat striate cortex: Suppressive surrounds and 'feedback' inactivation. *The Journal of Physiology*, 574(3):731–750, 2006.

[20] A. Bartsch and J. van Hemmen. Combined Hebbian development of geniculocortical and lateral connectivity in a model of primary visual cortex. *Biol Cybern*, 84:41–55, 2001.

[21] M. F. Bear, B. Connors, and M. Paradiso. *Neuroscience: Exploring the Brain (Third Edition)*. Lippincott Williams & Wilkins, 2006.

[22] J. A. Bednar. Topographica: Building and analyzing map-level simulations from Python, C/C++, MATLAB, NEST, or NEURON components. *Frontiers in Neuroinformatics*, 3:8, 2009.

[23] J. A. Bednar, Y. Choe, J. De Paula, R. Miikkulainen, J. Provost, and T. Tversky. Modeling cortical maps with Topographica. *Neurocomputing*, 58–60:1129–1135, 2004.

[24] J. A. Bednar and R. Miikkulainen. Tilt aftereffects in a self-organizing model of the primary visual cortex. *Neural Computation*, 12(7):1721–1740, 2000.

[25] R. Ben-Yishai, R. L. Bar-Or, and H. Sompolinsky. Theory of orientation tuning in visual cortex. *Proc Natl Acad Sci U S A*, 92(9):3844–3848, 1995.

[26] S. Bennett. *A History of Control Engineering 1930-1955*. Peter Peregrinus, Hitchin, Herts., UK, 1993.

[27] T. Binzegger, R. J. Douglas, and K. A. C. Martin. A quantitative map of the circuit of cat primary visual cortex. *The Journal of Neuroscience*, 24:8441–8453, 2004.

[28] T. Binzegger, R. J. Douglas, and K. A. C. Martin. Topology and dynamics of the canonical circuit of cat V1. *Neural Networks*, 22(8):1071–1078, 2009.

[29] P. O. Bishop, J. S. Coombs, and G. H. Henry. Interaction effects of visual contours on the discharge frequency of simple striate neurones. *The Journal of physiology*, 219(3):659–687, December 1971.

[30] C. Blakemore and G. F. Cooper. Development of the brain depends on the visual environment. *Nature*, 228(5270):477–478, 1970.

[31] C. Blakemore and D. J. Price. The organization and post-natal development of area 18 of the cat's visual cortex. *The Journal of Physiology*, 384:263–292, 1987.

[32] C. Blakemore and E. A. Tobin. Lateral inhibition between orientation detectors in the cat's visual cortex. *Experimental brain research. Experimentelle Hirnforschung. Expérimentation cérébrale*, 15(4):439–440, 1972.

[33] G. G. Blasdel. Orientation selectivity, preference, and continuity in monkey striate cortex. *Journal of Neuroscience*, 12:3139–3161, 1992.

[34] D. M. Blitz and W. G. Regehr. Timing and specificity of feed-forward inhibition within the lgn. *Neuron*, 45(6):917–928, 2005.

[35] V. Bonin, V. Mante, and M. Carandini. The suppressive field of neurons in lateral geniculate nucleus. *The Journal of Neuroscience*, 25(47):10844–10856, 2005.

[36] W. H. Bosking, Y. Zhang, B. Schofield, and D. Fitzpatrick. Orientation selectivity and the arrangement of horizontal connections in tree shrew striate cortex. *J Neurosci*, 17(6):2112–2127, Mar 1997.

[37] J. P. Bourgeois, P. J. Jastreboff, and P. Rakic. Synaptogenesis in visual cortex of normal and preterm monkeys: Evidence for intrinsic regulation of synaptic overproduction. *Proceedings of the National Academy of Sciences, USA*, 86:4297–4301, 1989.

[38] A. J. Bray and H. G. Barrow. Simple cell adaptation in visual cortex: A computational model of processing in the early visual pathway. Technical Report CSRP 331, School of Cognitive and Computing Sciences, University of Sussex, Brighton, UK, 1996.

[39] F. Briggs and E. M. Callaway. Laminar patterns of local excitatory input to layer 5 neurons in macaque primary visual cortex. *Cereb. Cortex*, 15(5):154–488, 2004.

[40] V. Bringuier, F. Chavane, L. Glaeser, and Y. Frégnac. Horizontal propagation of visual activity in the synaptic integration field of area 17 neurons. *Science*, 283(5402):695–699, 1999.

[41] T. Burger and E. W. Lang. Self-organization of local cortical circuits and cortical orientation maps: A nonlinear hebbian model of the visual cortex with adaptive lateral couplings. *Z Naturforsch [C]*, 56(5-6):464–478, 2001.

[42] P. Buzás, K. Kovács, A. S. Ferecskó, J. M. Budd, U. T. Eysel, and Z. F. Kisvárday. Model-based analysis of excitatory lateral connections in the visual cortex. *The Journal of comparative neurology*, 499(6):861–881, December 2006.

[43] P. Buzás, M. Volgushev, U. Eysel, and Z. Kisvrday. Independence of visuotopic representation and orientation map in the visual cortex of the cat. *Eur. J. Neurosci.*, 18:957–968, 2003.

[44] E. M. Callaway. Local circuits in primary visual cortex of the macaque monkey. *Annual review of neuroscience*, 21:47–74, 1998.

[45] E. M. Callaway and A. K. Wiser. Contributions of individual layer 2–5 spiny neurons to local circuits in macaque primary visual cortex. *Visual Neuroscience*, 13:907–922, 1996.

[46] M. W. Cannon and S. C. Fullenkamp. Spatial interactions in apparent contrast: inhibitory effects among grating patterns of different spatial frequencies, spatial positions and orientations. *Vision research*, 31(11):1985–1998, 1991.

[47] M. Carandini, D. J. Heeger, and J. A. Movshon. Linearity and normalization in simple cells of the macaque primary visual cortex. *J. Neurosci.*, 17(21):8621–8644, November 1997.

[48] C. E. Carr. Processing of temporal information in the brain. *Annual review of neuroscience*, 16:223–243, 1993.

[49] J. R. Cavanaugh, W. Bair, and J. A. Movshon. Nature and interaction of signals from the receptive field center and surround in macaque V1 neurons. *J Neurophysiol*, 88(5):2530–2546, 2002.

[50] F. S. Chance, L. F. Abbott, and A. D. Reyes. Gain modulation from background synaptic input. *Neuron*, 35(4):773–782, August 2002.

[51] F. S. Chance, S. B. Nelson, and L. F. Abbott. Complex cells as cortically amplified simple cells. *Nature Neuroscience*, 2(3):277–282, March 1999.

[52] B. Chapman and T. Bonhoeffer. Overrepresentation of horizontal and vertical orientation preferences in developing ferret area 17. *Proceedings of the National Academy of Sciences, USA*, 95:2609–2614, 1998.

[53] B. Chapman and M. P. Stryker. Development of orientation selectivity in ferret visual cortex and effects of deprivation. *J Neurosci*, 13(12):5251–5262, 1993.

[54] B. Chapman, M. P. Stryker, and T. Bonhoeffer. Development of orientation preference maps in ferret primary visual cortex. *The Journal of Neuroscience*, 16(20):6443–6453, 1996.

[55] H. J. Chisum and D. Fitzpatrick. The contribution of vertical and horizontal connections to the receptive field center and surround in V1. *Neural Networks*, 17(5-6):681–693, 2004.

[56] D. Contreras and L. Palmer. Response to contrast of electrophysiologically defined cell classes in primary visual cortex. *J. Neurosci.*, 23(17):6936–6945, 2003.

[57] M. Crair, D. Gillespie, and M. Stryker. The role of visual experience in the development of columns in cat visual cortex. *Science*, 279:566–570, 1998.

[58] M. C. Crair and R. C. Malenka. A critical period for long-term potentiation at thalamocortical synapses. *Nature*, 375(6529):325–328, May 1995.

[59] N. A. Crowder, J. van Kleef, B. Dreher, and M. R. Ibbotson. Complex cells increase their phase sensitivity at low contrasts and following adaptation. *J Neurophysiol*, 98(3):1155–1166, 2007.

[60] G. C. DeAngelis, R. D. Freeman, and I. Ohzawa. Length and width tuning of neurons in the cat's primary visual cortex. *Journal of neurophysiology*, 71(1):347–374, 1994.

[61] G. C. DeAngelis, G. M. Ghose, I. Ohzawa, and R. D. Freeman. Functional Micro-Organization of Primary Visual Cortex: Receptive Field Analysis of Nearby Neurons. *The Journal of Neuroscience*, 19(10):4046–4064, 1999.

[62] N. S. Desai, L. C. Rutherford, and G. G. Turrigiano. Plasticity in the intrinsic excitability of cortical pyramidal neurons. *Nature neuroscience*, 2(6):515–520, June 1999.

[63] M. R. Diamond, J. Ross, and M. C. Morrone. Extraretinal control of saccadic suppression. *The Journal of Neuroscience*, 20(9):3449–3455, 2000.

[64] M. A. Dichter and G. F. Ayala. Cellular mechanisms of epilepsy: a status report. *Science (New York, N.Y.)*, 237(4811):157–164, July 1987.

[65] D. M. Eagleman. Visual illusions and neurobiology. *Nature Reviews Neuroscience*, 2(12):920–926, 2001.

[66] E. D. Eggers and P. D. Lukasiewicz. Interneuron circuits tune inhibition in retinal bipolar cells. *J Neurophysiol*, 103(1):25–37, 2010.

[67] W. Einhäuser, C. Kayser, P. König, and K. P. Körding. Learning the invariance properties of complex cells from their responses to natural stimuli. *European Journal of Neuroscience*, 15:475–486, 2002.

[68] U. A. Ernst, K. R. Pawelzik, C. Sahar-Pikielny, and M. V. Tsodyks. Intracortical origin of visual maps. *Nat Neurosci*, 4(4):431–436, 2001.

[69] E. Erwin, K. Obermayer, and K. Schulten. Models of orientation and ocular dominance columns in the visual cortex: A critical comparison. *Neural Comput*, 7(3):425–468, 1995.

[70] D. Ferster. Spatially opponent excitation and inhibition in simple cells of the cat visual cortex. *J. Neurosci.*, 8(4):1172–1180, 1988.

[71] D. J. Field, A. Hayes, and R. Hess. Contour integration by the human visual system: evidence for a local ”association field”. *Vision research*, 33(2):173–193, January 1993.

[72] I. M. Finn, N. J. Priebe, and D. Ferster. The emergence of contrast-invariant orientation tuning in simple cells of cat visual cortex. *Neuron*, 54(1):137–152, 2007.

[73] P. Földiák. Learning invariance from transformation sequences. *Neural Computation*, 3(2):194–200, 1991.

[74] W. S. Geisler and D. G. Albrecht. Cortical neurons: isolation of contrast gain control. *Vision Res*, 32(8):1409–1410, August 1992.

[75] A. P. Georgopoulos, A. B. Schwartz, and R. E. Kettner. Neuronal population coding of movement direction. *Science*, 233:1416–1419, 1986.

[76] C. D. Gilbert and T. N. Wiesel. Columnar specificity of intrinsic horizontal and corticocortical connections in cat visual cortex. *J Neurosci*, 9(7):2432–2442, Jul 1989.

[77] I. Gödecke and T. Bonhoeffer. Development of identical orientation maps for two eyes without common visual experience. *Nature*, 379:251–254, 1996.

[78] I. Gödecke, D. S. Kim, T. Bonhoeffer, and W. Singer. Development of orientation preference maps in area 18 of kitten visual cortex. *Eur J Neurosci*, 9(8):1754–1762, 1997.

[79] A. Grabska-Barwinska and C. von der Malsburg. Establishment of a scaffold for orientation maps in primary visual cortex of higher mammals. *J. Neurosci.*, 28:249–257, 2008.

[80] A. Grinvald, E. E. Lieke, R. D. Frostig, and R. Hildesheim. Cortical point-spread function and long-range lateral interactions revealed by real-time optical imaging of macaque monkey primary visual cortex. *The Journal of Neuroscience*, 14(5):2545–2568, 1994.

[81] S. Grossberg and S. J. Olson. Rules for the cortical map of ocular dominance and orientation columns. *Neural Networks*, 7:883–894, 1994.

[82] M. Grubb, F. Rossi, J. Changeux, and I. Thompson. Abnormal functional organization in the dorsal lateral geniculate nucleus of mice lacking the beta 2 subunit of the nicotinic acetylcholine receptor. *Neuron*, 40:1161–1172, 2003.

[83] A. Gupta, Y. Wang, and H. Markram. Organizing principles for a diversity of GABAergic interneurons and synapses in the neocortex. *Science*, 287(5451):273–278, 2000.

[84] D. J. Heeger. Normalization of cell responses in cat striate cortex. *Visual neuroscience*, 9(2):181–197, 1992.

[85] J. Hegde and D. C. Van Essen. A comparative study of shape representation in macaque visual areas V2 and V4. *Cereb. Cortex*, 17(5):1100–1116, 2007.

[86] J. E. Heiss, Y. Katz, E. Ganmor, and I. Lampl. Shift in the balance between excitation and inhibition during sensory adaptation of s1 neurons. *J. Neurosci.*, 28(49):13320–13330, December 2008.

[87] T. K. Hensch, M. Fagiolini, N. Mataga, M. P. Stryker, S. Baekkeskov, and S. F. Kash. Local GABA circuit control of experience-dependent plasticity in developing visual cortex. *Science*, 282:1604–1608, 1998.

[88] J. L. Herrero, M. J. Roberts, L. S. Delicato, M. A. Gieselmann, P. Dayan, and A. Thiele. Acetylcholine contributes through muscarinic receptors to attentional modulation in V1. *Nature*, 454(7208):1110–1114, 2008.

[89] R. Hess and D. J. Field. Integration of contours: new insights. *Trends in Cognitive Sciences*, 3(12):480–486, December 1999.

[90] J. A. Hirsch, J.-M. Alonso, R. C. Reid, and L. M. Martinez. Synaptic integration in striate cortical simple cells. *J. Neurosci.*, 18(22):9517–9528, 1998.

[91] J. A. Hirsch and C. D. Gilbert. Synaptic physiology of horizontal connections in the cat's visual cortex. *J Neurosci*, 11(6):1800–1809, 1991.

[92] J. A. Hirsch and L. M. Martinez. Laminar processing in the visual cortical column. *Current opinion in neurobiology*, 16(4):377–384, 2006.

[93] B. hua Liu, P. Li, Y. J. Sun, L. Ya-tang, L. I. Zhang, and H. W. Tao. Intervening inhibition underlies simple-cell receptive field structure in visual cortex. *Nature Neuroscience*, 13(1):89–96, January 2010.

[94] D. H. Hubel and T. N. Wiesel. Receptive fields, binocular interaction and functional architecture in the cat's visual cortex. *Journal Physiology*, 160:106–154, 1962.

[95] D. H. Hubel and T. N. Wiesel. Sequence regularity and geometry of orientation columns in the monkey striate cortex. *The Journal of Comparative Neurology*, 158:267–294, 1974.

[96] J. J. Hunt, C. E. Giacomantonio, H. Tang, D. Mortimer, S. Jaffer, V. Vorobyov, G. Ericksson, F. Sengpiel, and G. J. Goodhill. Natural scene statistics and the structure of orientation maps in the visual cortex. *NeuroImage*, 47(1):157–172, August 2009.

[97] J. M. Hupé, A. C. James, P. Girard, S. G. Lomber, B. R. Payne, and J. Bullier. Feedback connections act on the early part of the responses in monkey visual cortex. *J Neurophysiol*, 85(1):134–145, 2001.

[98] J. M. Hupé, A. C. James, B. R. Payne, S. G. Lomber, P. Girard, and J. Bullier. Cortical feedback improves discrimination between figure and background by V1, V2 and V3 neurons. *Nature*, 394(6695):784–787, 1998.

[99] A. Hyvärinen and P. O. Hoyer. A two-layer sparse coding model learns simple and complex cell receptive fields and topography from natural images. *Vision research*, 41(18):2413–2423, 2001.

[100] J. M. Ichida, L. Schwabe, P. C. Bressloff, and A. Angelucci. Response facilitation from the "suppressive" receptive field surround of macaque V1 neurons. *J Neurophysiol*, 98(4):2168–2181, 2007.

[101] A. Ishikawa, S. Shimegi, H. Kida, and H. Sato. Temporal properties of spatial frequency tuning of surround suppression in the primary visual cortex and the lateral geniculate nucleus of the cat. *European Journal of Neuroscience*, 31(11):2086–2100, 2010.

[102] N. P. Issa, J. T. Trachtenberg, B. Chapman, K. R. Zahs, and M. P. Stryker. The critical period for ocular dominance plasticity in the ferret's visual cortex. *The Journal of Neuroscience*, 19(16):6965–6978, 1999.

[103] M. Ito and C. D. Gilbert. Attention modulates contextual influences in the primary visual cortex of alert monkeys. *Neuron*, 22(3):593–604, 1999.

[104] J. Z. Jin, C. Weng, C.-I. I. Yeh, J. A. Gordon, E. S. Ruthazer, M. P. Stryker, H. A. Swadlow, and J.-M. M. Alonso. On and off domains of geniculate afferents in cat primary visual cortex. *Nature neuroscience*, 11(1):88–94, 2008.

[105] H. E. Jones, I. M. Andolina, N. M. Oakely, P. C. Murphy, and A. M. Sillito. Spatial summation in lateral geniculate nucleus and visual cortex. *Experimental brain research. Experimentelle Hirnforschung. Expérimentation cérébrale*, 135(2):279–284, November 2000.

[106] H. E. Jones, K. L. Grieve, W. Wang, and A. M. Sillito. Surround suppression in primate V1. *J Neurophysiol*, 86(4):2011–2028, 2001.

[107] H. E. Jones, W. Wang, and A. M. Sillito. Spatial organization and magnitude of orientation contrast interactions in primate V1. *J Neurophysiol*, 88(5):2796–2808, 2002.

[108] G. J. Kalarickal and J. A. Marshall. Rearrangement of receptive field topography after intracortical and peripheral stimulation: The role of plasticity in inhibitory pathways. *Network: Computation in Neural Systems*, 13(1):1–40, 2002.

[109] Y. Karklin and M. S. Lewicki. Emergence of complex cell properties by learning to generalize in natural scenes. *Nature*, 457(7225):83–86, 2008.

[110] A. Kayser, N. J. Priebe, and K. D. Miller. Contrast-dependent nonlinearities arise locally in a model of contrast-invariant orientation tuning. *J Neurophysiol*, 85(5):2130–2149, 2001.

[111] A. S. Kayser and K. D. Miller. Opponent inhibitiona developmental model of layer 4 of the neocortical circuit. *Neuron*, 33(1):131–142, 2002.

[112] A. M. Kerlin, M. L. Andermann, V. K. Berezovskii, and R. C. Reid. Broadly tuned response properties of diverse inhibitory neuron subtypes in mouse visual cortex. *Neuron*, 67(5):858–871, September 2010.

[113] D. Kerschensteiner and R. O. L. Wong. A precisely timed asynchronous pattern of on and off retinal ganglion cell activity during propagation of retinal waves. *Neuron*, 58(6):851–858, 2008.

[114] Z. F. Kisvarday, A. S. Ferecsko, K. Kovacs, P. Buzas, J. M. L. Budd, and U. T. Eysel. One axon-multiple functions: Specificity of lateral inhibitory connections by large basket cells. *J Neurocytol*, 31(3-5):255–264, 2002.

[115] J. J. Knierim and D. C. van Essen. Neuronal responses to static texture patterns in area V1 of the alert macaque monkey. *J Neurophysiol*, 67(4):961–980, 1992.

[116] A. A. Koulakov and D. B. Chklovskii. Orientation preference patterns in mammalian visual cortex: a wire length minimization approach. *Neuron*, 29(2):519–527, February 2001.

[117] V. A. Lamme. The neurophysiology of figure-ground segregation in primary visual cortex. *The Journal of Neuroscience*, 15(2):1605–1615, 1995.

[118] T. Z. Lauritzen, A. E. Krukowski, and K. D. Miller. Local correlation-based circuitry can account for responses to multi-grating stimuli in a model of cat V1. *J Neurophysiol*, 86(4):1803–1815, 2001.

[119] J. S. Law. *Modeling the Development of Organization for Orientation Preference in Primary Visual Cortex*. PhD thesis, School of Informatics, The University of Edinburgh, Edinburgh, UK, 2009.

[120] J. B. Levitt and J. S. Lund. Contrast dependence of contextual effects in primate visual cortex. *Nature*, 387:73–76, 1997.

[121] Z. Li. Visual segmentation by contextual influences via intra-cortical interactions in the primary visual cortex. *Network: Computational Neural Systems*, 10:187–212, 1999.

[122] Z. Liu, J. Gaska, L. Jacobson, and D. Pollen. Interneuronal interaction between members of quadrature phase and anti-phase pairs in the cat's visual cortex. *Vision Research*, 32(7):1193–1198, 1992.

[123] M. London, A. Roth, L. Beeren, M. Hausser, and P. E. Latham. Sensitivity to perturbations in vivo implies high noise and suggests rate coding in cortex. *Nature*, 466(7302):123–127, July 2010.

[124] J. S. Lund. Anatomical organization of macaque monkey striate visual cortex. *Annu Rev Neurosci*, 11:253–288, 1988.

[125] M. B. Luskin and C. J. Shatz. Neurogenesis of the cat's primary visual cortex. *The Journal of comparative neurology*, 242(4):611–631, 1985.

[126] H. Markram, M. Toledo-Rodriguez, Y. Wang, A. Gupta, G. Silberberg, and C. Wu. Interneurons of the neocortical inhibitory system. *Nat Rev Neurosci*, 5(10):793–807, 2004.

[127] L. M. Martinez and J.-M. M. Alonso. Complex receptive fields in primary visual cortex. *The Neuroscientist*, 9(5):317–331, 2003.

[128] R. H. Masland. The fundamental plan of the retina. *Nature Neuroscience*, 4(9):877–886, 2001.

[129] C. J. McAdams. and J. H. R. Maunsell. Effects of attention on the reliability of individual neurons in monkey visual cortex. *Neuron*, 23(4):765–773, August 1999.

[130] D. McLaughlin, R. Shapley, M. Shelley, and D. J. Wielaard. A neuronal network model of macaque primary visual cortex (V1): orientation selectivity and dynamics in the input layer 4Calpha. *Proc Natl Acad Sci U S A*, 97(14):8087–8092, Jul 2000.

[131] R. Miikkulainen. Self-organizing process based on lateral inhibition and synaptic resource redistribution. In T. Kohonen, K. Mäkisara, O. Simula, and J. Kangas, editors, *Proceedings of the 1991 International Conference on Artificial Neural Networks*, pages 415–420. Amsterdam: North-Holland, 1991.

[132] R. Miikkulainen, J. A. Bednar, Y. Choe, and J. Sirosh. *Computaional Maps In The Visual Cortex*. Springer, 2005.

[133] K. Miller. A model for the development of simple cell receptive fields and the ordered arrangement of orientation columns through activity-dependent competition between ON- and OFF-center inputs. *J. Neurosci.*, 14:409–441, Jan 1994.

[134] K. D. Miller, J. B. Keller, and M. P. Stryker. Ocular dominance column development: Analysis and simulation. *Science*, 245:605–615, 1989.

[135] K. D. Miller and D. J. C. MacKay. The role of constraints in Hebbian learning. *Neural Computation*, 6:100–126, 1994.

[136] C. Monier, F. Chavane, P. Baudot, L. J. Graham, and Y. Frégnac. Orientation and direction selectivity of synaptic inputs in visual cortical neurons: A diversity of combinations produces spike tuning. *Neuron*, 37(4):663–680, 2003.

[137] B. C. Motter. Focal attention produces spatially selective processing in visual cortical areas V1, V2, and V4 in the presence of competing stimuli. *J Neurophysiol*, 70(3):909–919, 1993.

[138] J. A. Movshon, I. D. Thompson, and D. J. Tolhurst. Receptive field organization of complex cells in the cat's striate cortex. *The Journal of Physiology*, 283(1):79–99, 1978.

[139] P. C. Murphy, S. G. Duckett, and A. M. Sillito. Feedback connections to the lateral geniculate nucleus and cortical response properties. *Science.*, 286(5444):1552–1554, November 1999.

[140] M. Murray, S. Sharma, and M. A. Edwards. Target regulation of synaptic number in the compressed retinotectal projection of goldfish. *Journal of Computational Neurology*, 209:374–385, 1982.

[141] T. Nagano and K. Kurata. A self-organizing neural network model for the development of complex cells. *Biological Cybernetics*, 40(3):195–200, 1981.

[142] I. Nauhaus, A. Benucci, M. Carandini, and D. L. Ringach. Neuronal selectivity and local map structure in visual cortex. *Neuron*, 57(5):673–679, 2008.

[143] L. G. Nowak, M. V. Sanchez-Vives, and D. A. McCormick. Lack of orientation and direction selectivity in a subgroup of fast-spiking inhibitory interneurons: Cellular and synaptic mechanisms and comparison with other electrophysiological cell types. *Cerebral Cortex*, 18(5):1058–1078, May 2008.

[144] K. Obermayer, H. Ritter, and K. Schulten. A principle for the formation of the spatial structure of cortical feature maps. *Proc Natl Acad Sci U S A*, 87(21):8345–8349, 1990.

[145] K. Ohki, S. Chung, Y. H. Ch'ng, P. Kara, and R. C. Reid. Functional imaging with cellular resolution reveals precise micro-architecture in visual cortex. *Nature*, 433(7026):597–603, 2005.

[146] I. Ohzawa, G. Sclar, and R. D. Freeman. Contrast gain control in the cat visual cortex. *Nature*, 298(5871):266–268, July 1982.

[147] T. O'Leary, M. C. W. van Rossum, and D. J. A. Wyllie. Homeostasis of intrinsic excitability in hippocampal neurones: dynamics and mechanism of the response to chronic depolarization. *The Journal of Physiology*, 588(1):157–170, January 2010.

[148] B. Olshausen and D. Field. What is the other 85% of V1 doing? In *23 Problems in Systems Neuroscience*, pages 182–213. Oxford Scholarship Online Monographs, 2006.

[149] S. J. Olson and S. Grossberg. A neural network model for the development of simple and complex cell receptive fields within cortical maps of orientation and ocular dominance. *Neural Netw.*, 11(2):189–208, 1998.

[150] H. Ozeki, O. Sadakane, T. Akasaki, T. Naito, S. Shimegi, and H. Sato. Relationship between excitation and inhibition underlying size tuning and contextual response modulation in the cat primary visual cortex. *The Journal of Neuroscience*, 24(6):1428–1438, 2004.

[151] C. M. Palmer. *Topographic and Laminar Models for the Development and Organisation of Spatial Frequency and Orientation in V1*. PhD thesis, School of Informatics, The University of Edinburgh, Edinburgh, UK, 2009.

[152] J. W. Peirce. The potential importance of saturating and supersaturating contrast response functions in visual cortex. *Journal of vision*, 7(6), 2007.

[153] D. Purves. *Body and Brain: A Trophic Theory of Neural Connections*. Harvard University Press, Cambridge, MA, 1988.

[154] D. Ringach. On the origin of the functional architecture of the cortex. *PLoS ONE*, 2:251, 2007.

[155] D. L. Ringach, R. M. Shapley, and M. J. Hawken. Orientation selectivity in macaque V1: Diversity and laminar dependence. *The Journal of Neuroscience*, 22(13):5639–5651, 2002.

[156] M. Roberts and A. Thiele. Attention and contrast differently affect contextual integration in an orientation discrimination task. *Experimental Brain Research*, 187(4):535–549, 2008.

[157] K. S. Rockland and J. S. Lund. Intrinsic laminar lattice connections in primate visual cortex. *The Journal of comparative neurology*, 216(3):303–318, 1983.

[158] R. W. Rodieck. Quantitative analysis of cat retinal ganglion cell response to visual stimuli. *Vision Research*, 5(11):583–601, 1965.

[159] M. P. Sceniak, S. Chatterjee, and E. M. Callaway. Visual spatial summation in macaque geniculocortical afferents. *J Neurophysiol*, 96(6):3474–3484, 2006.

[160] M. P. Sceniak, D. L. Ringach, M. J. Hawken, and R. Shapley. Contrast's effect on spatial summation by macaque V1 neurons. *Nat Neurosci*, 2(8):733–739, Aug 1999.

[161] L. Schwabe, K. Obermayer, A. Angelucci, and P. C. Bressloff. The role of feedback in shaping the extra-classical receptive field of cortical neurons: A recurrent network model. *J Neurosci*, 26(36):9117–9129, 2006.

[162] P. Schwindt, J. A. O'Brien, and W. Crill. Quantitative analysis of firing properties of pyramidal neurons from layer 5of rat sensorimotor cortex. *J Neurophysiol*, 77(5):2484–2498, 1997.

[163] G. Sclar, J. H. Maunsell, and P. Lennie. Coding of image contrast in central visual pathways of the macaque monkey. *Vision research*, 30(1):1–10, 1990.

[164] G. Sclar, I. Ohzawa, and R. D. Freeman. Contrast gain control in the kitten's visual system. *J Neurophysiol*, 54(3):668–675, 1985.

[165] F. Sengpiel, A. Sen, and C. Blakemore. Characteristics of surround inhibition in cat area 17. *Experimental Brain Research*, 116(2):216–228, 1997.

[166] P. Series, J. Lorenceau, and Y. Fregnac. The "silent" surround of V1 receptive fields: Theory and experiments. *J Physiol Paris*, 97(4-6):453–474, 2003.

[167] C. J. Shatz and P. Rakic. The genesis of efferent connections from the visual cortex of the fetal rhesus monkey. *The Journal of comparative neurology*, 196(2):287–307, 1981.

[168] H. Shouval, D. Goldberg, J. Jones, M. Beckerman, and L. Cooper. Structured long-range connections can provide a scaffold for orientation maps. *J. Neurosci.*, 20:1119–1128, 2000.

[169] H. Shouval, N. Intrator, C. C. Law, and L. N. Cooper. Effect of binocular cortical misalignment on ocular dominance and orientation selectivity. *Neural Comput.*, 8(5):1021–1040, 1996.

[170] O. Shriki, D. Hansel, and H. Sompolinsky. Rate models for conductance-based cortical neuronal networks. *Neural Comput.*, 15(8):1809–1841, 2003.

[171] A. M. Sillito. The contribution of inhibitory mechanisms to the receptive field properties of neurones in the striate cortex of the cat. *The Journal of physiology*, 250(2):305–329, September 1975.

[172] A. M. Sillito, J. A. Kemp, J. A. Milson, and N. Berardi. A re-evaluation of the mechanisms underlying simple cell orientation selectivity. *Brain research*, 194(2):517–520, August 1980.

[173] L. C. Sincich and G. G. Blasdel. Oriented axon projections in primary visual cortex of the monkey. *The Journal of Neuroscience*, 21:4416–4426, 2001.

[174] S. G. Solomon, B. B. Lee, and H. Sun. Suppressive surrounds and contrast gain in magnocellular-pathway retinal ganglion cells of macaque. *J Neurosci*, 26(34):8715–8726, 2006.

[175] S. G. Solomon and P. Lennie. The machinery of colour vision. *Nat Rev Neurosci*, 8(4):276–286, 2007.

[176] D. C. Somers, S. B. Nelson, and M. Sur. An emergent model of orientation selectivity in cat visual cortical simple cells. *The Journal of Neuroscience*, 15(8):5448–5465, 1995.

[177] D. C. Somers, E. V. Todorov, A. G. Siapas, L. J. Toth, D. S. Kim, and M. Sur. A local circuit approach to understanding integration of long-range inputs in primary visual cortex. *Cereb. Cortex*, 8(3):204–217, 1998.

[178] D. Stellwagen and C. J. Shatz. An instructive role for retinal waves in the development of retinogeniculate connectivity. *Neuron*, 33(3):357–367, 2002.

[179] D. D. Stettler, A. Das, J. Bennett, and C. D. Gilbert. Lateral connectivity and contextual interactions in macaque primary visual cortex. *Neuron*, 36(4):739–750, 2002.

[180] K. J. Stratford, K. Tarczy-Hornoch, K. A. C. Martin, N. J. Bannister, and J. J. B. Jack. Excitatory synaptic inputs to spiny stellate cells in cat visual cortex. *Nature*, 382(6588):258–261, 1996.

[181] T. Sullivan and V. Desa. A temporal trace and som-based model of complex cell development. *Neurocomputing*, 58-60:827–833, 2004.

[182] N. V. Swindale. A model for the formation of ocular dominance stripes. *Proceedings of the Royal Society of London. Series B, Biological Sciences*, 215:243–264, 1980.

[183] N. V. Swindale. The development of topography in the visual cortex: A review of models. *Network*, 7(2):161–247, 1996.

[184] C. Tailby, S. G. Solomon, J. W. Peirce, and A. B. Metha. Two expressions of "surround suppression" in V1 that arise independent of cortical mechanisms of suppression. *Visual neuroscience*, 24(1):99–109, 2007.

[185] S. Tanaka. Theory of self-organization of cortical maps: Mathematical framework. *Neural Networks*, 3:625–640, 1990.

[186] D. Tolhurst and J. M. A. Dean. The statistical reliability of signals in single neurons in cat and monkey visual cortex. *Vision Research*, 23(8):775–785, 1983.

[187] S. Treue and J. C. M. Trujillo. Feature-based attention influences motion processing gain in macaque visual cortex. *Nature*, 399(6736):575–579, June 1999.

[188] J. Triesch. A gradient rule for the plasticity of a neuron's intrinsic excitability. *ICANN - Lecture Notes in Computer Science*, 3696(2):65–70, 2005.

[189] T. W. Troyer, A. E. Krukowski, N. J. Priebe, and K. D. Miller. Contrast-invariant orientation tuning in cat visual cortex: thalamocortical input tuning and correlation-based intracortical connectivity. *The Journal of Neuroscience*, 18(15):5908–5927, 1998.

[190] J. Z. Tsien. Linking Hebb's coincidence-detection to memory formation. *Current Opinion in Neurobiology*, 10(2):266–273, April 2000.

[191] G. G. Turrigiano, K. R. Leslie, N. S. Desai, L. C. Rutherford, and S. B. Nelson. Activity-dependent scaling of quantal amplitude in neocortical neurons. *Nature*, 391:892–896, February 1998.

[192] M. S. V. Dragoi. Dynamic properties of recurrent inhibition in primary visual cortex: contrast and orientation dependence of contextual effects. *J Neurophysiol*, 83(2):1019–1030, Feb 2000.

[193] J. D. Victor. The dynamics of the cat retinal x cell centre. *The Journal of physiology*, 386:219–246, May 1987.

[194] C. von der Malsburg. Self-organization of orientation-sensitive cells in the striate cortex. *Kybernetik*, 15:85–100, 1973.

[195] G. A. Walker, I. Ohzawa, and R. D. Freeman. Asymmetric suppression outside the classical receptive field of the visual cortex. *J Neurosci*, 19(23):10536–10553, 1999.

[196] C. Wang, C. Bardy, J. Y. Y. Huang, T. FitzGibbon, and B. Dreher. Contrast dependence of center and surround integration in primary visual cortex of the cat. *Journal of vision*, 9(1), 2009.

[197] D. Warren, E. Fernandez, and R. Normann. High-resolution two-dimensional spatial mapping of cat striate cortex using a 100-microelectrode array. *Neuroscience*, 105:19–31, 2001.

[198] C. Weber. Self-organization of orientation maps, lateral connections, and dynamic receptive fields in the primary visual cortex. In *Proceedings of the International Conference on Artificial Neural Networks*, Lecture Notes in Computer Science 2130, pages 1147–1152, Berlin, 2001. Springer.

[199] M. Wehr and A. M. Zador. Balanced inhibition underlies tuning and sharpens spike timing in auditory cortex. *Nature*, 426(6965):442–446, November 2003.

[200] M. Weliky, K. Kandler, D. Fitzpatrick, and L. C. Katz. Patterns of excitation and inhibition evoked by horizontal connections in visual cortex share a common relationship to orientation columns. *Neuron*, 15(3):541–552, 1995.

[201] L. White and D. Fitzpatrick. Vision and cortical map development. *Neuron*, 56:327–338, 2007.

[202] L. E. White, D. M. Coppola, and D. Fitzpatrick. The contribution of sensory experience to the maturation of orientation selectivity in ferret visual cortex. *Nature*, 411(6841):1049–1052, 2001.

[203] J. Wielaard and P. Sajda. Circuitry and the classification of simple and complex cells in v1. *J Neurophysiol*, 96(5):2739–2749, November 2006.

[204] J. Wielaard and P. Sajda. Extraclassical receptive field phenomena and short-range connectivity in V1. *Cereb Cortex*, 16(11):1531–1545, 2006.

[205] W. B. Wilent and D. Contreras. Dynamics of excitation and inhibition underlying stimulus selectivity in rat somatosensory cortex. *Nature Neuroscience*, 8(10):1364–1370, September 2005.

[206] D. J. Willshaw and C. von der Malsburg. How patterned neural connections can be set up by self-organization. *Proceedings of the Royal Society of London. Series B, Biological Sciences*, 194:431–445, 1976.

[207] L. Wiskott and T. J. Sejnowski. Slow feature analysis: Unsupervised learning of invariances. *Neural computation*, 14(4):715–770, 2002.

[208] R. O. Wong. Retinal waves and visual system development. *Annu. Rev. Neurosci.*, 22:29–47, 1999.

[209] C.-I. I. Yeh, D. Xing, and R. M. Shapley. "Black" responses dominate macaque primary visual cortex V1. *The Journal of Neuroscience*, 29(38):11753–11760, 2009.

[210] S.-C. Yen, J. Baker, and C. M. Gray. Heterogeneity in the responses of adjacent neurons to natural stimuli in cat striate cortex. *J Neurophysiol*, 97(2):1326–1341, 2007.

[211] M. Zhang, F. S. Hung, Y. Zhu, Z. Xie, and J.-H. H. Wang. Calcium signal-dependent plasticity of neuronal excitability developed postnatally. *Journal of neurobiology*, 61(2):277–287, November 2004.

[212] L. Y. Zhao and B. E. Shi. Integrating contrast invariance into a model for cortical orientation map formation. *Neurocomput.*, 72(7-9):1887–1899, 2009.

[213] L. Zhaoping. Border ownership from intracortical interactions in visual area v2. *Neuron*, 47(1):143–153, July 2005.